NAVIGATION ACCURACY AND INTERFERENCE REJECTION FOR GPS ADAPTIVE ANTENNA ARRAYS

A DISSERTATION

SUBMITTED TO THE DEPARTMENT OF AERONAUTICS AND ASTRONAUTICS

AND TO THE COMMITTEE ON GRADUATE STUDIES

OF STANFORD UNIVERSITY

IN PARTIAL FULFILLMENT OF THE REQUIREMENTS

FOR THE DEGREE OF

DOCTOR OF PHILOSOPHY

David S. De Lorenzo

August 2007

I certify that I have read this dissertation and that in my opinion it is fully adequate, in scope and in quality, as a dissertation for the degree of Doctor of Philosophy.

_____

(Per K. Enge)
Principal Advisor

I certify that I have read this dissertation and that in my opinion it is fully adequate, in scope and in quality, as a dissertation for the degree of Doctor of Philosophy.

_____

(Stephen M. Rock)

I certify that I have read this dissertation and that in my opinion it is fully adequate, in scope and in quality, as a dissertation for the degree of Doctor of Philosophy.

_____

(Dennis M. Akos)

Approved for the University Committee on Graduate Studies.

ABSTRACT

The classic problem in signal processing is to enhance signal while suppressing noise. In this investigation, the signal is timing information from satellites of the Global Positioning System (GPS). The noise originates from jammers at disparate locations. The first step in the solution is to develop a software receiver that implements an adaptive directional antenna array which points (electronically) to individual GPS satellites while suppressing jammers. This software receiver and the associated space-time adaptive algorithms represent a robust and efficient architecture for follow-on hardware implementation. The second step is to analyze the tradeoff between allocating resources to reject radio frequency interference and allocating resources to mitigate measurement biases in the GPS timing information. This analysis leads to deterministic corrections that reduce navigation biases to acceptable levels while preserving the interference rejection capabilities of the adaptive array. The final step is experimental verification by exercising the software receiver with operational hardware in the loop. This investigation demonstrates that adaptive antenna arrays can enable systems that meet the aggressive accuracy and integrity requirements for piloted and autonomous aircraft landing while simultaneously providing significant attenuation of radio frequency interference.

ACKNOWLEDGEMENTS

The acknowledgements in my dissertation are important to me because so many people have helped me in this journey. My fear is that someone deserving of mention may be left out.

My first thanks go to my advisor, Professor Per Enge of the Department of Aeronautics and Astronautics. Thanks also go to Professors Dennis Akos, Steve Rock, and Jason Rife. The work in this thesis has been helped immeasurably by collaboration with my colleagues, Sherman Lo, Tsung-Yu Chiou, Grace Gao, Todd Walter, Lee Boyce, Doug Archdeacon, Seebany Datta-Barua, Alan Chen, Steve Waslander, Eric Phelts, Juan Blanch, Sam Pullen, Alex Ene, Mike Koenig, Hiro Konno, Ung-Suok Kim, Jenny Gautier, Santiago Alban, Sasha Mitelman, Felix Antreich, Godwin Zhang, Gil Gutterman, Morgan Quigley, Pieter Abbeel, Sherann Ellsworth, Dana Parga, and Lynn Kaiser. The significance of my work I owe to you all, the shortcomings are completely my own.

Throughout my life I have been fortunate to receive guidance, inspiration, and encouragement from my family. Foremost I am grateful to my loving wife Truc, our wonderful children Carina and Robin, my parents Bob and Nancy, Truc's parents Quang and My Ho, my brother Mike and his wife Kristin, and Truc's sister Tung and her brothers Quan and Quyen. Thanks also go to my friends Eric and Sally Wang, George and Mary Frances Fisk, Herb and Margie Rauch, Mari Ormiston, Mont Hubbard, Maury Hull, Ted Price, and Ken Struckmeyer.

Finally, the author gratefully acknowledges the support of the JPALS Program Office and the Naval Air Warfare Center Aircraft Division through contract N00421-05-C-0068, and the Federal Aviation Administration on Cooperative Agreement 97-G-012.

TABLE OF CONTENTS

LIST OF TABLES

LIST OF FIGURES

CHAPTER 1: INTRODUCTION

The classic problem in signal processing is to enhance signal while suppressing noise. In this investigation, the signal is timing information from satellites of the Global Positioning System (GPS). The noise originates from jammers at disparate locations. The first step in the solution is to develop a software receiver that implements an adaptive directional antenna array which points (electronically) to individual GPS satellites while suppressing jammers. The second step is to analyze the tradeoff between allocating resources to reject radio frequency interference and allocating resources to mitigate measurement biases in the GPS timing information. The final step is experimental verification by exercising the software receiver with operational hardware in the loop.

These three steps are accomplished in this investigation. Chapter 2 treats software implementation of the space-time adaptive antenna array. Chapter 3 discusses the tradeoff between interference rejection and navigation biases. Chapter 4 addresses experimental verification. Chapter 5 briefly outlines future work. Before leading the reader through these steps, it is useful to present some background information.

1.1 BACKGROUND

Global navigation satellite systems, led by the NAVSTAR Global Positioning System (GPS), are the world's premier technology for positioning and timing [1]. GPS provides typical accuracies of meters in position and nanoseconds in time. These accuracies make GPS a critical technology for aviation, where safety-of-life requires strict limits on navigation errors. GPS maintains its availability through all phases of flight, from taxi and takeoff, through flight en route, and during final approach and landing. This availability is attractive for aviation, in contrast to the phase-of-flight-specific availability of traditional navigation technologies.

Virtually all civil and military aircraft are equipped with GPS receivers. For most phases of flight, safety requirements can be met by stand-alone GPS navigation or by GPS with

wide-area augmentation [2]. However, aviation authorities have not certified GPS as a primary means of navigation for landing operations. Local-area augmentation, required to ensure navigation system integrity during landing, is still under development [3]. The ultimate aviation objective for GPS is auto-land. Fully-automated GPS landings require the highest levels of outside assistance and performance validation [4]. An important research area in both civil and military aviation is ensuring GPS accuracy and integrity during final approach and landing.

A significant challenge to landing with GPS, particularly for military users, is to reject radio frequency interference, which can jam reception of the GPS signals [5]. Among the most aggressive anti-jam technologies is the multi-element antenna array equipped with adaptive beamforming and nullsteering [6]. Antenna arrays that use space-time adaptive processing significantly improve the signal to interference plus noise ratio (SINR). However, this spatial and temporal filtering can introduce time-varying biases into the GPS measurements [7, 8, 9, 10, 11, 12, 13, 14, 15]. This investigation evaluates the tradeoff between interference rejection and GPS measurement biases. It demonstrates that adaptive antenna arrays can enable systems that meet the aggressive accuracy and integrity requirements for piloted and autonomous aircraft landing while simultaneously providing significant attenuation of radio frequency interference.

1.2 PROBLEM STATEMENT

The Joint Precision Approach and Landing System (JPALS) is a United States Navy and Air Force program designed to provide local-area augmentation to GPS navigation [16]. Sea-based JPALS, shown conceptually in Figure 1.1, is intended to support piloted and autonomous landings in demanding maritime environments [17]. Four challenges for these landings are: (a) all-weather around-the-clock blue-water operations, (b) crowded and moving landing area, (c) ship-generated or inadvertent radio frequency interference, and (d) hostile jamming. Safety-of-life considerations drive requirements for high integrity, for high accuracy, and for rejection of narrowband and wideband interference. These requirements are shown in Table 1.1 [18].

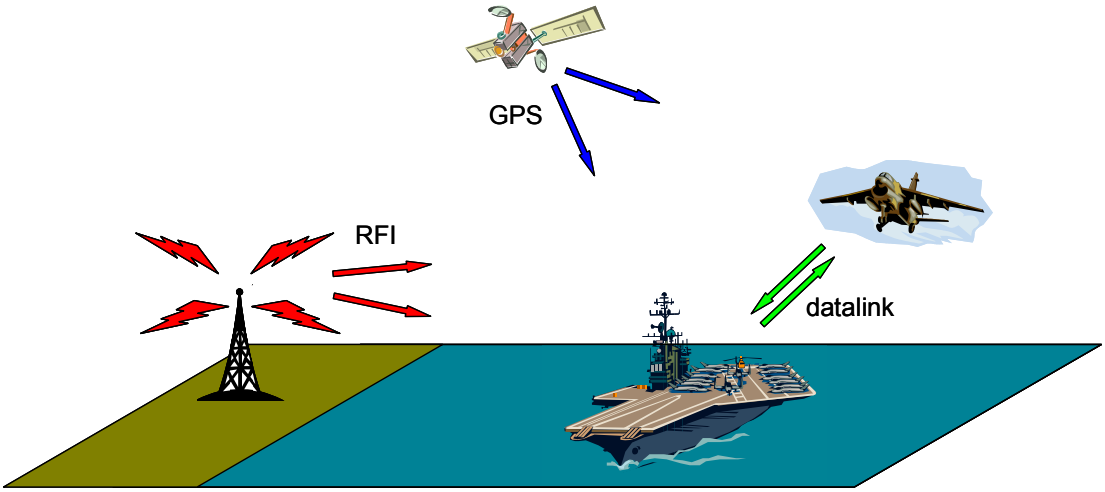

Figure 1.1. Sea-based JPALS overview and operational environment.

Table 1.1. High-Level Requirements for Sea-based JPALS [18].

Feature	Requirement
Accuracy (vertical, 95%)	0.4 meters
Integrity (loss probability)	1 part in 10^{6} / approach
Vulnerability to Jamming	95% availability under specified jamming scenarios

1.3 BASELINE ARCHITECTURE

The baseline architecture is intended to meet the accuracy, interference-rejection, and integrity requirements of Sea-based JPALS. To do this, the system will utilize carrier-phase differential navigation and multi-element adaptive antenna arrays [18, 19], two elements that have not been previously combined.

Sea-based JPALS accuracy requirements are addressed through carrier-phase differential navigation, whereas current or next-generation civilian landing systems use carrier-smoothed code-phase navigation [20, 21]. Code-phase navigation is not suitable for Sea-based JPALS because it does not meet the accuracy requirement shown in Table 1.1.

The accuracy of a GPS position estimate can be no better than the ability of the receiver to resolve the arrival times of the incoming satellite signals. For code-phase positioning, this accuracy is related to the chip length of the pseudo-random noise (PRN) code. The PRN code is the spreading code modulating the GPS sinusoidal carrier. The length of a PRN code chip is about 300 m for C/A code (1.023 Mchips/sec) and 30 m for P-code (10.23 Mchips/sec). This leads to a lower bound on code-phase estimation accuracies of several meters for C/A code and tens of centimeters for P-code [22]. Code-phase estimates may be smoothed substantially with rate-aiding from the carrier-tracking loop. However, even the sub-meter accuracy of a differential code-phase system that uses carrier-smoothing is insufficient to meet Sea-based JPALS accuracy requirements [18].

In contrast, a position solution that leverages the greater precision of GPS carrier-phase measurements can achieve Sea-based JPALS accuracy requirements. However, each carrier sinusoid is not uniquely identifiable, so absolute range in carrier cycles cannot directly be observed. The solution is carrier-phase differential navigation, where a user shares code-phase and carrier-phase estimates with another receiver (the "base station"). By differencing these measurements, a relative position solution with respect to the base station may be found. Relative positioning is acceptable for Sea-based JPALS since the goal is to locate an aircraft precisely with respect to the landing zone on a moving ship. (The drawbacks to carrier-phase differential navigation include increased complexity, reduced tracking robustness, and the need for a data link between user and base station.)

With this method, a relative position is calculated from the difference in the number of carrier cycles separating the base station from the airborne user, projected along vectors extending up to each tracked GPS satellite. The carrier-phase difference is comprised of an unknown number of whole carrier cycles (the integer cycle ambiguity) and a fractional carrier-phase that is the difference of measurements made within each receiver. Once the integer ambiguities are resolved, then instead of a code-phase-based absolute position estimate, it is possible to achieve relative positioning accuracies on the order of fractions of a carrier wavelength. For the GPS L1 carrier at 1575.42 MHz, which has a wavelength of 19 cm, a lower bound on carrier-phase differential navigation accuracies

(in real-time operation with uninterrupted carrier-phase tracking) is on the order of one centimeter [22]. This is well within Sea-based JPALS accuracy requirements of 0.4 m.

Sea-based JPALS requirements for interference rejection are addressed by controlled reception pattern antenna (CRPA) arrays both on the airborne platform and on the ship. A CRPA can increase the signal to interference plus noise ratio (SINR) in two ways: (a) by enhancing the array gain in the direction of desired signals above the gain from a fixed reception pattern antenna (FRPA), and (b) by attenuating interference signals that arrive from off of the main beam boresight (here, interference refers to any undesirable signal, e.g., jamming, spoofing, unintentional interference, multipath, etc.). The weighting coefficients for each antenna in a CRPA array may be computed either deterministically or adaptively [23].

Deterministic methods have been considered for Sea-based JPALS because they are simpler to implement than adaptive algorithms. However, the deterministic CRPA suffers deficiencies in interference rejection when compared to an adaptive array. For GPS, the deterministic CRPA simply points a beam at each GPS satellite. To this end, it computes coefficients for each antenna using knowledge of array geometry and satellite ephemeris (see Figure 1.2). Beamforming increases gain in a desired look direction (or directions, if multiple signals are being tracked by the same beamformer). However, the sidelobes and nulls of the array are uncontrolled and may not adequately suppress interference. An additional step of interference detection and localization can produce nullsteering constraints that significantly reduce the array gain in the direction of undesired signals. In practice, this method of nullsteering has difficulties because performance falls off dramatically with only small errors in interference localization [24].

Adaptive algorithms control sidelobes and steer nulls without the same sensitivity to small interference localization errors. Adaptive array processing increases the SINR by using feedback to optimize some characteristic of the array output. Suppression of narrowband or continuous-wave (CW) interference can be achieved by adaptive spatial filtering [7, 25, 26, 27]. Greater interference rejection (particularly of multiple, high-

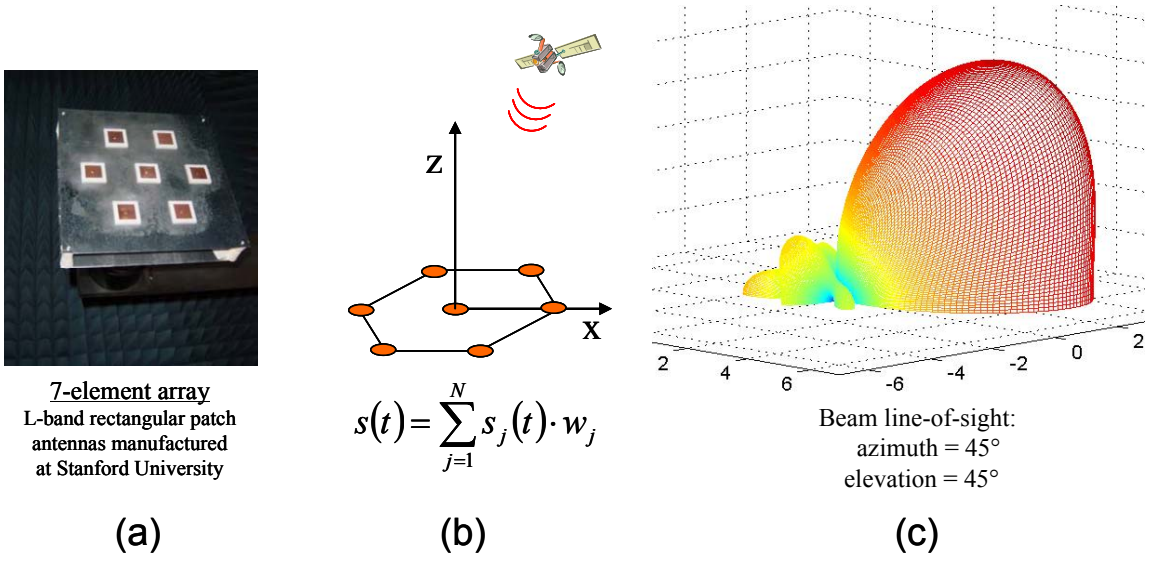

Figure 1.2. Controlled reception pattern antenna (CRPA) arrays:
(a) Stanford's 7-element array in the anechoic chamber
(b) beamforming for reception of an incoming satellite signal
(c) array gain pattern showing main beam and sidelobes

power, or wideband sources) can be realized by incorporating temporal filtering as well, for example with a tapped-delay-line antenna array [8, 28]. In order to achieve maximum performance to meet Sea-based JPALS interference rejection requirements, the best choice of weighting algorithm for the CRPA array is space-time adaptive processing [18], because it provides the greatest improvement in SINR.

Sea-based JPALS integrity requirements are met by high-performance integer ambiguity resolution algorithms that are used during carrier-phase differential base station to aircraft initialization [18, 29]. Carrier-phase differential navigation achieves its remarkable accuracy by the elimination of common-mode nuisance parameters in the measurements made at the base station and at the aircraft [22]. Extended filtering of the GPS code-phase and carrier-phase measurements reduces the impact of random errors, allowing reliable determination of the number of integer carrier cycles separating the base station from the aircraft, projected along each satellite direction. However, the ambiguity resolution algorithms still are sensitive to measurement biases, as biases are not reduced

Table 1.2. Integrity-Driven Bias Requirements for Sea-based JPALS [29].

Feature	Bias Requirement
Code-phase bias	< 8 centimeters
Carrier-phase bias	< 0.5 centimeter (< 10° phase)

by filtering and can cause algorithm convergence to an erroneous integer solution set. For this reason, integrity analysis leads to derived requirements for code-phase and carrier-phase biases, as shown in Table 1.2 [29]. These bias requirements are substantially tighter than the vertical accuracy limit of 0.4 m shown in Table 1.1.

Common-mode biases in GPS estimates do not affect integer ambiguity resolution or integrity. Here, common-mode refers to biases which apply equally to all code-phase or carrier-phase measurements made by a receiver, such as biases caused by analog filter-induced signal distortion, processing delays, or receiver clock errors. Biases which are not common-mode, however, do affect ambiguity resolution and integrity. A bias that is not common-mode is one which is different for each received GPS signal, such as biases due to satellite clock errors, atmospheric delays, or multipath.

The non-common-mode biases that will have the greatest impact on Sea-based JPALS integrity calculations are those which result from antenna-induced signal distortion and from signal distortion caused by array spatial and temporal filtering [18]. Including a space-time adaptive antenna array in the Sea-based JPALS design in order to reject interference can increase satellite-specific code-phase and carrier-phase tracking biases.

Figure 1.3 summarizes how Sea-based JPALS accuracy, integrity, and interference rejection requirements, shown in blue, lead to the architectural solutions just described, shown in green. However, the bias limitations derived from integrity analysis are at odds with the biases caused by antennas and by space-time adaptive antenna array processing (these appear in yellow). Bridging the gap between these two aspects of Sea-based

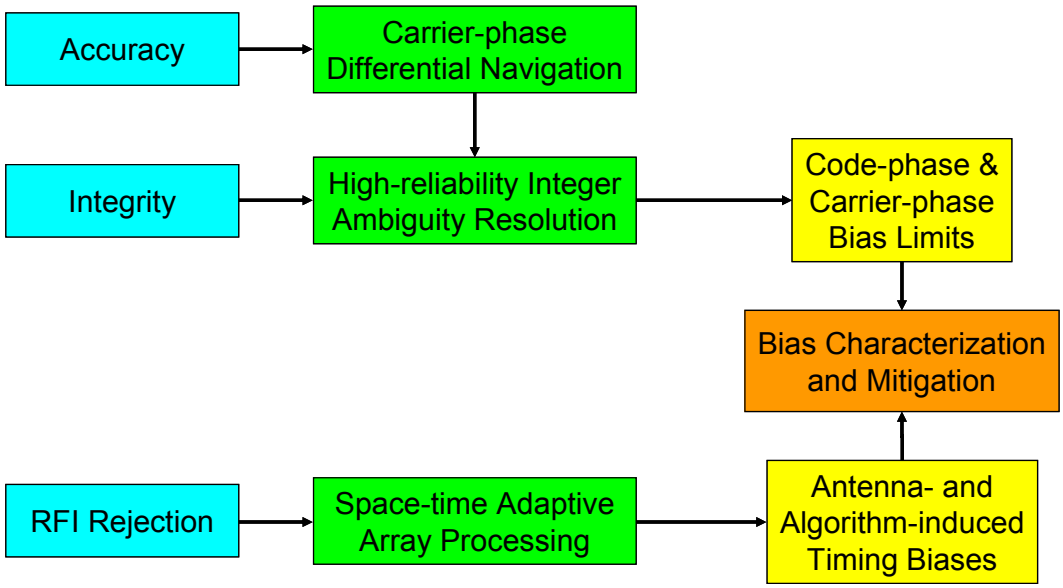

Figure 1.3. Summary of accuracy, integrity, and interference rejection requirements for Sea-based JPALS.

JPALS is the task of bias characterization and mitigation, which is shown in orange in Figure 1.3. The next section shows how to mitigate biases so that residual errors are below the limits derived from integrity analysis.

1.4 CHALLENGES TO IMPLEMENTING THE BASELINE ARCHITECTURE

The key challenge to implementing a GPS adaptive antenna array for Sea-based JPALS is to reject interference while limiting or mitigating navigation biases. First, strict limits on code-phase and carrier-phase biases have been identified in order to meet accuracy and integrity requirements. Second, there is a need for space-time adaptive antenna arrays in order to meet interference rejection requirements. However, there is a conflict between integrity-driven bias requirements and the requirement to reject interference through use of an adaptive antenna array. The mechanisms whereby adaptive antenna arrays increase code-phase and carrier-phase biases are discussed next.

Antennas and multi-element antenna arrays can introduce biases in estimates of code-phase and carrier-phase. An ideal isotropic antenna will receive incoming signals

identically for all frequencies and line-of-sight arrival directions. However, the response of an actual GPS antenna varies as a function of incoming signal azimuth, elevation, and frequency. The GPS signal is transmitted on two frequencies, L1 at 1575.42 MHz and L2 at 1227.6 MHz (the frequency treated in this investigation is L1). Figure 1.4 characterizes an L1-band right-hand circularly polarized rectangular patch antenna, with gain versus frequency in the left subplot and phase versus frequency in the right subplot [30]. The 40 MHz band centered on the L1 carrier frequency includes the central peak of the P-code signal and the next higher and lower side-peaks. The plots in Figure 1.4 show the high degree of non-linearity in antenna gain and phase response between ten representative incoming signal arrival directions (signal azimuth and elevation are summarized in Table 1.3, where PRN 11 is the test satellite at zenith).

In addition to the frequency-domain characterization just described, an antenna also may be characterized according to the biases it introduces in the receiver's estimates of code-phase and carrier-phase. This is measurement-domain characterization.

In the ideal case, correlation between the incoming PRN code sequence and an on-board-generated replica sequence produces an output function with the shape of an isosceles

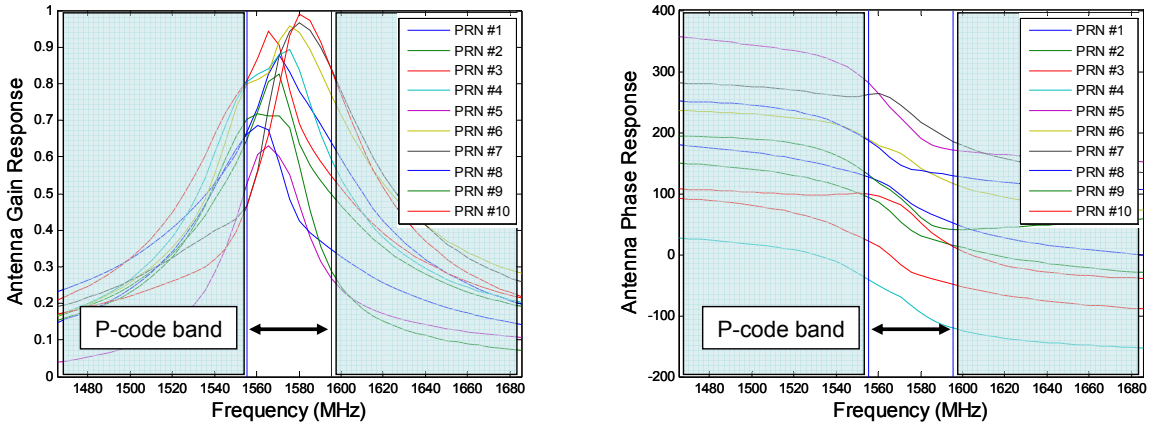

Figure 1.4. L-band patch antenna gain and phase response with respect to signal frequency and arrival direction [30]. Each signal is arriving from a different azimuth/elevation combination (refer to Table 1.3).

triangle having a base dimension that is two code chips wide. Finite signal bandwidth causes rounding of the triangular shape. Antenna anisotropy distorts the leading and trailing edges of the correlation function, and this distortion is dependent on signal arrival direction. Figure 1.5 illustrates the impact to the incoming-to-replica correlation function for the ten signal arrival directions whose frequency response was characterized in Figure 1.4 (for reference, the signal from PRN 11 is received undistorted).

Code-phase tracking estimates the peak of the incoming-to-replica correlation function. It does this by seeking to zero-out the difference between early and late correlation output values (the early and late correlators are commonly placed one-half chip before and after the central peak). Therefore, antenna-induced signal distortion leads to a biased estimate of code-phase that varies according to signal arrival direction (and which is dependent on the code-phase discriminator and the correlator spacing).

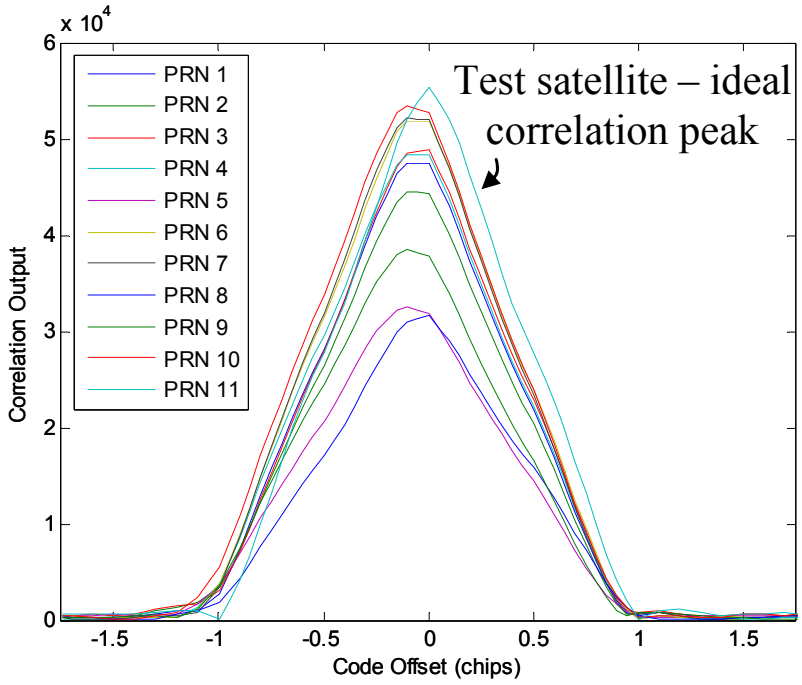

Figure 1.5. Distortion of the correlation function between the incoming signal and the onboard-generated replica produces a biased estimate of code-phase. Differences in gain cause varying degrees of signal attenuation. Each signal is arriving from a different azimuth/elevation combination (see Table 1.3).

Carrier-phase bias is a result of the non-zero phase response of the antenna at the carrier frequency, and this phase response also varies as a function of signal arrival direction. Carrier-phase bias measures the difference between the antenna's physical center and its instantaneous electromagnetic center. There also may be a reduction in received signal power as a function both of signal frequency and of arrival direction; as shown in Table 1.3, signal attenuation may exceed 6 dB in comparison to an isotropic receiving antenna (this effect is more pronounced at low elevations).

Table 1.3 shows code-phase and carrier-phase biases for the antennas characterized by Figures 1.4 and 1.5. The biases for this antenna (in particular the differential biases) do not meet Sea-based JPALS code-phase or carrier-phase bias requirements [29].

A multi-element antenna array may introduce additional biases in the estimates of code-phase and carrier-phase. Two primary mechanisms which generate biases specific to CRPA arrays are electromagnetic mutual coupling and spatial and temporal filtering. Mutual coupling between the elements of the array changes the electromagnetic response of each antenna and can cause biases by increasing the degree of frequency-dependant

Table 1.3. Code-phase and carrier-phase biases for the center antenna of a 7-element array, as a function of incoming signal line-of-sight; incident signal power of 40 dB-Hz.

PRN	Incoming Signal Line-of-Sight		Code-phase Bias (m)	Carrier-phase Bias (deg)	C/No (dB-Hz)
	Az	El			
1	0	40	-2.0	85	37.5
2	30	30	-1.9	42	36.8
3	60	40	-1.5	-27	37.6
4	90	50	-2.3	-83	38.1
5	120	20	-2.8	-154	34.3
6	150	60	-2.2	154	38.7
7	210	70	-2.4	-129	38.9
8	240	20	-0.5	141	33.6
9	270	30	-3.0	76	35.9
10	300	80	-2.7	67	38.8

distortion in the received signals [30, 31, 32, 33, 34, 35]. Biases also are caused by the spatial and temporal weighting used to form the array output signal. Incorporating temporal processing, in particular, exacerbates signal distortion and the biases due to that distortion [6, 36].

Bias mitigation is necessary in order to increase the probability of correctly estimating integer ambiguities for carrier-phase differential navigation. Two methods of bias mitigation proposed for Sea-based JPALS are antenna equalization and line-of-sight-based bias compensation [35]. Antenna equalization is outlined in Figure 1.6. Line-of-sight-based bias compensation is outlined in Figure 1.7.

As shown in Figure 1.6, antenna equalization takes the form of frequency-domain filtering of the incoming satellite signals to undo distortion caused by each antenna's non-isotropic gain and phase response [7, 8, 11]. However, since each antenna's response is a strong function of the incoming signal arrival direction, the equalization filters likewise are antenna and line-of-sight dependent, requiring not only a massive database of filter coefficients but also parallel equalization for each antenna in the array and for each receiver tracking channel. Furthermore, this filtering must be done at the sampling frequency or as a block-processing operation on buffered samples. These considerations result in significant processing demands placed on the receiver.

As shown in Figure 1.7, line-of-sight-based bias compensation applies code-phase and carrier-phase bias corrections to the tracking estimates [14, 15, 35]. The corrections are stored in a look-up table and applied based on signal arrival direction. This method of bias compensation is done at the tracking loop output frequency (~kHz), rather than at the sampling frequency (~MHz), reducing the computational burden on the receiver.

Bias mitigation via deterministic corrections is simpler to implement, less demanding on the receiver, and more amenable to verification than frequency-domain equalization. The look-up table approach applies predetermined bias compensation values, so each set of code-phase and carrier-phase corrections is valid for only one combination of arrival

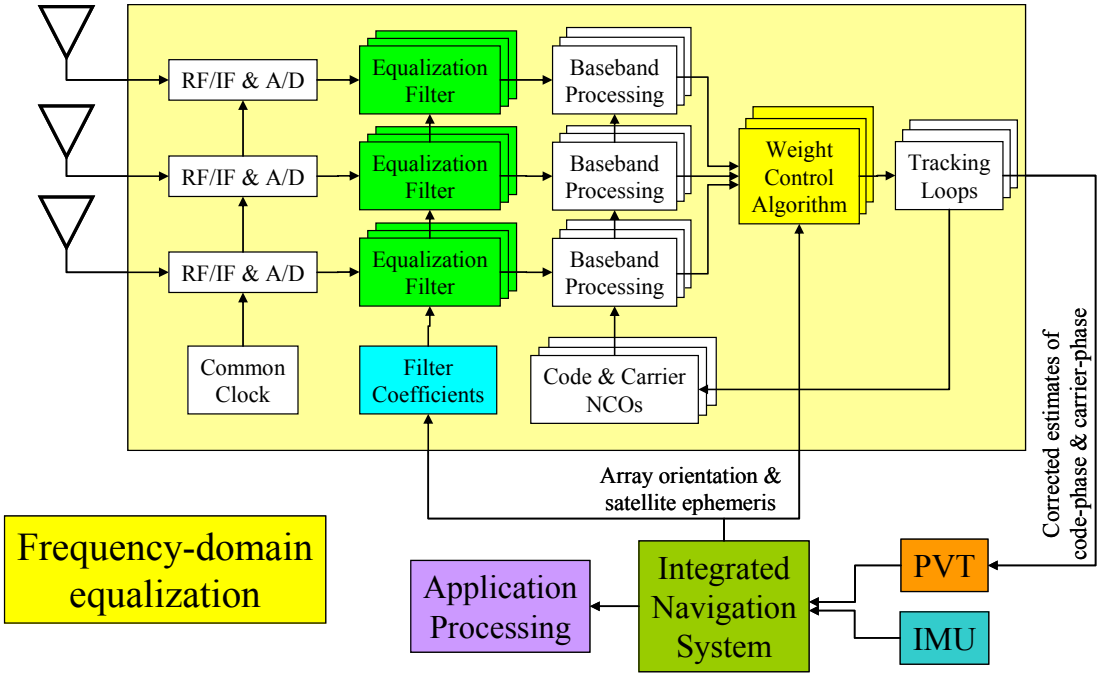

Figure 1.6. Frequency-domain equalization of antenna-induced signal distortion.

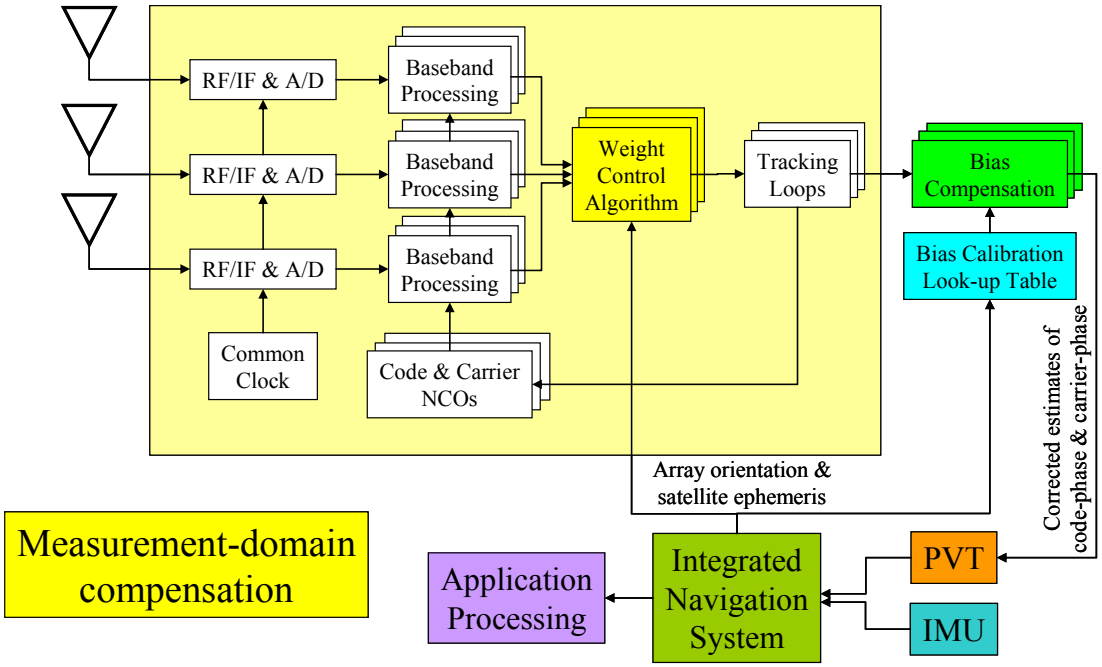

Figure 1.7. Measurement-domain compensation of code-phase and carrier-phase biases caused by antenna-induced signal distortion.

direction and signal frequency (e.g., L1, L2, etc.). This mitigation method, if successful in meeting Sea-based JPALS requirements, is considered preferable to frequency-domain equalization and is the approach studied in the remainder of this investigation.

1.5 APPROACH TO IMPLEMENTING THE BASELINE ARCHITECTURE

The approach to mitigating GPS navigation biases developed here has two parts. First, the code-phase and carrier-phase biases are calibrated. Second, these calibrated biases are used as corrections that are subtracted from code-phase and carrier-phase estimates made by the GPS receiver. The corrections are functions of the azimuth and elevation of the satellite in the antenna frame.

Code-phase and carrier-phase biases are the results of antenna anisotropy and array spatial and temporal filtering. Mitigation of code-phase and carrier-phase biases will take the form of deterministic corrections applied to the tracking loop output. The corrections are derived from single-antenna FRPA and multi-antenna CRPA calibration.

For a deterministic beamforming CRPA, the weighting coefficients used to combine the antenna signals are deterministic functions of array geometry and satellite ephemeris. For this reason, the biases likewise are deterministic and may be calibrated, e.g., through electromagnetic simulation or anechoic chamber testing. Deterministic measurement-domain compensation, as shown in Figure 1.7, will exactly correct these biases.

However, for an adaptive array, the antenna weights are dependent on the signal and noise environment (which includes interference). Thus the biases no longer are deterministic and cannot be calibrated *a priori*. For this reason, deterministic corrections, when applied to the tracking outputs of an adaptive antenna array, may leave residual uncompensated code-phase and carrier-phase biases. Consequently, deterministic look-up-table-based compensation may be insufficient in reducing biases to the required level.

This section described how Sea-based JPALS performance requirements will be met through carrier-phase differential navigation (accuracy) and through multi-element

adaptive antenna arrays (interference rejection), with specific limits on code-phase and carrier-phase biases (integrity). The predominant challenge of the current analysis is managing or mitigating the biases due to antennas and adaptive arrays while at the same time meeting interference rejection requirements.

1.6 THESIS CONTRIBUTIONS

For a GPS receiver with space-time adaptive array processing, there is a clear tradeoff between rejection of radio frequency interference and mitigation of biases in the code-phase and carrier-phase measurements. This investigation shows how to meet accuracy, integrity, and interference rejection requirements with a combination of an adaptive antenna array and deterministic bias compensation.

The three main contributions of this thesis are the following:

1. Chapter 2 develops a software receiver that implements a space-time adaptive multi-antenna array. The architecture is modular and scalable. The software is more computationally efficient than existing approaches. The method solves several adaptive-processing-related issues previously identified in the literature.

2. Chapter 3 analyzes the tradeoff between rejecting radio frequency interference and mitigating navigation biases. This analysis leads to deterministic corrections that are sufficient to reduce measurement biases below the levels required by Sea-based JPALS.

3. Chapter 4 provides experimental verification by exercising the software receiver with operational hardware in the loop.

The impact of these contributions is summarized in Table 1.4. The results in the right-most column show that for isotropic antennas, space-time adaptive processing introduces no code-phase or carrier-phase biases. This no-bias finding is demonstrated for LMS and MVDR adaptive arrays. Other adaptive algorithms also may introduce no navigation biases, but this has not been evaluated here.

Table 1.4. Antenna anisotropy, adaptive algorithms, and residual code-phase and carrier-phase biases.

Antenna Type	Array Type	Compensation and Bias Residuals
Isotropic	FRPA	no biases, compensation not required
	CRPA	no biases, compensation not required
	STAP	no biases, compensation not required [1]
Non-isotropic	FRPA	bias compensation successful [2]
	CRPA	bias compensation successful [2]
	STAP	bias compensation success depends on antenna anisotropy and J/S ratio [1] [2]

[1] results apply to Widrow/LMS and Applebaum/MVDR STAP algorithms and wideband-Gaussian RFI

[2] successful compensation means meeting Sea-based JPALS accuracy- and integrity-derived limits

FRPA: fixed reception pattern antenna

CRPA: controlled reception pattern antenna (array)

STAP: space-time adaptive processor (array)

J/S: jammer-to-signal power

For non-isotropic antennas and space-time adaptive processing, deterministic corrections are sufficient to reduce code-phase and carrier-phase biases below Sea-based JPALS limits, depending on the degree of antenna anisotropy. For the L-band patch antennas implemented at Stanford University and analyzed in this investigation, the code-phase bias residuals in the presence of wideband interference exceed the limits established for Sea-based JPALS and therefore do not meet the auto-land requirements. However, with antennas that exhibit less signal distortion as a function of frequency and arrival direction (i.e., reduced non-linearity), bias mitigation is successful (since isotropic antennas do meet the bias requirements). Therefore, with a suitable antenna design, space-time adaptive processing would be enabled for carrier-phase differential navigation, allowing aircraft auto-land while providing the benefits of interference rejection to the receiver.

This investigation demonstrates that a combination of space-time adaptive processing and deterministic measurement-domain bias compensation will meet Sea-based JPALS

requirements. This means that the accuracy, integrity, and interference-rejection requirements of Sea-based JPALS can be met with a system architecture incorporating carrier-phase differential navigation and multi-element adaptive antenna arrays.

CHAPTER 2: SPACE-TIME ADAPTIVE PROCESSING FOR A SOFTWARE RECEIVER

This chapter describes a GPS software receiver, developed specifically in the course of this investigation, which implements a space-time adaptive antenna array. The adaptive directional antenna can point (electronically) to each GPS satellite while nulling some number of disparate jammers. The GPS receiver described herein quantifies interference rejection, characterizes code-phase and carrier-phase biases due to antennas and to array processing, and evaluates performance of a deterministic bias compensation scheme. The algorithms in the receiver implement antenna array processing for adaptive beamforming and nullsteering, known as space-time adaptive processing or STAP. This section begins with a discussion of deterministic and adaptive antenna array processing for GPS, and then describes in detail the specific STAP-related contributions of this investigation.

2.1 SOFTWARE RECEIVER OVERVIEW

This section presents an overview of the Stanford University GPS multi-antenna space-time adaptive software receiver [14], shown conceptually in Figure 2.1. The basic processing of the receiver follows traditional design practices, e.g., [22, 37, 38, 39, 40]. An FFT-based acquisition module performs a rapid search across Doppler frequency and code-phase for satellite signals present in the input data. Following acquisition, normal GPS signal processing takes place: carrier wipeoff, code wipeoff, early/prompt/late inphase and quadrature correlators, and then execution of code and carrier tracking loops.

The non-standard feature of this software receiver is the inclusion of a weight control algorithm which supports single-antenna FRPA, multi-antenna deterministic CRPA, and space-time adaptive antenna array processing. The execution of the adaptive weight control algorithm either can occur between the carrier and code wipeoff steps as shown in Figure 2.1, or it can occur downstream of the correlation operation as will be discussed later. In the development of antenna array processing that follows, computation of the

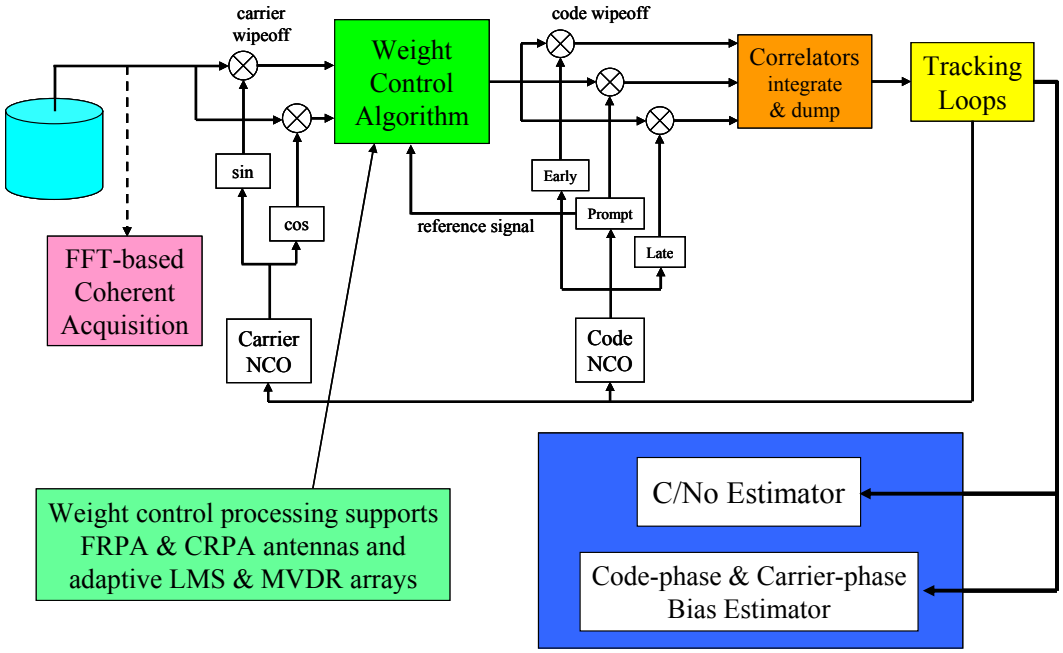

Figure 2.1. Software receiver block diagram [14].

weight vector, whether by deterministic or by adaptive means, will utilize information on array orientation, satellite ephemeris, and/or signal covariance. This is introduced in Figure 2.2 and will be expanded upon in the following sections.

The desired characterization data for this investigation are present in the code-phase, carrier-phase, and carrier to noise ratio (C/N_0) estimates from receiver processing. For this reason, computation of a navigation solution is not required. Any code-phase or carrier-phase biases introduced by the software receiver are isolated to the spatial and temporal filtering of the weight control algorithm, since the rest of the software receiver contains traditional and well-understood elements.

2.2 ANTENNA ARRAY PROCESSING

The next sections describe the approach to antenna array processing for GPS. This discussion starts with a review of the adaptive array literature for GPS, describes deterministic and then adaptive array processing, shows how adaptive algorithms work in a GPS receiver, and concludes with an illustrative example.

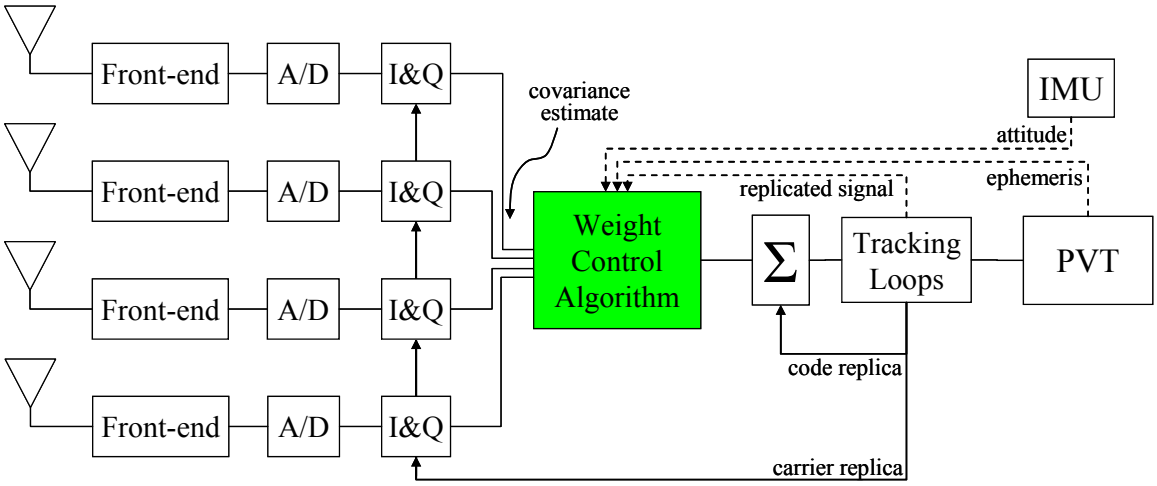

Figure 2.2. Array processing and inputs
to the weight control algorithm.

There is a substantial history of adaptive signal processing for radar systems and wireless communication [23, 41, 42, 43], with the primary goals being to increase the signal to interference plus noise ratio (SINR) and to reduce the bit-error-rate of transmitted data. Current GPS methods build on this existing technology base. For GPS, there is an additional critical goal of limiting timing errors (or equivalently, of limiting delays) in the code-phase and carrier-phase estimates. A unique constraint for GPS is that the signals tracked by the receiver are below the thermal noise floor prior to code de-spreading. This limitation makes reference-signal-based adaptation more challenging and has led much of the previous research to focus strictly on power minimization methods.

The military legacy of adaptive array processing and anti-jam for GPS dates from the late 1970s, but this work is not available in the published literature. The earliest published work on adaptive array processing for GPS dates to the early 1990s, e.g., [44, 45, 46], but these studies either were completely analytical or relied on exact replicas of the tracked signals. More recent papers focused on analytical studies of STAP performance [47, 48, 49, 50], required *a priori* knowledge of the signal, of the interference, or of the complete space-time covariance matrix [47, 51], or leveraged the low power of the GPS signals to simplify implementation of power minimization processing [25, 48, 49, 50, 51].

The first truly practical descriptions of GPS STAP receivers came next, with treatments now including discussion of antenna mutual coupling, channel-to-channel variation and equalization, and measurement domain errors, e.g., [7, 8, 31, 52]. These papers were followed by an increasingly mature treatment of adaptive array processing in the GPS literature, including modular or cascaded anti-jam designs [27, 53, 54], practical hardware-based testing [53, 55], equalization or adaptation constraints to limit code-phase and carrier-phase bias errors [10, 26, 53, 56, 57], and more aggressive interference scenarios or adaptive algorithm performance [9, 26, 28, 58].

The most recent GPS STAP literature focuses on robust GPS receiver designs that can lead to practical hardware implementation [11, 14, 15, 59, 60, 61, 62, 63], on system-level integrated testing [11, 13, 14, 15, 61, 62, 63], on characterization of antenna-induced code-phase and carrier-phase errors [11, 12, 13, 14, 15, 61, 63, 64, 65], and on evolved adaptive algorithms for spatial and temporal filtering, e.g., [66, 67, 68, 69].

Gaps still exist in the GPS STAP-related literature, and a number of these gaps are addressed directly by the algorithms and methods developed during the course of this investigation. The contributions in this area include the creation and demonstration of a multi-antenna space-time adaptive GPS software receiver that:

- Completely integrates space-time adaptive array processing into the GPS receiver.
- Ties convergence speed of the adaptive algorithms to the noise bandwidth of the carrier-tracking loop.
- Implements an adaptation constraint that eliminates carrier-phase errors caused by weight vector phase rotation, without reducing spatial or temporal degrees of freedom in the adaptive algorithm.
- Addresses navigation data bit ambiguity for reference-signal-based adaptation.
- Provides a MATLAB-based GPS software receiver development environment that enables STAP analysis [14, 64, 70], tracking loop architecture studies [71], next-

generation satellite navigation signal analysis [72, 73, 74], and multi-antenna GPS receiver hardware development for real-time operation [75].

This chapter describes a way to: (a) implement STAP for high-integrity GPS, and (b) provide a software environment for end-to-end bias characterization and interference rejection studies. The following discussion begins with a brief overview of deterministic and adaptive array processing and then presents in detail the implementation of STAP for a GPS receiver. Real data from a variety of sources are processed by the software receiver to show the efficacy of the STAP algorithms.

2.2.1 Deterministic Beamforming

The goal of a multi-element antenna array is to combine received signals in such a way that the ratio of desirable to undesirable content in the array output is maximized. Multi-element antenna array technology is well-described in the literature, particularly as applied to deterministic beamforming, nullsteering, and gain-pattern computation, e.g., [76, 77] as well as for adaptive antenna array processing, e.g., [6, 36, 78, 79].

There are several methods for combining the received signals in a multi-antenna array, but the simplest conceptually is to multiply the signal vector (one sample per antenna element per sampling epoch) by the complex array weight vector and then to sum over the N antenna elements in the array:

$$s(t) = \sum_{j=1}^{N} s_j(t) \cdot w_j(t) = \mathbf{w}^T \mathbf{s}(t) \tag{2.1}$$

(In the subsequent discussion, the explicit time-dependence of the array weight vector is omitted for clarity.)

For an array with temporal as well as spatial extent, signals from the current sampling epoch are added to the signal vector with their previous-time neighbors in a first-in-first-out sense. For beamforming that occurs after carrier wipeoff, as developed in this

investigation, the weight vector entries for all temporal samples for any particular antenna element and satellite are identical. This is because, after carrier wipeoff, no further phase-shifting needs to occur beyond that required to compensate for satellite and array geometry. Therefore, the summation over *K* time-taps is omitted for clarity.

For a deterministic CRPA array with maximum gain achieved for a particular incoming signal vector, weights are calculated given knowledge of antenna baselines and incoming signal azimuth and elevation:

$$w_j = \exp\left[-j\left(2\pi \frac{\vec{p}_j \cdot \hat{r}_{boresight}}{\lambda_{L1}}\right)\right] \tag{2.2}$$

Here, $\vec{p}_j$ is the baseline vector to the j^{th} antenna in body-fixed coordinates, $\hat{r}_{boresight}$ is a unit-vector in the direction of the satellite, and λ_{L1} is the wavelength for the signal frequency to be processed. The phase rotation provided by antenna weight w_j in Eq. (2.2) removes the phase shift due to antenna array and satellite geometry (i.e., geometric phase), as shown in Figure 2.3. Referring back to Figure 2.2, $\vec{p}_j$ is known *a priori* and $\hat{r}_{boresight}$ is calculated with input from the IMU (inertial measurement unit) and PVT

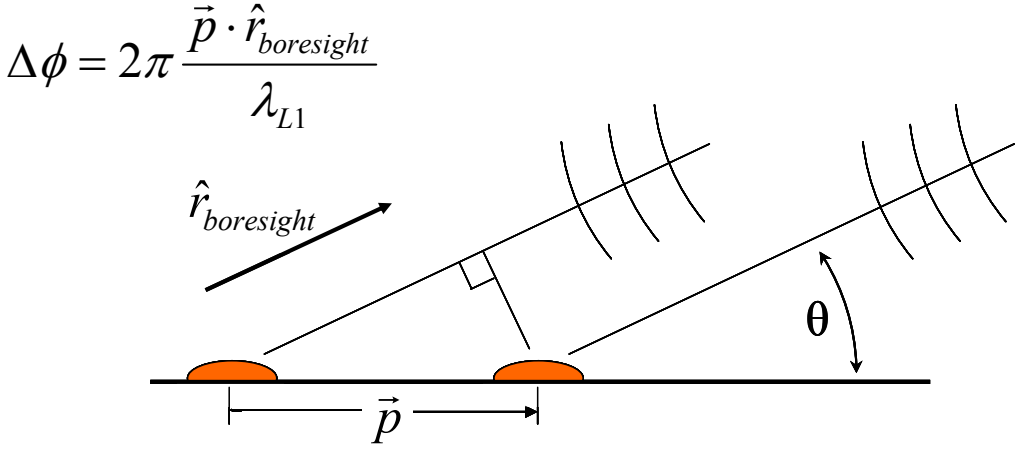

Figure 2.3. Antenna geometry showing calculation of Δφ.

(position, velocity, and time) elements in the GPS receiver block diagram. Note that non-isotropic antennas change the array response and can cause the optimal weight coefficients to differ from those given in Eq. (2.2).

This array yields maximum constructive interference in the desired look direction and for the signal center frequency, but the sidelobes and nulls are uncontrolled and may not adequately suppress interference or multipath. Figure 2.4 shows examples of the array gain pattern for a seven-element planar array with λ/2 inter-element separation and for a variety of boresight directions. For a boresight azimuth of 45°, the figures show gain patterns for elevation angles of 20°, 45°, and 80°. In the three-dimensional depiction of the first row, the shape corresponds to the array gain and the color scale is in dB. The

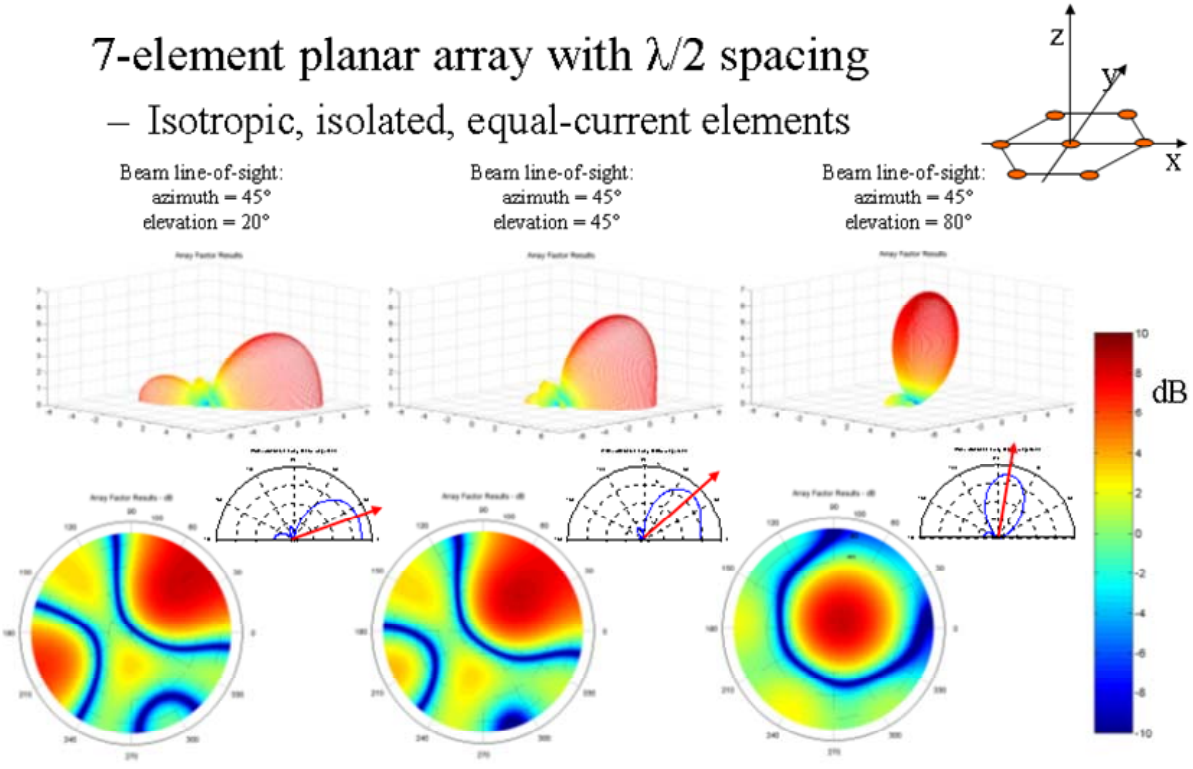

Figure 2.4. Array factor magnitude – 7-element controlled-reception pattern antenna with λ/2 inter-element spacing.

second row of figures shows a two-dimensional slice, or section, through the three-dimensional gain plot, in this case through the boresight azimuth of 45°. Finally, the last row of figures shows the dB-gain color scale of the upper hemisphere (+z-axis) projected onto a two-dimensional polar plot. In this way, the entire information of the three-dimensional plot in the first row is preserved in a two-dimensional representation, clearly showing the characteristics of the array main beam, sidelobes, and nulls.

Figure 2.4 shows the gain pattern calculated deterministically for a desired array boresight. If directions of arrival for interfering signals or multipath are available, then additional constraints can be incorporated into the array weight vector. Note, however, that this first requires localization and estimation of the undesired signal vectors.

2.2.2 Space-Time Adaptive Processing

In contrast to the deterministic array, an adaptive antenna array uses feedback to optimize some performance index (see Figure 2.5 and Compton, 1988 [6]). "Adaptive" in this

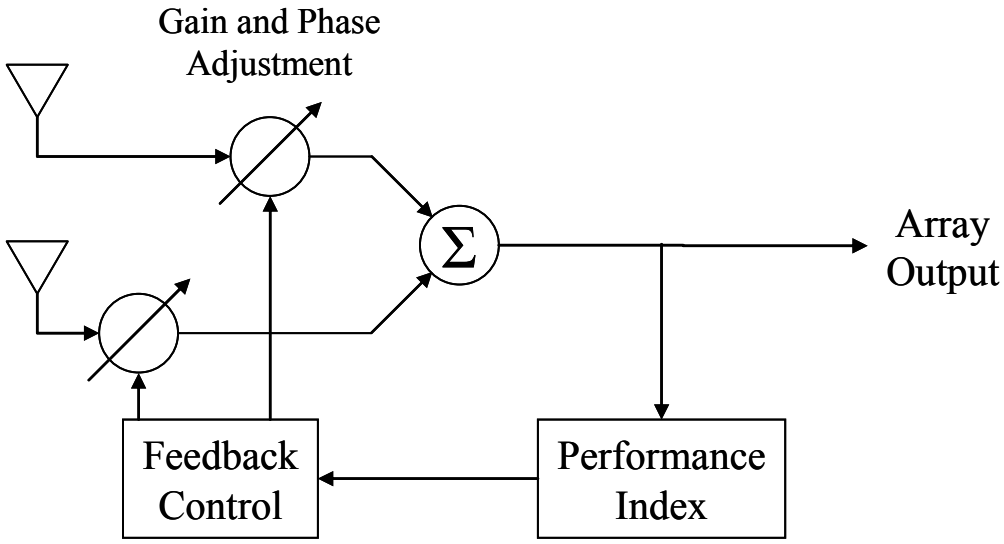

Figure 2.5. Generic adaptive antenna array
(after Compton, 1988 [6]).

context means that the array gain pattern adapts to the signal and noise environment, subject to user-specified constraints. The constraint or optimization criteria can be broadly classified either as maximizing the signal to interference plus noise ratio (SINR) at the array output, e.g., [80, 81], or as minimizing the mean-square error (MSE) between the actual array output and the ideal array output, e.g., [82]. In both of these cases, the array adapts to maximize the desired signal and to reject interference.

For the purposes of this investigation, two adaptation schemes are studied. The Applebaum beamformer [81], or minimum variance distortionless response (MVDR) array, is in the SINR class of methods. This algorithm constrains to unity the array gain in a particular look direction (it also may have side constraints for nullsteering), while rejecting coherent interference down to the noise floor. The MVDR beamsteering constraint is equal to the weight vector calculated for the deterministic CRPA in Eq. (2.2). The Widrow beamformer [82] is in the MSE class of methods. This algorithm seeks a weight vector that causes the array output to match a desired reference signal, while again rejecting coherent interference present at the array input. For GPS, the reference signal is the PRN code sequence and the navigation data bits (for adaptation that occurs prior to code wipeoff and accumulation), or it is just the navigation data bits (for adaptation that occurs after code wipeoff and accumulation). This method is termed a least-mean-square (LMS) approach as it uses an LMS-based error cost function.

The Widrow/LMS and Applebaum/MVDR optimization criteria were chosen in this investigation for the following reasons: (a) they exemplify each class of adaptive weight control method described above, (b) these methods are ones against which other adaptive schemes typically are compared, (c) they are straightforward to implement and relatively efficient to execute, (d) they are well-represented in the radar, wireless, and GPS literature, and (e) they have well-understood convergence properties, and stability can be guaranteed with an appropriate choice of the adaptation parameters.

In both the MVDR and LMS cases, the optimal steady-state weight vectors satisfy the Wiener solution. This means that for stationary signals with known autocorrelation and

crosscorrelation statistics, the adaptive arrays minimize the mean-square error between the array output and a reference (the Wiener condition), whether that optimization is based on a beamsteering constraint (MVDR) or on a reference signal constraint (LMS). The steady-state weight vectors may be computed according to:

$$\begin{aligned} \mathbf{W}_{MVDR} &= \mu\boldsymbol{\Phi}^{-1}\mathbf{T}^{*} \quad Applebaum/MVDR \\ \mathbf{W}_{LMS} &= \boldsymbol{\Phi}^{-1}\mathbf{S} \quad Widrow/LMS \end{aligned} \tag{2.3}$$

This notation, and that used henceforth, comes from Compton, 1988 [6]. Here **T*** is the array steering vector, μ is a signal power scaling factor, **S** is the reference correlation vector, and **Φ** is the signal covariance matrix. All are explained below.

The signal covariance matrix, **Φ**, is defined as the expected value of $\mathbf{X}^{*}\mathbf{X}^{\mathrm{T}}$, where the measurement vector, **X**, is composed of the signals input to the adaptive array computation. For pre-correlation adaptation, **X** is the sample vector after carrier wipeoff (one complex sample per antenna element per time-tap). For post-correlation adaptation, **X** is the inphase and quadrature prompt correlator output vector (one complex correlator output value per antenna element per time-tap). In the interference-free case, the signal covariance matrix, **Φ**, is diagonal and the adaptive weight vector, **W**, is equal to the constraint vector scaled according to the gain of each antenna.

Referring to Figure 2.2, the MVDR steering vector, **T***, is calculated given knowledge of array orientation and satellite ephemeris, and so is equivalent to the deterministic CRPA weight vector, **w**, from Eq. (2.2), $\mathbf{T}^{*} = \mathbf{w}$. The LMS reference vector, **S**, is the product of the sample vector, **X**, and the reference signal, $r(t)$ (i.e., the PRN code sequence and/or the navigation data bit), $\mathbf{S} = \mathbf{X}^{*} \cdot r(t)$.

Note that solution of the equations in the form of Eq. (2.3) requires estimation and then inversion of the covariance matrix, **Φ**. This is the sample matrix inverse (SMI) approach. Estimation of **Φ** can require significant signal buffering capacity (placing large memory demands on the receiver) and time-averaging (introducing latency and reducing the

ability of the array to adapt quickly to changing interference environments), while matrix inversion requires computational complexity. However, this is an approach that has been employed successfully in adaptive beamforming and nullsteering GPS architectures, e.g., [31, 59, 61].

In recursive form, these adaptive algorithms look like:

$$\begin{aligned} \mathbf{W}_{n+1} &= \left[\mathbf{I} - \gamma\mathbf{\Phi}_n\right]\mathbf{W}_n + \gamma\mu\mathbf{T}^* \quad && \textit{Applebaum / MVDR} \\ \mathbf{W}_{n+1} &= \left[\mathbf{I} - \gamma\mathbf{\Phi}_n\right]\mathbf{W}_n + \gamma\mathbf{S}_n \quad && \textit{Widrow / LMS} \end{aligned} \tag{2.4}$$

With this formulation, estimation of $\mathbf{\Phi}$ is not tied to SMI buffer size, but may be done at each sample epoch, so $\mathbf{\Phi}_n = \mathbf{X}_n^* \mathbf{X}_n^T$. Thus, solving for the weight vector subject to the adaptive constraints requires no buffering or matrix inversion, and with suitable pre-conditioning adapts quickly and robustly to a changing signal environment. The execution of Eq. (2.4) is shown in Figure 2.6.

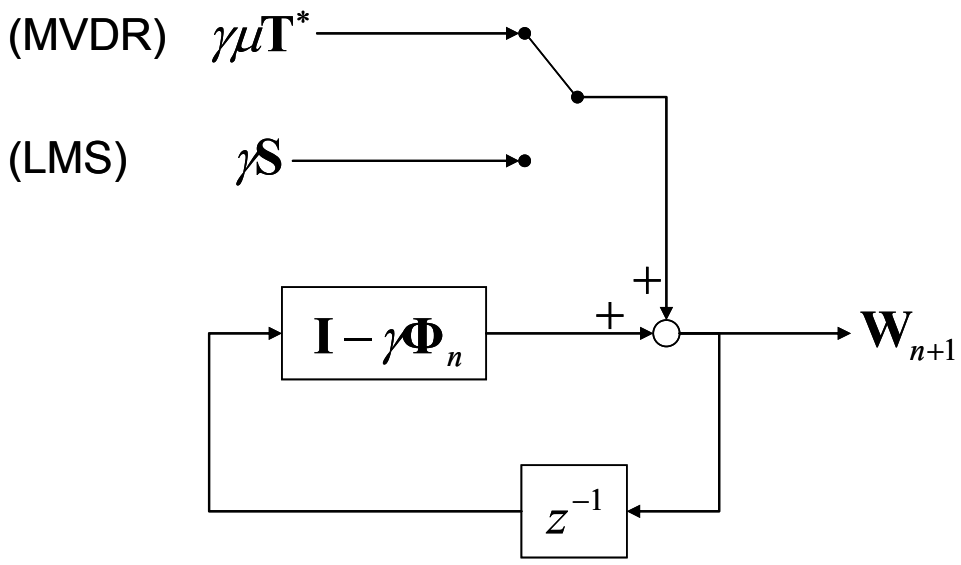

Figure 2.6. Recursive weight vector calculation
for the GPS adaptive array – see Eq. (2.4).

In addition to the composite signal output calculation from Eq. (2.1), there is the simple calculation of $\mathbf{\Phi}$ at each weight update epoch, and the calculation of $\mathbf{S}$ for LMS. Calculation of $\mathbf{T}^*$ can be done on a schedule commensurate either with platform dynamics or with satellite constellation motion (whichever is faster), or on the time scale of the changes in the interference environment if nullsteering constraints are implemented deterministically.

As update equations, the algorithms become:

$$\begin{aligned} \Delta\mathbf{W}_n &= \gamma\left[\mu\mathbf{T}^* - \mathbf{\Phi}_n\mathbf{W}_n\right] \quad Applebaum/MVDR \\ \Delta\mathbf{W}_n &= \gamma\left[\ \mathbf{S}_n - \mathbf{\Phi}_n\mathbf{W}_n\right] \quad Widrow/LMS \\ \mathbf{W}_{n+1} &= \mathbf{W}_n + \Delta\mathbf{W}_n \end{aligned} \tag{2.5}$$

This last form is actually the most instructive. Eq. (2.5) shows that the algorithms reach steady-state when the bracketed terms in the $\Delta\mathbf{W}_n$ equations go to zero, i.e., when the weight vector suppresses from the covariance matrix everything but the steering or reference vector. This is equivalent to cancellation of the terms within the dashed box of Figure 2.7. Of course, since only an estimate of the covariance matrix, $\mathbf{\Phi}$, is available, this yields an approximate solution. It is the misadjustment parameter γ (equivalent to 2μ in the treatment of Widrow and Stearns, 1985 [36]) that controls convergence speed and, as the name implies, steady-state misadjustment.

The computation of the desired array output signal (LMS) or of the array steering-vector constraint (MVDR), as well as the estimation of the space-time covariance matrix, are specific to each receiver tracking channel. Therefore, the STAP algorithms compute weight vector coefficients that are unique to each satellite and frequency being tracked, providing the maximum increase in each channel's signal to noise ratio (SNR). In contrast, power minimization methods that do not rely either on a steering-vector constraint or on a desired reference signal may suffer if the array nulls happen to coincide with the direction of a desired incoming signal (either due to jammer nulling constraints or from array synthesis).

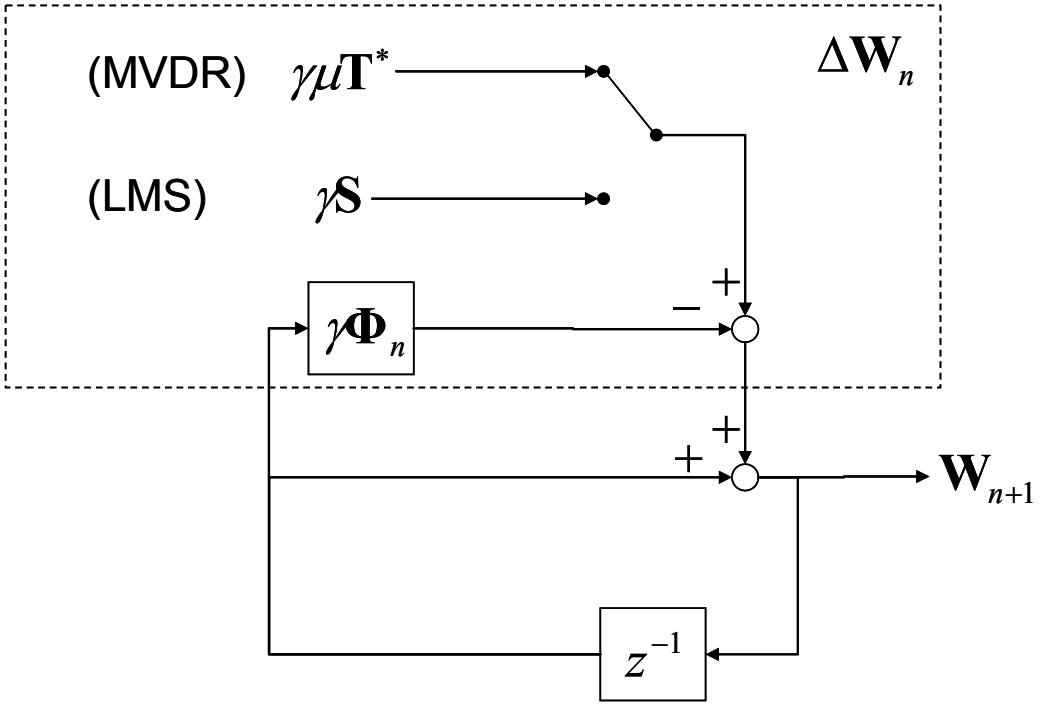

Figure 2.7. Iterative weight vector calculation for the GPS adaptive array – see Eq. (2.5).

This brings up an interesting characteristic of the steady-state gain pattern calculated by an adaptive algorithm: the depths of the pattern nulls and the levels of sidelobes are optimized to balance interference rejection with the suppression of noise. In other words, if interference power goes up, then nulls get deeper, while if white noise power goes up, then sidelobe get smaller. Unlike white noise, every signal incident on the array (whether desirable or undesirable) is correlated in space and in time across antenna elements, lending structure to the covariance matrix. The constraint vector preserves desirable signals in the array output. However, the structure in the covariance matrix due to interference is suppressed by the adaptive algorithms. If no interference is present, then the covariance matrix is diagonal (except for the contribution from desired signals) and the expected value of the steady-state weight vector is equal to the Wiener solution.

2.2.3 Array Processing in a GPS Receiver

In a GPS receiver, code wipeoff follows carrier wipeoff, and uses the estimated code-phase from the code numerically-controlled oscillator (NCO). This is followed by accumulation (with the integration period usually from one to tens of milliseconds):

$$S = \frac{1}{T}\sum_{t=1}^{T} s(t)\cdot x(t-\hat{\tau}) \tag{2.6}$$

Eq. (2.6) is executed for the prompt code replica, as well as for early and late versions of the code replica sequence. The accumulator outputs are used in the code-phase and carrier-phase discriminators, which drive the code and carrier tracking loops.

For a multi-antenna GPS receiver, weight vector multiplication can occur either pre-correlation or post-correlation. In pre-correlation beamforming, the antenna weights are applied to the antenna signals directly (after carrier wipeoff, as developed here), as shown in Eq. (2.1). In post-correlation beamforming, the antenna weights are applied after the complex correlation operation. Since both accumulation and beamforming are linear operations, they can be done in either order:

$$\begin{aligned} S &= \frac{1}{T}\sum_{t=1}^{T}\left(\sum_{j=1}^{N} s_j(t)\cdot w_j\right)\cdot x(t-\hat{\tau}) \qquad pre-correlation \\ &= \frac{1}{T}\sum_{j=1}^{N}\left(\sum_{t=1}^{T} s_j(t)\cdot x(t-\hat{\tau})\right)\cdot w_j \qquad post-correlation \end{aligned} \tag{2.7}$$

Eq. (2.7) expands $s(t)$ from Eq. (2.6), and shows that weight vector multiplication and code wipeoff and accumulation are order-independent.

Figure 2.8 shows this interchangeability. (This discussion does not cover beamforming that occurs outside of the main receiver processing flow, e.g., beamforming as a separate stand-alone anti-jam module or STAP appliqué.) Note that pre-correlation beamforming occurs at the sampling frequency (~MHz speeds) while post-correlation beamforming occurs at the integrate-and-dump frequency (~kHz). The reference signal shown in

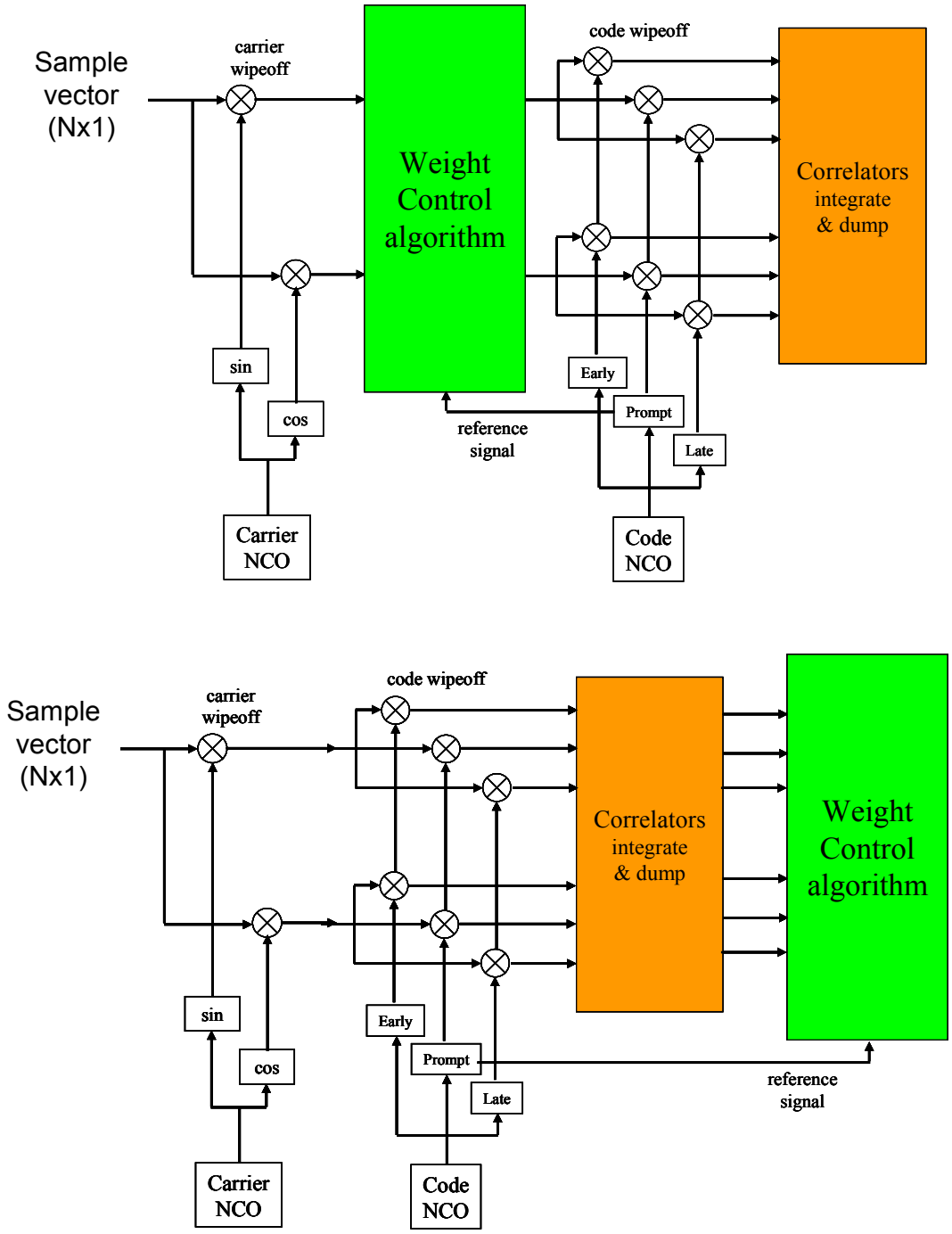

Figure 2.8. Pre- vs. post-correlation beamforming – accumulation and beamforming are linear and therefore order-independent.

Figure 2.8, and which is required for LMS-based adaptation, is the PRN code sequence and the navigation data bits for pre-correlation adaptation, or it is just the navigation data bits for post-correlation adaptation.

2.2.4 Illustrative Example

Figure 2.9 shows the convergence behavior of an adaptive algorithm tracking a desired signal in the presence of jamming. This example simulation shows tracking with a 12-element circular array having $\lambda/2$ inter-element separation. There are five continuous-wave jammers each with a jammer to signal (J/S) power ratio of unity. The array uses an omnidirectional initial gain pattern (in other words "blind" initialization), an LMS-based error cost function, and spatial processing to counter jamming (no temporal processing is needed). Misadjustment has been set to 2%, meaning that convergence speed is relatively slow but that steady-state weight vector errors are small.

In Figure 2.9, notice how the adaptive algorithm reacts quickly to steer spatial nulls in the directions of the jammers and then responds more slowly to drive null depths deeper while reducing sidelobe levels. In this relatively simple scenario, jammer suppression for the five interference sources is [10.6, 11.1, 10.9, 14.5, 11.0] dB, while the desired signal experiences virtually no attenuation. Contrast the nearly uniform suppression from the adaptive array with the more variable suppression from the deterministic CRPA, where the jammers are down [5.4, 13.3, 15.8, 6.4, 9.6] dB. The deterministic CRPA gain pattern, shown in the upper-right subplot, does not control the array sidelobes. It should be noted that while the gain patterns shown in Figure 2.9 are interesting visually, a better measure of adaptive algorithm performance remains output SINR.

Figure 2.10 shows that for a conventional beamsteering antenna array without feedback or adaptation (the deterministic CRPA), the required inputs to the weight control algorithm are signal arrival direction, array orientation, and baseline geometry or array manifold. The Applebaum/MVDR array requires an additional measure or estimate of signal covariance, allowing it to control sidelobes, steer nulls, and reject interference.

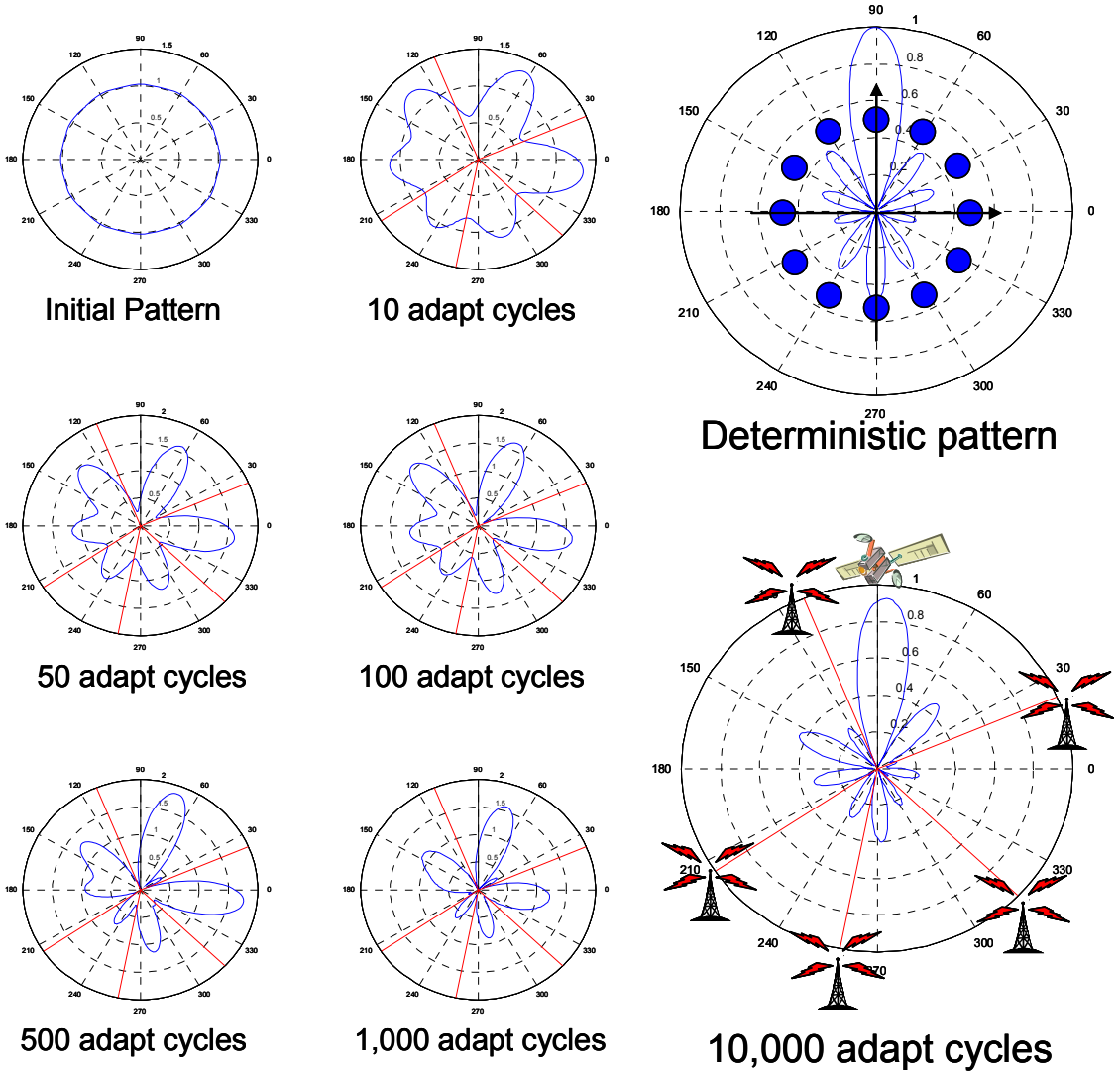

Figure 2.9. Adaptive antenna array showing blind initialization, LMS-based adaptation, and converged array gain pattern. This scenario consists of a 12-element planar array, the desired signal arriving from the 12-o'clock position, and five narrow-band jammers located as shown in the lower-right plot. This contrasts the adaptive array gain pattern with that of a deterministic array which allows jamming energy in on the array sidelobes.

The Widrow/LMS array requires signal covariance as well as a desired reference signal (the PRN code sequence and navigation data bits for pre-correlation adaptation, or just the navigation data bits for post-correlation adaptation).

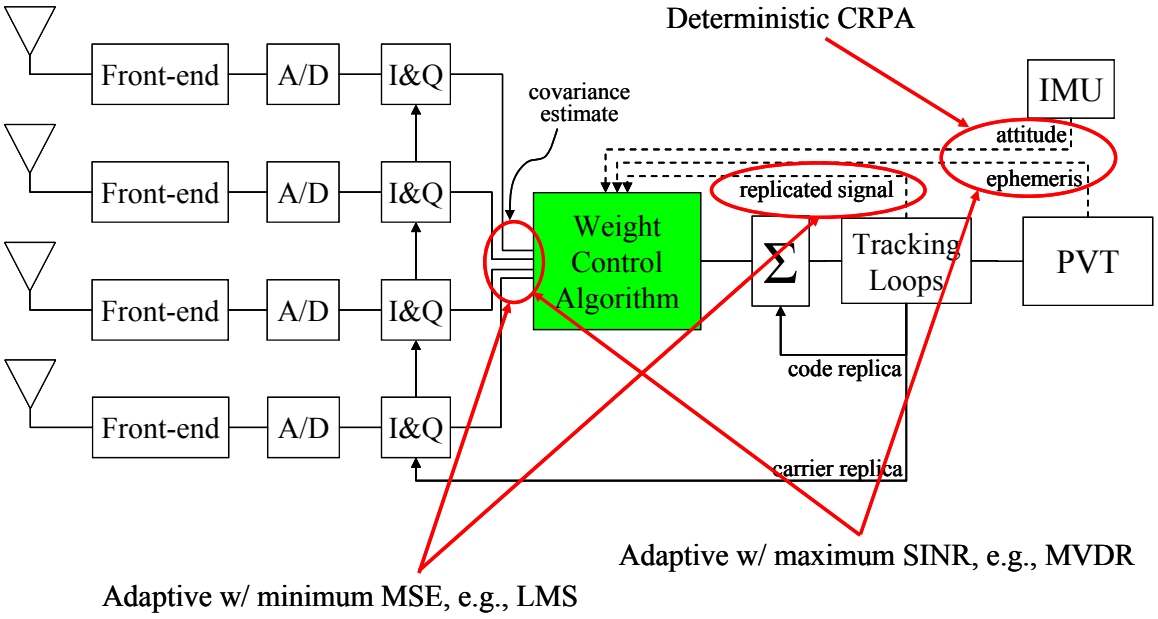

Figure 2.10. Array processing and inputs
to the weight control algorithm.

The LMS algorithm controls array response to align the output signal with a locally-generated reference signal. For the case of pre-correlation adaptive array processing for GPS, this ideal array output signal is derived from the code tracking loop (the carrier already having been removed from the signal in the architecture under discussion). However, note that there is a reference signal ambiguity if navigation data are encoded onto the incoming signal. This ambiguity can be addressed through buffering the navigation message, by suitable logic in the weight control algorithm (i.e., by monitoring the polarity of the weight at the reference antenna tap), or by running two weight computations in parallel, one each for +1 and –1 data bit encoding.

From the previous discussion, it becomes apparent that the Applebaum/MVDR array is well-suited to situations of known signal arrival direction and known antenna response, but unknown signal waveform. In fact, MVDR array performance is negatively impacted

by channel errors, line biases, or unmodeled antenna effects. If **T*** includes nullsteering constraints, then the MVDR array also is sensitive to interference localization errors. In contrast, the Widrow/LMS array is appropriate for unknown signal arrival direction but known (or correlated) reference waveform. While the LMS array is resistant to the error sources just listed for the MVDR array, it may be susceptible to multipath-induced errors, since the LMS cost function may steer array sidelobes to capture multipath energy. The MVDR array will not suffer this effect.

In an adaptive antenna array, the spatial degrees of freedom (the number of antennas less any spatial weight coefficient constraints) correspond to the geometry of the array gain pattern and to the number and depth (selectivity) of beams and nulls. The temporal degrees of freedom (the number of time-taps less any temporal weight coefficient constraints) determine the spectral response of the array and allow nulling of wideband interference.

Processing in the spatial and temporal domains (STAP) can be compared to processing in the spatial and frequency domains (space-frequency adaptive processing or SFAP). Narrowband (i.e., suboptimal) SFAP outperforms STAP when the number of frequency bins is greater than the number of time-taps [57]. However, when the temporal and frequency degrees of freedom are equal, then STAP and SFAP are equivalent [83, 84].

This concludes the general overview of STAP algorithms for GPS receivers. The discussion that follows will describe in more detail the GPS STAP algorithms and methods developed in the course of this investigation.

2.3 RECEIVER IMPLEMENTATION

The STAP algorithms contained in the GPS software receiver developed as part of this work include features that are novel with regard to the existing literature on GPS adaptive array processing. In addition, the STAP algorithms implement distinct features that are combined together for the first time in a single GPS receiver. The subsections in this section present these distinct and novel features.

2.3.1 Integrated Adaptive Array Processing

In many cases described in the literature, STAP algorithms are implemented as stand-alone anti-jam modules or as "appliqués" that exist outside of the main structure of the GPS receiver, e.g., [8, 26, 85]. For these cases, the STAP algorithms exist either completely upstream of GPS receiver signal processing or completely downstream of the correlation operation.

The GPS software receiver developed and described here completely integrates the STAP algorithms, as shown earlier in the block diagram of Figure 2.1. This integration provides several benefits over stand-alone anti-jam modules or appliqués: (a) simplified weight coefficient calculation, (b) easy scalability in numbers of antennas, frequencies, and tracking channels, (c) seamless support of both pre-correlation and post-correlation adaptation (see Eq. (2.7)), and (d) simplified generation and handling of the adaptation constraints, whether these are the steering-vector constraints of MVDR or the reference signal constraints of LMS. The ease of integrating the STAP algorithms into this receiver is a consequence of starting from a clean-sheet design and coding in a high-level programming language (MATLAB).

The receiver architectures for pre-correlation and post-correlation beamforming and nullsteering are shown in Figure 2.11 and Figure 2.12, respectively. The analog signal processing section of this architecture applies both to test-bed hardware and to signals created entirely in a software simulation environment. In either case, signals are received by an array of antennas and are conditioned by the RF (radio frequency) front-ends: amplification, filtering, mixing and downconversion, and finally analog to digital (A/D) sampling. The RF processing for all antennas shares timing from a common clock. At this point, digital samples are stored to disk for later retrieval, as the software receiver developed for this investigation runs exclusively in a post-processing mode.

Digital processing comes next. For pre-correlation beamforming, as shown in Figure 2.11, inphase and quadrature carrier wipeoff is followed by the weight control algorithm.

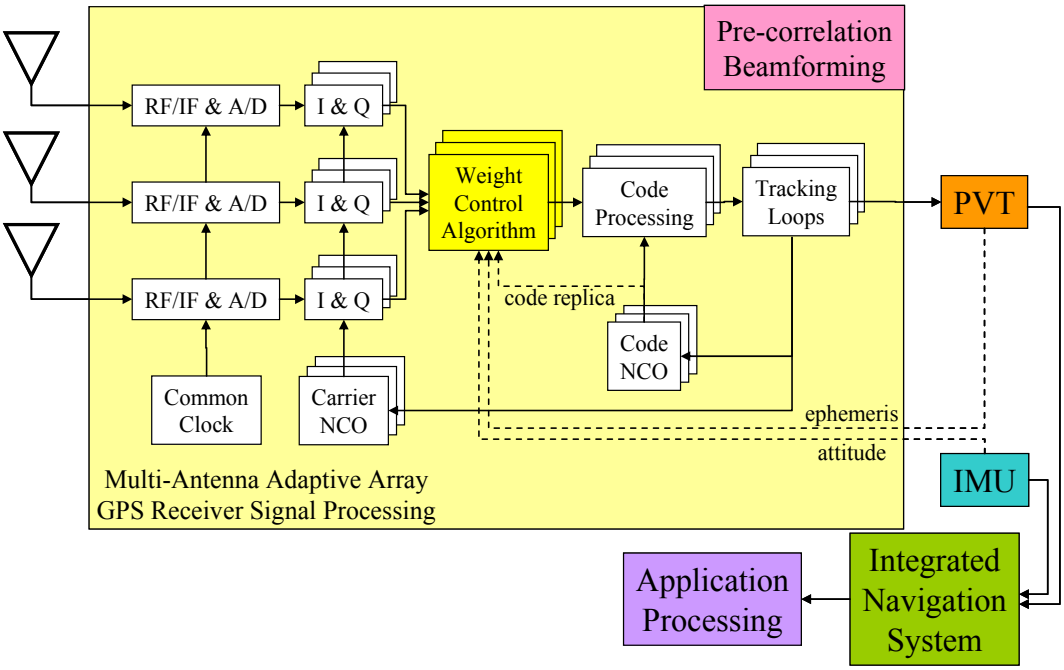

Figure 2.11. GPS STAP receiver architecture utilizing pre-correlation beamforming (LMS and MVDR and Deterministic).

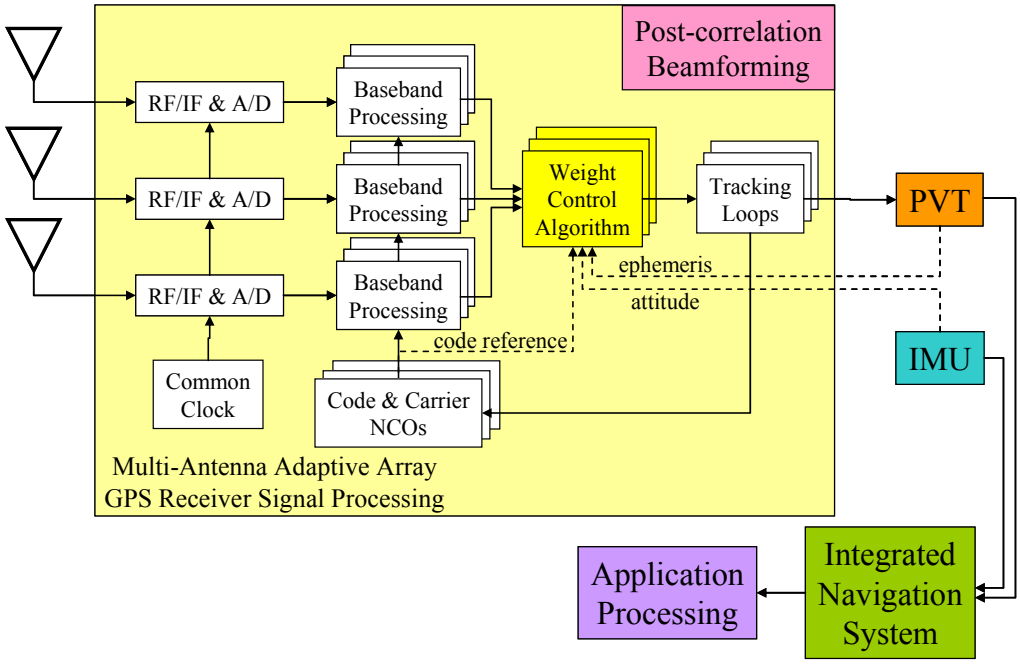

Figure 2.12. GPS STAP receiver architecture utilizing post-correlation beamforming (LMS and MVDR and Deterministic).

At this point, the signals are summed at each sample instant and a single complex sample stream goes to code wipeoff and accumulation. The signals then enter tracking loops just as they would for a traditional GPS receiver. For post-correlation beamforming, as shown in Figure 2.12, all code and carrier processing occurs prior to the weight control algorithm. In post-correlation adaptation, the quantities upon which the weight control algorithm operates are the inphase and quadrature prompt correlator outputs. For both pre-correlation and post-correlation weight adaptation, all processing steps after A/D conversion are satellite-specific.

Code-phase and carrier-phase estimates come out of the tracking loops and enter the GPS position, velocity, and time (PVT) processing block. In the architecture shown here, the PVT outputs are combined with outputs from an inertial measurement unit (IMU) by an integrated navigation filter. The navigation filter feeds subsequent downstream applications. Closer integration between GPS signal tracking and the IMU could be enabled (e.g., tightly-coupled or ultra-tightly-coupled GPS/INS integration), but this topic is not explored further here.

The architectures described here scale with commercial off-the-shelf (COTS) technologies in the RF front-end and in the correlation engine. Post-correlation adaptation operates on the outputs of the code accumulators, so that the entire baseband signal processing chain from RF amplification, filtering, and downconversion, through A/D sampling, to carrier and code wipeoff and accumulation remains the same as for a traditional single-antenna GPS receiver. The only difference in this case is that baseband processing is now replicated for each antenna and signal frequency that is processed.

Similarly, pre-correlation adaptation can leverage single-antenna GPS building blocks, but now the adaptive beamforming module is inserted into the baseband processing chain. As can be seen, these receiver architectures support growth in the number of GPS signals, transmission frequencies, and satellites. This makes these architectures well-suited to processing all available global navigation satellite system signals, e.g., from modernized GPS, GLONASS, Galileo, Beidou/Compass, etc.

2.3.2 Convergence Speed

The convergence speed of an adaptive algorithm is a tradeoff between fast convergence to react quickly to a changing signal/noise environment, and slow convergence to reduce noise in the array output due to weight vector misadjustment. Due to the high rate of weight coefficient iteration, especially for pre-correlation adaptation, convergence within tens or hundreds of microseconds is achievable. However, fast convergence speeds are beneficial only for interference environments that change on these time scales.

For a GPS receiver, selection of convergence speed also must consider the bandwidth of the receiver's phase-locked loop (PLL). If the interference environment is slowly-changing, then there is no discernable benefit to ultra-fast convergence in regards to the primary metric of GPS receiver tracking robustness, i.e., the resistance to a cycle slip in the carrier-tracking loop.

The carrier-tracking loop represents the weakest link in the GPS receiver, and the PLL can only tolerate a limited number of corrupted carrier-phase discriminator output values before suffering a cycle slip. The maximum output from an arctangent discriminator is 90 degrees, meaning that no matter how high the J/S ratio or how little interference is rejected by the adaptive algorithm, no error larger than 90 degrees can be output by the carrier-phase discriminator. The following discussion considers several successive carrier-phase discriminator output samples all of either +90 degrees or –90 degrees, rather than a step error in the PLL of either +90 degrees or –90 degrees. This represents the absolute worst-case outcome from jamming, so this analysis is conservative.

For a 7 Hz PLL noise bandwidth (a typical value for a low-dynamics unaided GPS receiver), a second-order PLL tolerates a maximum of two navigation data bits worth of corrupted discriminator output values before a cycle slip occurs. If three navigation data bits worth of PLL discriminator output values all are corrupted to maximum extent (i.e., all either +90 degrees or –90 degrees), then a cycle slip occurs. See Figure 2.13, where a cycle slip is visible as an inversion of the decoded navigation data bit. (The above

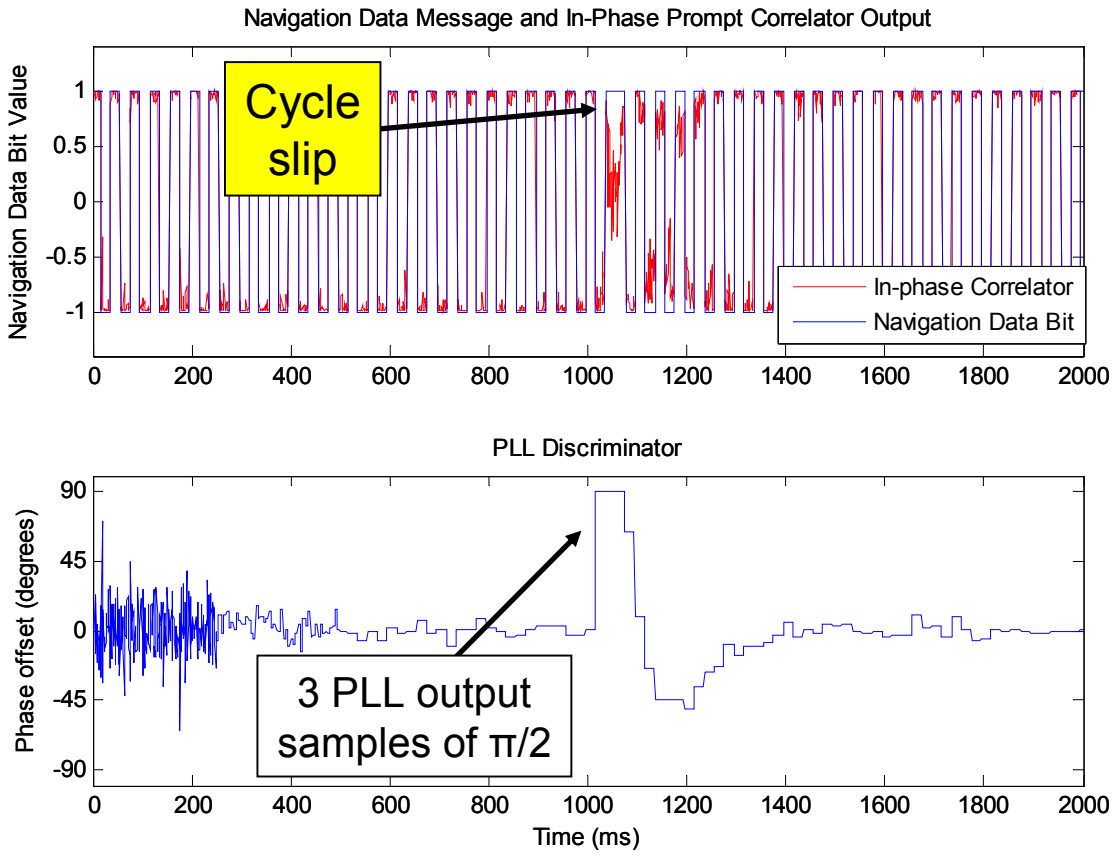

Figure 2.13. Three navigation data epochs of corrupted PLL samples causing a carrier-phase cycle slip.

method decouples convergence speed from interference power. The analysis of cycle slip probability also could be done using an estimate of the tracked C/N_0 [86]. The present method is appropriate for the investigation of interference rejection versus navigation biases contained in Chapter 3.)

The preceding considerations show that for a PLL noise bandwidth of 7 Hz, the adaptive weight vector needs to reach steady-state within approximately 60 milliseconds in order to reject interference. In other words, it is desirable to correct the majority of the initial weight vector error in that amount of time. Of course, this requires that the convergence speed be compatible both with the variation speed of the interference environment as well

as with the time scale of platform dynamics. If the carrier-tracking loop has a lower bandwidth than that assumed here (which is desirable and is possible with inertial aiding of the PLL), then even slower convergence of the adaptive weight vector is enabled (for example, this might apply to stationary receivers in urban environments).

The adaptive weight coefficients can be plotted versus time to give an indication of their convergence behavior. Figure 2.14 shows weight coefficient evolution as a function of time for pre-correlation adaptation using an LMS-based optimization criterion. The different curves in this figure are for different choices of adaptation speed, which is selected via the misadjustment parameter of Eq. (2.5). The weight coefficient behavior of

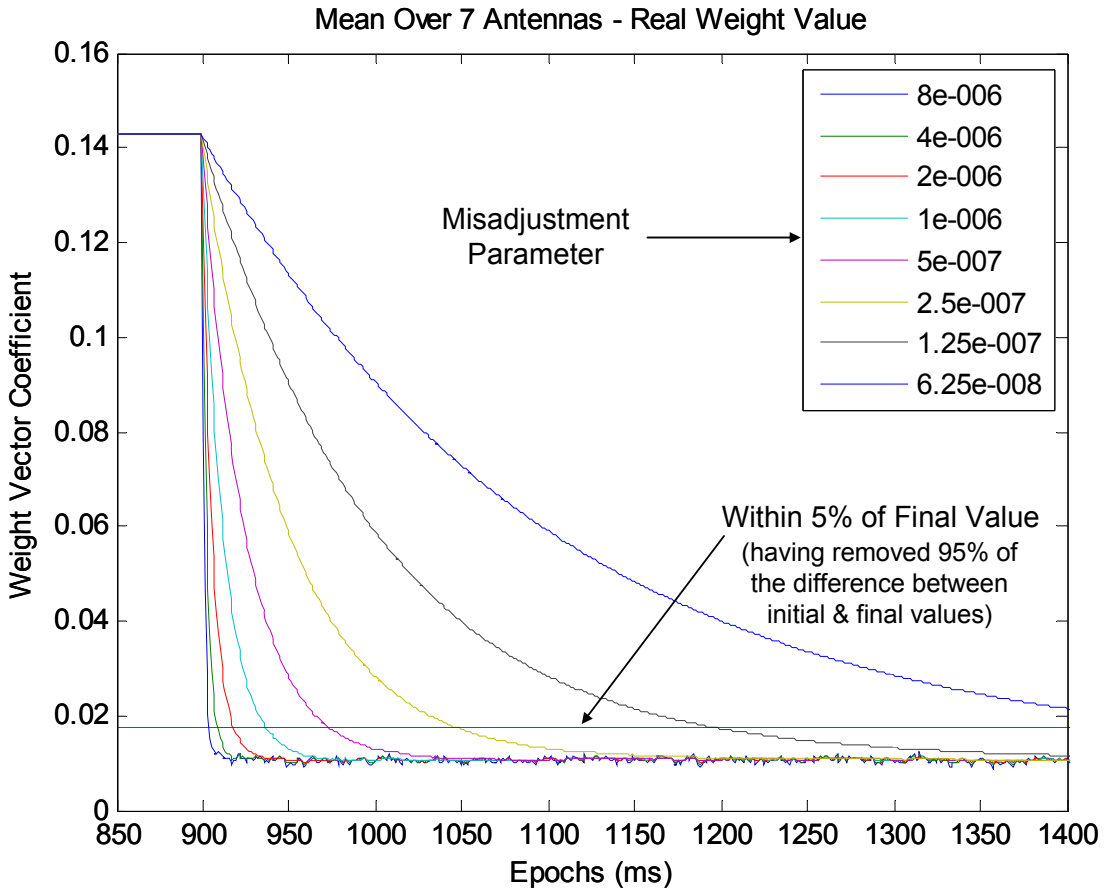

Figure 2.14. Weight coefficient evolution versus time, pre-correlation LMS-based adaptive beamforming.

Figure 2.14 is dependent on sampling frequency and C/N_0, so the easiest way to choose the convergence speed parameter is through a characterization study as described next.

Figure 2.15 plots convergence speed versus misadjustment parameter both for LMS and for MVDR processing, and both for pre-correlation and for post-correlation adaptation.

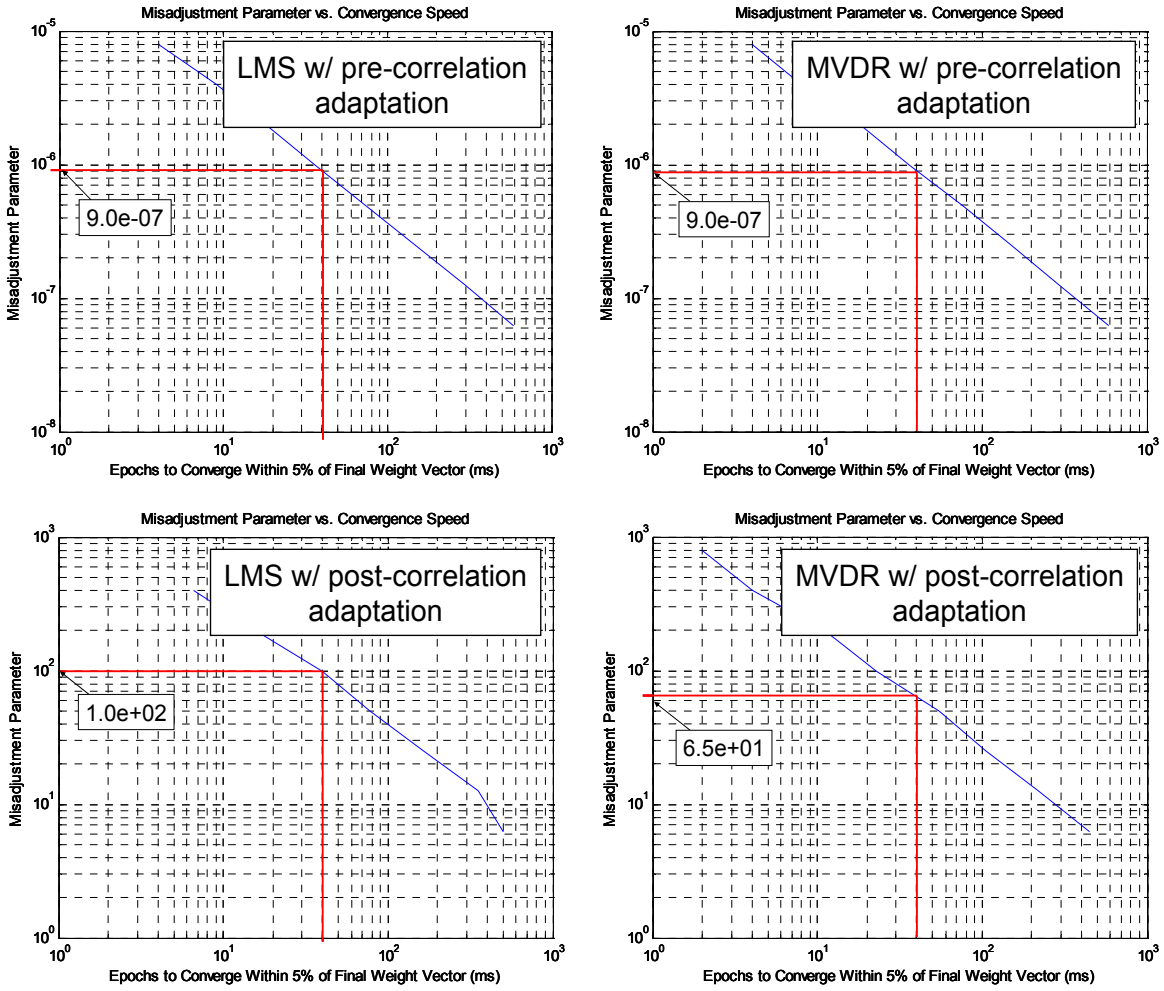

Figure 2.15. Misadjustment versus convergence speed, LMS and MVDR STAP with pre- and post-correlation adaptation. These scenarios show simulated P-code data for a seven-element antenna array with f_S = 80 MHz and C/N_0 = 40 dB-Hz. The convergence speed versus misadjustment parameter relationship changes with number of antennas and time-taps, f_S, and C/N_0.

These scenarios show data for a seven-element antenna array tracking simulated P-code signals, with f_S = 80 MHz and C/N_0 = 40 dB-Hz. (Note that the convergence speed versus misadjustment parameter relationship changes with the numbers of antennas and time-taps, f_S, and C/N_0.) The identification of the tradeoff between weight vector convergence speed, steady-state misadjustment, and PLL noise bandwidth is a new focus for a GPS STAP receiver, and the characterization method used to select convergence speed is new as well.

2.3.3 Phase De-Rotation Constraint

A GPS receiver that incorporates adaptive antenna array processing has two separate feedback mechanisms that alter the phase difference between the incoming satellite signal and the carrier NCO: the carrier tracking loop (the PLL) and the complex coefficients of the antenna weight vector. The PLL tracks carrier-phase changes (e.g., due to satellite-to-receiver motion or receiver clock drift) and adjusts the carrier NCO to maintain phase-lock between the receiver NCO and the input signal. The adaptive algorithm steers the phases of each antenna channel so that the signal-of-interest is constructively reinforced (whether the optimization criteria is reference-signal-based or steering-vector-based).

Since the antenna weights adapt on a time scale much faster than that of the PLL, carrier-phase errors will selectively be reduced by phase adjustment in the adaptive antenna weights. The consequence is that the PLL will not detect changes in carrier-phase as it should, there will be no adjustment in the carrier NCO, and there will be an accumulation of carrier-phase error. This drift or accumulation of carrier-phase error is shown in Figure 2.16. (In this figure, the initial carrier-phase excursion is due to tracking loop overshoot, settling, and convergence.) The error is due to the apparent motion of the central element, which is solely caused by the non-zero-phase weights applied thereon.

One remedy to the problem of carrier-phase drift is to impose a symmetric weight vector constraint [53, 59], although this reduces STAP degrees of freedom by half. A better remedy, and the one introduced here, is a “de-rotation” constraint as part of the adaptive

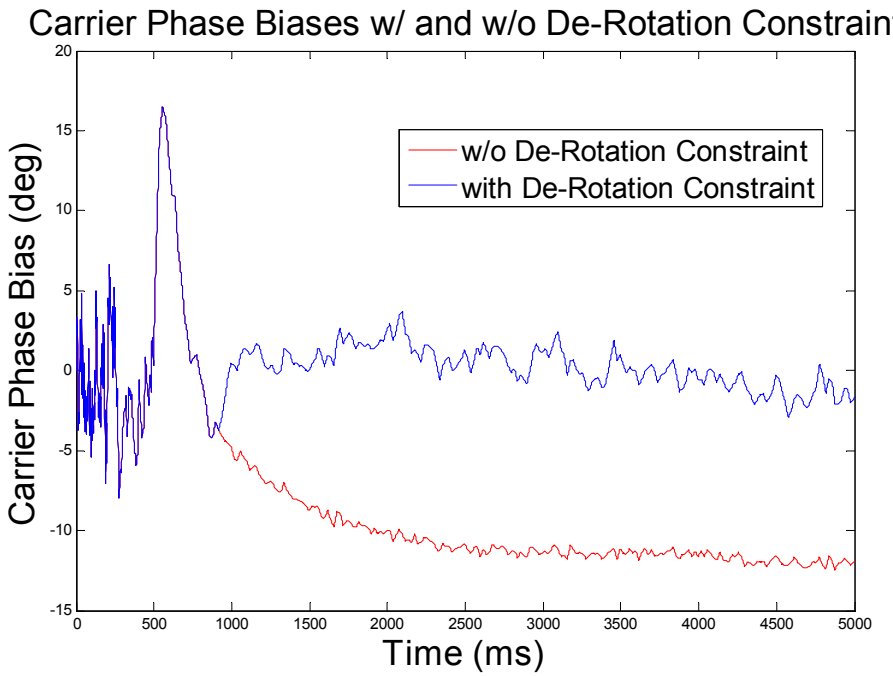

Figure 2.16. Carrier-phase drift caused by lack of phase de-rotation constraint in STAP weight update algorithm.

weight computation. With this constraint method, the updated weight vector, $\mathbf{W}_{n+1}$, is calculated as usual (see Eq. (2.5)), but then the weight vector is rotated back such that the weight applied to the central time-tap on the master antenna element is constrained always to zero degrees of phase:

$$\mathbf{W}_{n+1} = \mathbf{W}_{n+1} \cdot \frac{w_j^*}{|w_j|} \tag{2.8}$$

In Eq. (2.8), w_j is the weight vector coefficient for the central time-tap of the reference (master) antenna element. This equation "de-rotates" the updated weight vector, $\mathbf{W}_{n+1}$.

2.3.4 Navigation Data Bit Ambiguity

During adaptation of the antenna weights using the LMS-based optimization criterion, the reference signal must account for the polarity of the navigation data bits. For post-

correlation beamforming, the navigation data bit matches the sign of the inphase channel of the array output signal (with a possible sign ambiguity resolved by matching a navigation message preamble). For pre-correlation beamforming, the sign of the inphase channel of the array output matches the navigation data bit modulated by the PRN code sequence (again, with a possible sign ambiguity).

In either pre-correlation or post-correlation LMS adaptation, it is not possible to know *a priori* which polarity of navigation data bit to use as a reference, either +1 or –1 (unless the navigation message is buffered, is communicated on a different channel, or is otherwise forecast). The STAP implementation developed for this investigation runs separate weight vector calculations both for +1 and for –1 navigation data bit polarity. The algorithm then performs a variance test on the weight coefficient of the reference antenna element at the completion of each 20 millisecond navigation data bit. The weight vector that corresponds to the lower value of this test statistic is used to calculate the array output signal (i.e., less weight vector variation means that the array output signal more closely matches the LMS reference signal). This weight vector also is used to initialize the weight coefficients for the subsequent 20 milliseconds of adaptation.

2.4 TRACKING REAL SIGNALS WITH ADAPTIVE SOFTWARE RECEIVER

The end of this section provides tracking results of real GPS signals recorded with multi-antenna test-bed hardware. The data processing and receiver implementation are illustrated in Figures 2.17 and 2.18. Figure 2.17 shows tracking results for live L1 C/A-code data collected in Sweden with a multi-antenna custom hardware system [87, 88]. These tracking results represent a portion of a ten minute dataset collected on November 7th, 2006. Figure 2.18 shows tracking results for L1 C/A-code signals created with an RF hardware simulator and collected with a NordNav four-receiver system [89, 90, 91]. These tracking results represent one of a set of data records with varying levels of narrowband and wideband interference. The data in Figures 2.17 and 2.18 have receiver parameters as follows: f_S = 16.3676 MHz, f_{IF} = 4.1304 MHz, 2-bit A/D converters, and real-valued samples only.

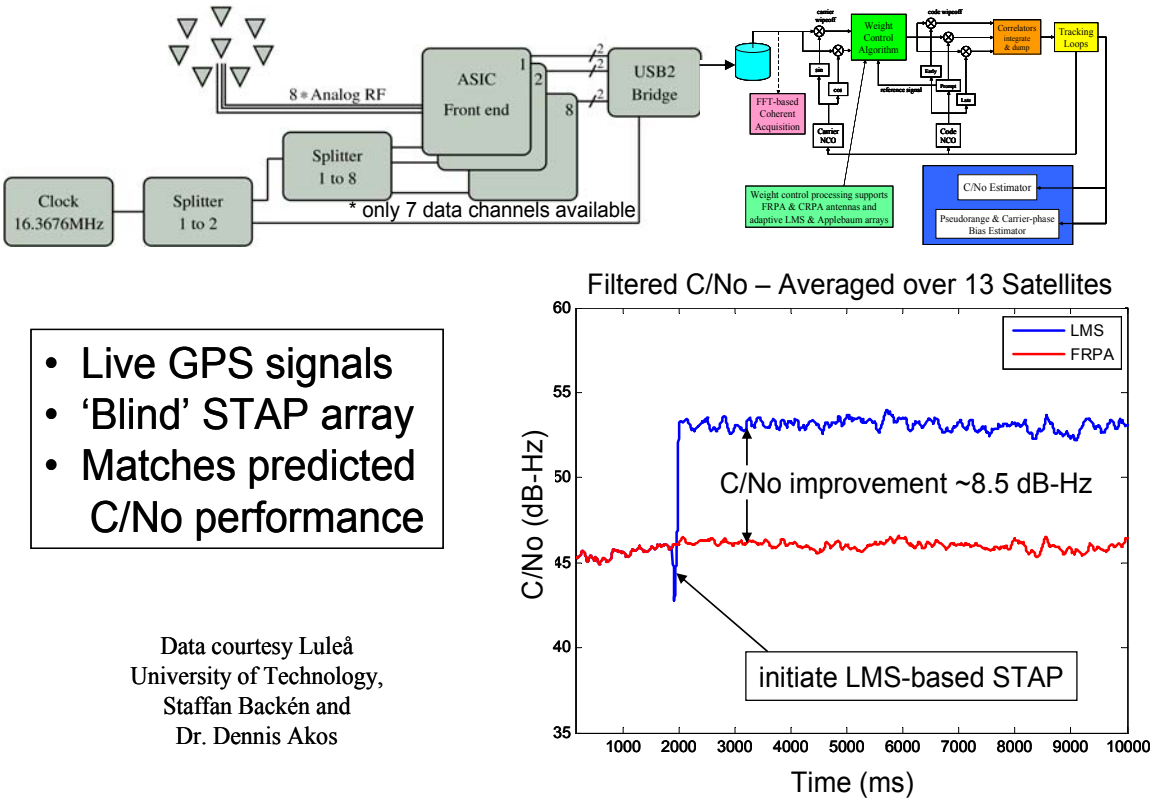

Figure 2.17. Processing real data from a seven-channel receiver.

The data were processed as follows. First, the satellite signals were acquired in single-antenna FRPA mode. Then, the satellites were tracked briefly in single-antenna mode in order to refine estimates of code-phase and Doppler frequency and to capture carrier-phase in order to align to the navigation data bit boundary (allowing 20 millisecond coherent integration). Finally, after 2000-4000 milliseconds of processing in single-antenna mode, the multi-antenna CRPA was enabled (either deterministic beamforming or LMS or MVDR adaptive beamforming and nullsteering).

The reasons for acquiring and pulling-in the signal in single-antenna mode were twofold. First, it is simpler to implement and faster computationally to perform single-antenna acquisition. Note, however, that acquisition performance for a deterministic CRPA was the focus of an earlier portion of this investigation [60]. Second, tracking performance is

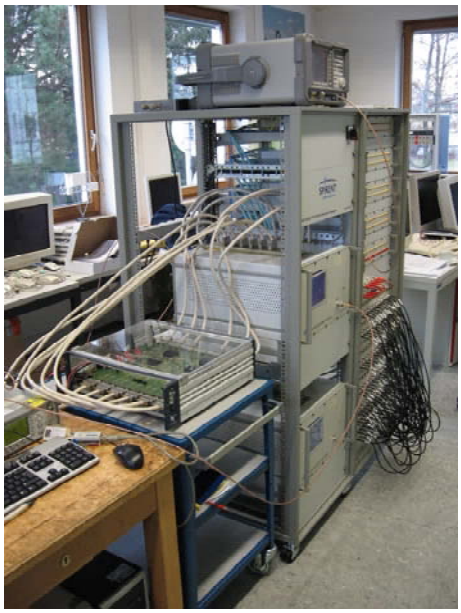

Data courtesy DLR Institute of
Communications and Navigation,
Felix Antreich and
Dr.-Ing. Achim Hornbostel

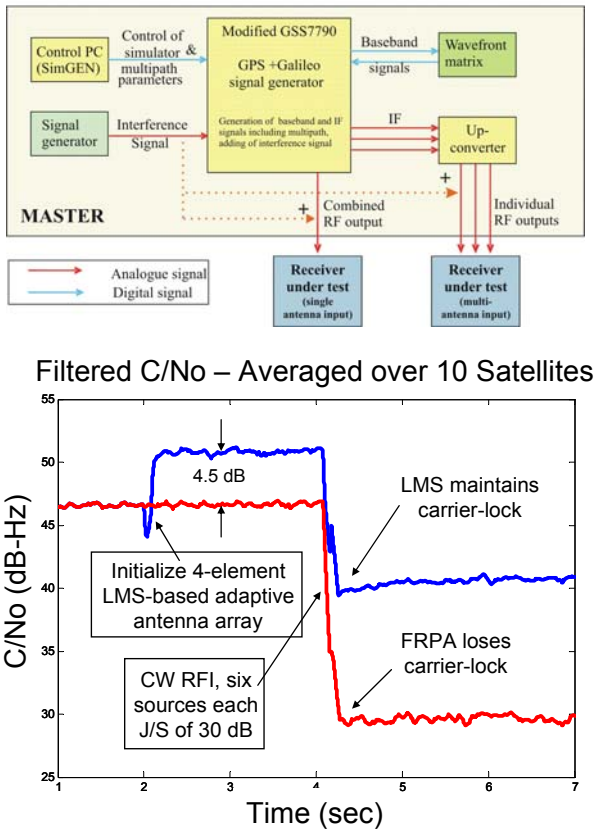

Figure 2.18. Processing data from Spirent simulator, DLR wavefront generator, and four-channel NordNav receiver.

more important to characterize than acquisition performance. The reason for this is that the operational scenarios considered for this investigation have the GPS receiver tracking satellite signals and then encountering elevated levels of jamming. At that point, every effort will be spent by the receiver and STAP algorithm to maintain carrier-lock. Since acquisition requires higher C/N_0 levels than tracking, if once carrier-lock is lost, then there is no expectation of reacquiring the signal until jamming levels subside.

LMS adaptive processing can use an initial weight vector calculated deterministically, or the weights can be initialized "blind." Blind initialization consists of setting each coefficient in the array weight vector identically to zero with the exception of the center

time-tap of the master antenna element, which receives a "1" entry. For the interference-free cases, this tracking allows estimation of the Wiener weight vector coefficients (as developed previously in Section 2.2.2). This is important because, in the absence of jamming, the LMS weight coefficients converge to the optimal Wiener values in steady-state regardless of their initial values.

Deterministic initialization of the antenna weights, whether for the beamforming CRPA or for the LMS or MVDR adaptive arrays, can be done in either of two ways: (a) by using knowledge of array geometry, satellite azimuth and elevation values, and receiver-to-receiver timing biases to compute the weight vector coefficients according to Eq. (2.2), or (b) by using the converged weight vector from the LMS-based adaptive processing in the interference-free case.

Method (a) is suitable for real or simulated signals where all of the required input data are known. However, for real test-bed hardware, there are difficulties in configuring the software receiver to initialize weights according to Method (a). First, Method (a) requires that the phase bias between signals recorded on each receiver is known. These receiver-to-receiver biases can be problematic to characterize, although it is possible to use the LMS weights to calibrate this response. This calibration is done by noting that the difference between the weights calculated according to Eq. (2.2) and the LMS-derived weights is equal to the receiver-to-receiver phase bias. In fact, phase calibration was determined according to this method for the data shown in Figure 2.18, and the results agreed with the phase bias results found through traditional antenna calibration means (see Figure 2.19). Second, Method (a) requires that the receiver location, array geometry and orientation, data collection time, and satellite ephemeris are known with a fair degree of certainty. Third, the antenna locations and array orientation must be specified in the coordinate system convention used for the software receiver weight initialization algorithm.

These three considerations make Method (b) the preferred method to initialize the antenna weight coefficients for deterministic CRPA and MVDR processing for these

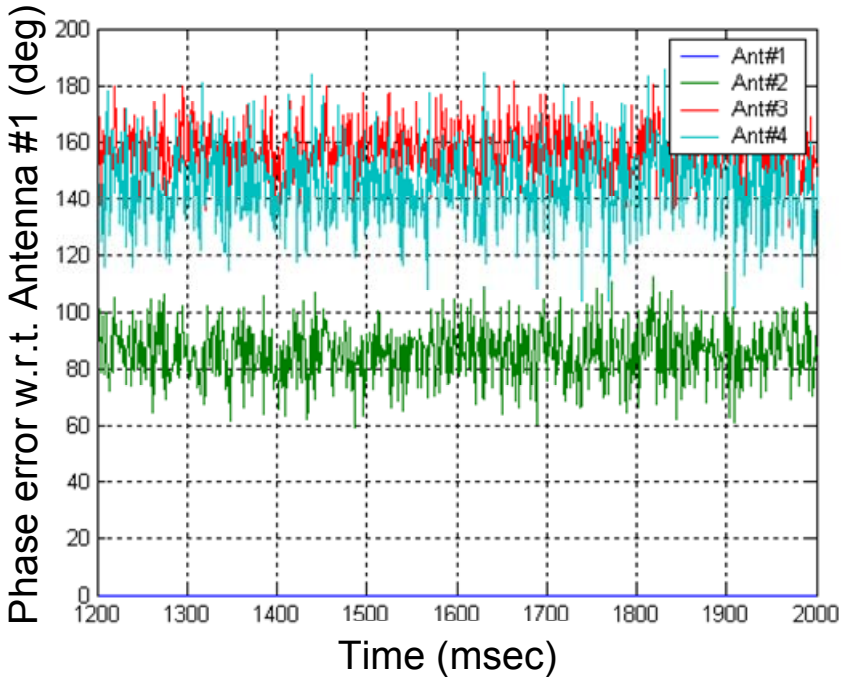

Figure 2.19. Phase calibration mismatch between receiver channels.

datasets. Simulated data and data collected locally (and for which the variables just described are well-characterized), were processed using Method (a) (where weight coefficient are initialized via Eq. (2.2)), but these results are not included here.

Figure 2.17 illustrates the average C/N_0 tracking values over a 13-satellite visible constellation. The red line plots C/N_0 versus time for the single-antenna FRPA; the average value of approximately 46 dB-Hz is typical for GPS open-sky signal reception. The blue line shows the average C/N_0 versus time for LMS-based adaptive processing, with spatial-only adaptation (in the interference-free case, no advantage would be realized with temporal processing). There is a slight drop in C/N_0 as the array initializes, but then the array weight vector converges to the steady-state values and C/N_0 recovers to outperform the single-element FRPA. As can be seen, when tracking with the seven-element array the average C/N_0 of the tracked signals goes up by approximately 8.5 dB (this is to be expected, as $10*\log_{10}(7) = 8.5$ dB).

Figure 2.18 illustrates the average C/N_0 tracking values over a ten satellite simulated constellation. In this case signals were produced with a high-fidelity Spirent GPS RF simulator with a wavefront generator front-end that introduces phase offsets to simulate a four-antenna array. The red line shows the average C/N_0 versus time for the single-antenna FRPA as before; the average tracked value is approximately 47 dB-Hz. The blue line plots the average C/N_0 versus time for LMS-based adaptive processing. For this four-antenna array, the average improvement in C/N_0 is approximately 4.5 dB (this slightly underperforms the predicted value of 6 dB, and this minor degradation is due to analog hardware imperfections).

As shown in Figure 2.18, at 4000 milliseconds into the tracking window, narrowband interference illuminates the antenna array, with a J/S power ratio of 30 dB for each of six narrowband jammers. This represents a significant level of interference, and it is well beyond the capacity of a single-antenna GPS receiver to maintain signal lock without special interference rejection processing. The LMS-based adaptive array suffers a 10 dB decrease in tracked C/N_0 in the presence of this jamming, but the tracked C/N_0 remains approximately 40 dB-Hz, which is well above the required level for this receiver to track signals.

2.5 SUMMARY OF ADAPTIVE PROCESSING

This chapter has described a multi-antenna space-time adaptive GPS software receiver. This receiver utilizes a modular and scalable building-block architecture, is more computationally efficient than existing methods, and solves several STAP-related processing issues previously identified in the literature.

The adaptive algorithms and GPS software receiver presented in this section:

- Completely integrates space-time adaptive array processing into the GPS receiver.
- Ties convergence speed of the adaptive algorithms to the noise bandwidth of the carrier-tracking loop.

- Implements an adaptation constraint that eliminates carrier-phase errors caused by weight vector phase rotation, without reducing spatial or temporal degrees of freedom in the adaptive algorithm.

- Addresses navigation data bit ambiguity for reference-signal-based adaptation.

The GPS STAP algorithms have been verified using simulated and actual GPS data. This concludes the discussion of space-time adaptive array processing for GPS.

CHAPTER 3: CHARACTERIZATION OF INTERFERENCE REJECTION VERSUS NAVIGATION BIASES

This chapter evaluates the tradeoff between allocating resources to reject radio frequency interference and allocating resources to mitigate navigation biases in the GPS timing information. The tradeoff is explored through high-fidelity software simulation that generates GPS signals for an antenna array and applies antenna anisotropy and mutual coupling effects. The simulation methodology allows verification of the phase response and quantifies the tradeoff between interference rejection and tracking biases. Chapter 4 will extend this analysis to testing with hardware in the loop.

For isotropic antennas, the MVDR and LMS space-time adaptive algorithms showed no navigation biases. For antennas models that simulate actual test hardware, navigation biases were reduced with a deterministic bias mitigation strategy, although not to the level required by Sea-based JPALS requirements. Taken together, these results suggest that for antennas of a suitably-improved design, bias mitigation is successful, enabling space-time adaptive processing in conjunction with carrier-phase differential navigation.

Figure 3.1 shows an overview of the GPS software receiver and the simulation environment. The simulation first creates GPS satellite signals. These signals are modified by the antennas in the multi-element array, by front-end filtering, and by analog to digital (A/D) conversion. The modified signals then are stored to disk. The next step is processing by GPS software receiver. This receiver runs in post-processing on stored data so the same data file can be processed in different configurations of the receiver and the results evaluated. Finally, deterministic bias compensation based on single-antenna or array calibration is applied to the code-phase and carrier-phase tracking estimates.

3.1 ANTENNA CHARACTERIZATION

This section describes the GPS antenna array. Antenna anisotropy and mutual coupling were critical inputs to the simulation study, and this investigation was able to leverage

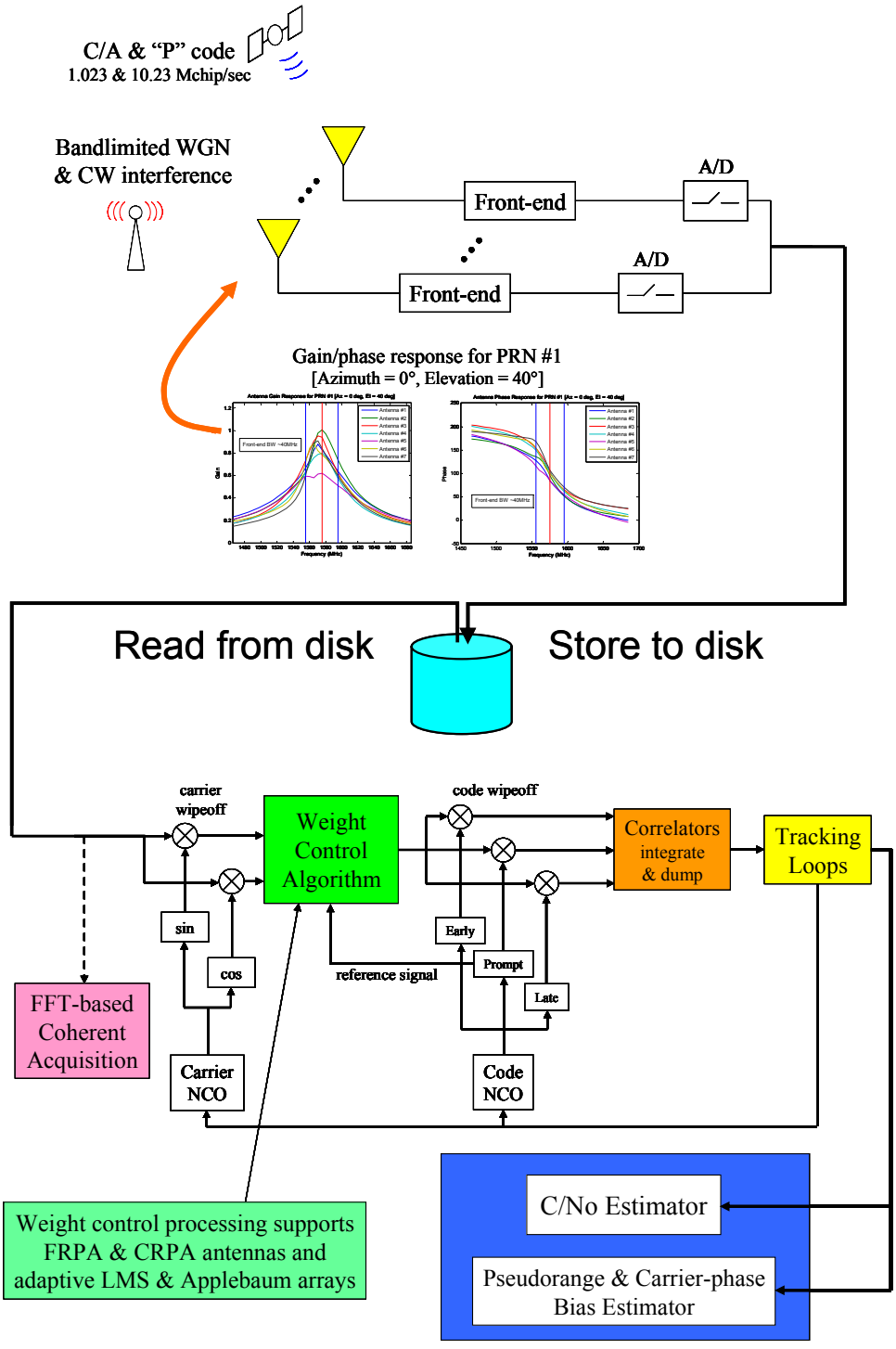

Figure 3.1. Block diagram of simulation environment, showing antenna characterization, signal and interference generation, adaptive weight computation, and signal tracking.

previous work on antenna and array characterization. An array of L-band single-probe-fed right-hand circularly polarized rectangular patch antennas was designed and fabricated at Stanford University in order to study mutual coupling and distortion-induced biases in GPS antenna arrays [92, 93]. The antenna response characteristics were determined through a combination of high-fidelity finite-element electromagnetic-field simulations and anechoic chamber testing, and this process is well-described in other literature [30, 35]. A seven-element hexagonal array with half-wavelength baselines was the standard array configuration. Figure 3.2 shows this array mounted on a ground-plane during testing in an anechoic chamber.

Characterization data for the Stanford-designed antennas are available for a 220 MHz wide band about the GPS L1 center frequency of 1575.42 MHz, for a seven-element antenna array, and for ten signal arrival directions. Figure 3.3 shows satellite and jammer locations, both in a sky-view plot in the center of the figure as well as listed by azimuth

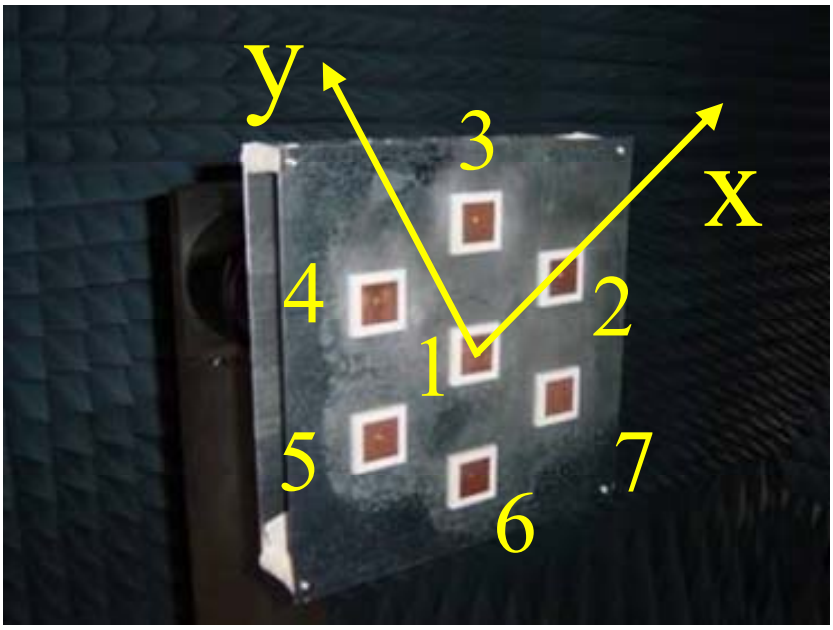

Figure 3.2. 7-element single-probe-fed rectangular patch antenna array, in anechoic chamber during testing.

PRN	Azimuth	Elevation
1	0	40
2	30	30
3	60	40
4	90	50
5	120	20
6	150	60
7	210	70
8	240	20
9	270	30
10	300	80

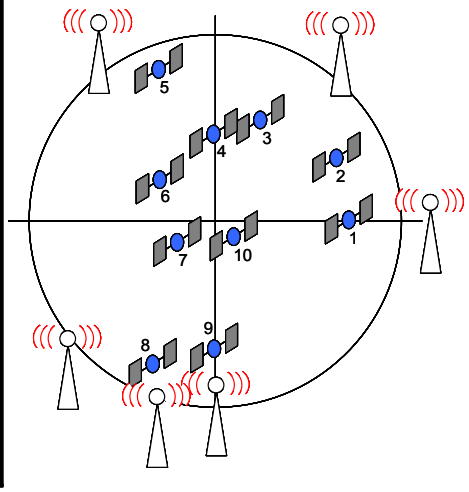

RFI	Azimuth	Elevation
1	0	0
2	45	0
3	120	0
4	225	0
5	250	0
6	270	10

Figure 3.3. The "standard constellation" of ten satellites as well as six near-horizon wideband interference sources.

and elevation in the two tables to either side. The satellite locations comprise the "standard constellation" for this investigation, and were chosen to maintain continuity with previous studies and because, for these antennas, the associated arrival directions produce the greatest degree of distortion on the received signals. Since the distortion is greatest for these arrival directions, it leads to extremes in the code-phase and carrier-phase biases, meaning that the simulation study results represent the worst-case outcome for this array. Complete characterization data by frequency, signal arrival direction, and gain and phase response are included in Appendix B.

The patch antennas utilized in this investigation have greater variation in response with respect to signal frequency and arrival direction when compared to high-quality commercial L-band GPS patch antennas. There are three reasons for using custom-designed antennas for the simulation portion of this investigation, rather than using those that are commercially-available: (a) for mutual coupling analysis, the necessary electromagnetic simulation models are proprietary to each antenna manufacturer and are not available in the open literature, (b) parameter sensitivity studies required that

Stanford University fabricate antennas to precise dimensional specifications, and (c) the results of this investigation are meant to apply to single-frequency L-band patch antennas in general, and not to those from a particular antenna manufacturer.

Since the antennas used in this simulation study have a greater degree of signal distortion than commercially-available antennas and arrays, the results described in this section are conservative. To whit, the hardware was not designed to minimize the biases. This means that the interference rejection performance is pessimistic and that the post-compensation code-phase and carrier-phase residual biases are larger than would be expected for commercial antennas. Therefore, implementing the adaptive algorithms and bias mitigation strategies from this investigation on commercial hardware will lead to improved results. The method of incorporating the antenna response data into the signal simulation will be described in the following paragraphs.

3.2 SIGNAL SIMULATION

This section describes the GPS signal simulation. The GPS signal simulation allows isolation and testing of receiver, environmental, antenna, and array processing parameters, and is a vital component of this investigation. A simulation-based approach was used for much of the analysis, rather than relying exclusively on hardware-based testing, for several reasons: (a) it was not practical to create a full suite of precisely-controlled signal and interference scenarios using real hardware, (b) it was not possible to easily control for code-phase and carrier-phase biases due to factors other than antennas and array processing (e.g., multipath, analog filter delays, atmospheric effects, clock or ephemeris errors, etc.), and (c) the use of simulated data, in conjunction with a GPS software receiver, allows for the highest levels of repeatability in the response of adaptive algorithms, tracking loops, and noise estimators.

A block diagram of the signal simulation environment is shown in Figure 3.4. This environment includes models of a multi-element antenna array, an intermediate-frequency-based signal generator, point-source wideband and narrowband interferers,

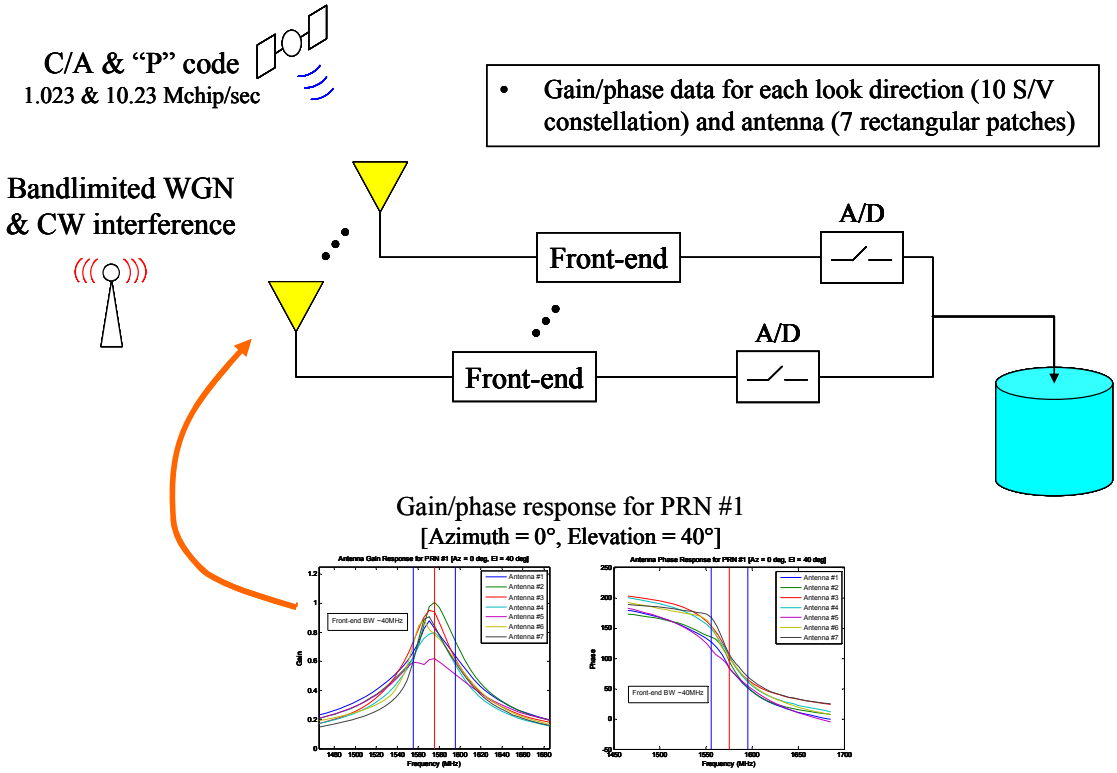

Figure 3.4. Block diagram of GPS signal simulation.

antenna anisotropy effects, and white Gaussian noise (WGN) on all channels. The simulation runs in MATLAB. The details and implementation of the GPS signal simulation are described next.

3.2.1 Intermediate Frequency Signal Simulation

The GPS signal simulation creates time-series of sampled data for a constellation of satellites and for an array of antennas, and stores this data to disk for post-processing. Rather than have the simulation run at RF and then down-convert and sample the signal, it is more computationally efficient to create signals at the sampling frequency directly. In order to capture the effects of array geometry, antenna anisotropy, and front-end downconversion and filtering, it is necessary to rigorously implement the received signal

model. This model accounts for the reception time offsets due to satellite ephemeris and antenna array geometry, and includes the impact of antenna anisotropy.

The signal transmitted on the GPS L1 frequency includes a civilian signal and a military signal broadcast in quadrature. Each signal is the product of a high-frequency sinusoidal carrier at f_{L1} = 1575.42 MHz, a PRN spreading code sequence $x(t)$ of 1.023 Mchip/sec for the civilian C/A-code and 10.23 Mchip/sec for the military P-code, and a navigation data sequence $D(t)$ transmitted at 50 bits/sec. The signal impinging on the reference, or master, antenna has the following form (applicable either to C/A-code or to P-code):

$$s_{L1}(t) = \sqrt{2P_S}\, D(t-\tau)x(t-\tau)\cos\left[2\pi(f_{L1}+f_D)t+\theta\right] \qquad 3.1$$

In Eq. (3.1), τ is the relative code offset between the receiver time-base and the PRN sequence start. The Doppler frequency, f_D, is due to transmitter/receiver line-of-sight motion. The angle, θ, is the relative phase of the transmitted signal with respect to the receiver's local oscillator. Without loss of generality, the master antenna is assumed to be at the array physical center (i.e., the origin of the local coordinate system).

The simulation portion of this investigation will focus on the military-specific P-code. This is done not only to support Sea-based JPALS but also so that the analysis is most relevant to next-generation satellite navigation signals (e.g., modernized GPS and Galileo) with their higher code chipping rates.

The GPS receiver front-end down-converts and filters the received signal to a frequency band suitable for sampling and digitization. The intermediate frequency, f_{IF}, is chosen so that the central peak in the signal spectrum (and usually the next-highest side-peaks) is resolved without unintentional aliasing. For C/A-code, f_{IF} is usually on the order of 1.5-4.0 MHz and for P-code. f_{IF} is usually on the order of 10 MHz or greater. The locally-generated downconversion mixing signal is:

$$s_{mix}(t) = \sqrt{2}\cos\left[2\pi(f_{L1}-f_{IF})t\right] \qquad 3.2$$

Single-stage downconversion is shown here without loss of generality. The effect of mixing the GPS L1 signal $s_{L1}(t)$ with $s_{mix}(t)$ is to split the signal into high-frequency and low-frequency parts, with frequencies of $(2f_{L1} - f_{IF} + f_D)$ and $(f_{IF} + f_D)$, respectively. After filtering to suppress the high-frequency component, the signal for one satellite on the master antenna channel at the intermediate frequency is:

$$s_{IF}(t) = \sqrt{P_S}\, D(t-\tau)x(t-\tau)\cos\left[2\pi\left(f_{IF} + f_D\right)t + \theta\right] \tag{3.3}$$

For a slave antenna, there will be a relative time advance or delay in the received signal with respect to the master antenna signal. The time advance or delay, Δt, as shown in Figure 3.5, is found as the dot-product of an antenna's baseline vector, $\vec{p}$, with the array to satellite "boresight" unit-vector, $\hat{r}_{boresight}$, divided by the wave propagation speed, c:

$$\Delta t = \frac{\vec{p} \cdot \hat{r}_{boresight}}{c} \tag{3.4}$$

For a half-wavelength baseline, Δt is on the order of 0.1 nanoseconds or less. Also notice that a signal arriving from the array broadside (for a linear array), or a signal arriving from a direction normal to the array (for a planar array), or a signal arriving from a

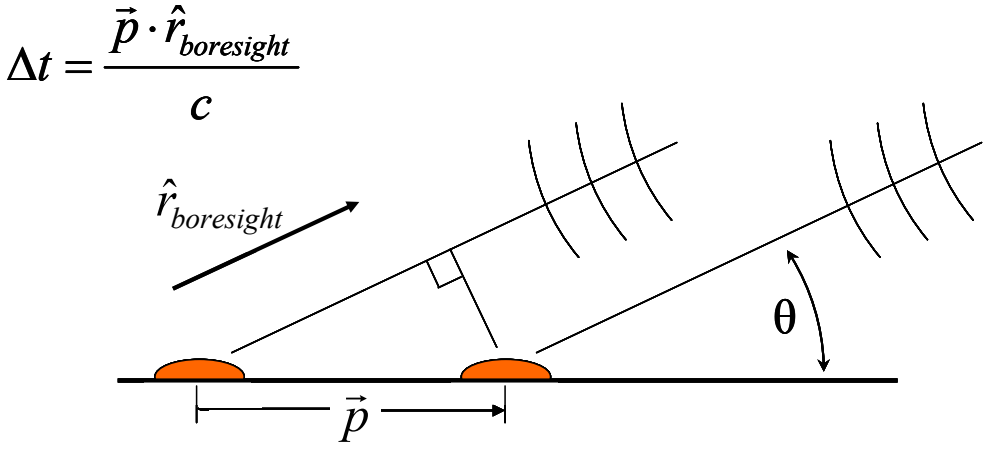

Figure 3.5. Antenna geometry showing calculation of Δt.

direction orthogonal to a particular master-to-slave baseline vector, will have $\Delta t = 0$. At the L1 carrier frequency, the impinging signal for a slave antenna is:

$$s_{slave}(t) = \sqrt{2P_S}\, D(t + \Delta t - \tau)\, x(t + \Delta t - \tau) \cos\left[2\pi (f_{L1} + f_D)(t + \Delta t) + \theta\right] \qquad 3.5$$

This equation underscores the importance of using a common oscillator for the RF front-ends of the master antenna and of all slave antennas, synchronizing analog mixing, downconversion, and sampling. Without a common clock, additional time skew would corrupt the signals on each slave antenna channel. Also, notice that the signal received by a slave antenna contains the time advance or delay in each term of the signal description (navigation data, code, and carrier). However, Δt is much smaller than either a navigation data bit (20 milliseconds) or a PRN code chip (1 μs for C/A-code or 0.1 μs for P-code). In fact, $\Delta t \approx \frac{|\vec{p}|}{c} \approx$ 0.3 nsec to 1.0 nsec.

After mixing, downconversion, and low-pass filtering, the signal at the intermediate frequency for a slave antenna becomes:

$$s_{slave,IF}(t) = \sqrt{P_S}\, D(t + \Delta t - \tau)\, x(t + \Delta t - \tau) \cos\left[2\pi (f_{IF} + f_D)t + \theta + 2\pi (f_{L1} + f_D)\Delta t\right] \qquad 3.6$$

The effect of a time advance or delay on the sinusoidal carrier is to introduce a phase advance or delay that is strictly a function of the original carrier frequency (L1 and Doppler), and not a characteristic of the intermediate frequency (or frequencies, for multi-stage downconversion). In consequence, generating in simulation the master and slave antenna signals at the intermediate frequency is relatively straightforward. The signal generator can employ either time-shifting (as developed here) or frequency-dependent phase-shifting (used later for wideband interference signals). (Note: these same methods can be used to introduce motion of each antenna's electromagnetic phase center, as a function of signal frequency or arrival-direction, without having to incorporate the detailed antenna response models in the manner described next.)

3.2.2 Effect of Antenna Gain and Phase

For a non-isotropic antenna, the gain and phase response vary as a function of the incident radiation frequency and the direction of signal arrival. This non-ideal response causes a distortion of the ideal triangular autocorrelation function shape, resulting in a code-phase bias, as well as a shift in the signal energy with respect to the inphase and quadrature processing channels, which yields a carrier-phase bias. In simulation, this distortion is modeled by first taking the Fourier transform of the simulated time-domain satellite signal, next multiplying this by the frequency-domain antenna response, and then finally performing the inverse Fourier transform. This process is illustrated in Figure 3.6.

3.2.3 Effect of Jamming

Interference in the GPS band can take several forms, including continuous-wave (CW) or wideband radio frequency interference, spoofing (mimicking the GPS signal in such a way as to bias or corrupt the navigation solution), and multipath. CW interference was not used in this simulation study for three reasons: (a) de-spreading the GPS signal confers to the receiver a substantial level of built-in CW interference resistance already,

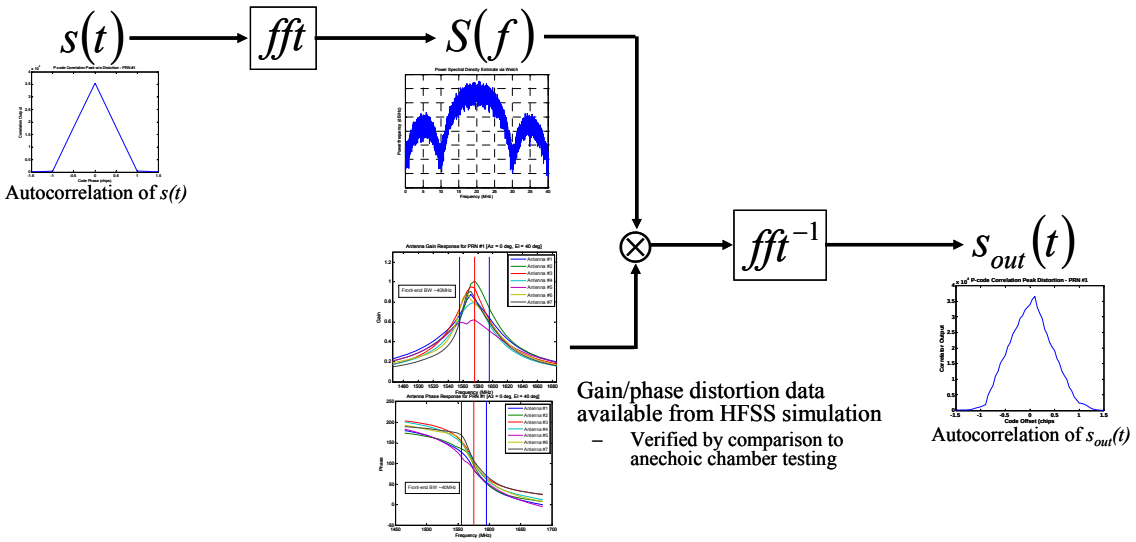

Figure 3.6. Modeling antenna-induced distortion effects in simulation.

(b) nullsteering antenna arrays (using either interference detection and localization or adaptive weight computation) are so effective against CW interference that this does not present a good opportunity to test their true capabilities, and (c) the interference scenarios for Sea-based JPALS may not be limited to CW interference only. Mitigation of spoofing and multipath are outside the scope of this investigation, although the spatial filtering associated with multi-element antenna arrays provides a substantial degree of resistance to these forms of interference.

For a wideband interference source, two simulation methods were explored although only the latter was used to create data for this investigation. In the first method, several co-located CW transmitters broadcast across a frequency band equivalent to the bandwidth of the desired wideband interference source, and then are scaled such that their combined power equals the desired J/S power ratio. In this method, the signal from each CW transmitter is created identically to that from a satellite, except without the navigation data or PRN spreading-code modulation (see Eq. (3.6)). Also, it is possible to sweep in frequency the CW transmitters so that the interference is not simply a line spectrum.

In the second method, wideband interference is created by bandpass filtering WGN. This method of interference generation is preferable, because the multi-tone approach described above could have enough spectral structure to enable an unrealistically high amount of processing gain from the adaptive temporal filter. This filtered WGN approach is the method of interference generation used in this investigation.

In this method, introducing the time offsets associated with transmitter geometry for a particular receiving antenna may be achieved through frequency-dependent phase-shifting. The slave antenna signal for a wideband interference source is determined as follows, where $j(t)$ is the bandlimited WGN signal received at the array center and Δt is the time-offset for that particular slave antenna and interference source combination:

$$j_{slave}(t) = FFT^{-1}\{FFT\{j(t)\}\cdot\exp(-j2\pi f\,\Delta t)\} \tag{3.7}$$

3.3 SIMULATION SCENARIOS

This section describes the simulation scenarios. The parameters chosen for the simulation are fairly standard. The reason for this is that the current investigation focuses on the tradeoff between interference rejection and mitigating tracking biases for adaptive arrays of non-isotropic antennas. This best could be done with a typical set of simulation parameters.

As summarized in Table 3.1, the software signal simulation produced P-code-like signals mixed-down from the GPS L1 frequency to a suitable intermediate frequency for sampling (f_S = 80MHz, f_{IF} = 20MHz, front-end bandwidth = 40MHz). The spreading-code modulation for each satellite used the P-code generator and a chipping rate of 10.23 Mchips/sec, but was short-cycled after one millisecond. One millisecond short-cycling simplified implementation of the software receiver with no significant impact on the signal spectrum. A standard constellation of ten satellites was used representing PRN codes 1-10 (refer back to Figure 3.4), with satellite Doppler frequencies ranging from –2 kHz to +2 kHz (these are not orbitally-correct Doppler frequencies, but were chosen for

Table 3.1. Simulation parameters.
f_S = 80 MHz; f_{IF} = 20 MHz; bandwidth = 40 MHz
P-code @ 10.23 Mchips/sec; 1 ms code length.

PRN	Incoming Signal Line-of-Sight		Carrier Doppler Frequency (Hz)	Received C/No for Master Antenna (dB-Hz)	
	Az	El		Isotropic	Non-Isotropic
1	0	40	-2000	40.0	37.5
2	30	30	-1556		36.8
3	60	40	-1111		37.6
4	90	50	-667		38.1
5	120	20	-222		34.3
6	150	60	222		38.7
7	210	70	667		38.9
8	240	20	1111		33.6
9	270	30	1556		35.9
10	300	80	2000		38.8

simulation purposes only). Since a position solution was neither required nor calculated, no valid navigation message or ephemeris information was needed. Instead, a random and unique sequence of navigation data bits was modulated onto each satellite signal.

Depending on the simulation case, the GPS signals were received either by an array of isotropic antennas or by an array whose gain and phase response characteristics were as determined previously through electronic simulation modeling and anechoic chamber testing (see Appendix B). Received signal power was within the normal range for unobstructed open-sky GPS reception, as low signal power *per se* was not under investigation. The ratio of signal to WGN yielded a C/N_0 of 40 dB-Hz for an isotropic receiving antenna. For the non-isotropic antennas modeled in the simulation study, there was an average of 3 dB loss, meaning that for these antennas the estimated C/N_0 during tracking was ~37 dB-Hz. Attenuation varied as function of signal arrival direction based on each antenna's unique response characteristics (see Table 3.2 and Appendix B).

Table 3.2. Received C/No (dB-Hz) for each antenna in the non-isotropic array - the C/No was 40 dB-Hz from simulation.

PRN	Antenna Number						
	1	2	3	4	5	6	7
1	37.5	39.1	38.7	37.8	35.2	37.4	38.1
2	36.8	37.9	36.1	34.9	35.8	36.7	36.6
3	37.6	38.6	38.9	36.0	36.4	34.7	36.8
4	38.1	40.4	39.7	39.5	39.0	37.1	37.5
5	34.3	36.8	35.6	36.9	33.3	31.7	29.2
6	38.7	38.5	38.7	39.9	39.2	39.4	38.0
7	38.9	39.5	37.9	40.0	40.3	41.0	39.2
8	33.6	32.1	31.4	32.7	34.1	35.3	31.8
9	35.9	35.0	33.6	35.0	37.3	37.3	37.2
10	38.8	39.4	41.6	39.6	40.3	39.7	41.5

Ensemble mean: 37.1 dB-Hz
Ensemble standard deviation: 2.6 dB-Hz

Six wideband interference sources were placed at or near the horizon, in some cases with small angular separation between interference and a satellite signal (refer to Figure 3.4). Interference power was varied to achieve a desired J/S power ratio, ranging from no interference up to a J/S power ratio of 50 dB for each of the six wideband sources. This level of interference was sufficient to cause the single-element FRPA to lose lock of the signal entirely (remember, there was no anti-jam software receiver processing other than that provided by the multi-element antenna array). This performance is consistent with that of commercially-available non-interference-hardened GPS receivers.

Antenna-induced signal distortion was not applied to the wideband interference. Treating the antennas as ideal in the arrival directions associated with interference (as opposed to using actual or estimated antenna response data) was not problematic, because distortion of these signals would only affect the performance of interference localization algorithms but not the performance of adaptive algorithms with cost functions that optimize SINR or minimize MSE (such as were used in this investigation). In fact, distortionless reception of interference was desirable since it de-couples the interference rejection performance of the adaptive algorithms from the low-elevation roll-off in patch antenna gain (it is usual for an antenna to have significant signal attenuation near the horizon).

The final operations of the signal simulation were an automatic gain-control stage to ensure good dynamic range performance, and then A/D conversion to store real-valued samples to disk at 4-bit resolution. The stored signals then were fed as inputs into a software-based GPS receiver, described previously in Chapter 2. Storing samples at higher resolution was not done for three reasons: (a) storage requirements would have been excessive, (b) it is usual for a GPS receiver to use only 1-4 bits of A/D resolution anyway, and (c) the signal power loss from using 4-bits of A/D resolution, rather than floating point values, is minimal (i.e., fractions of a dB). Insufficient dynamic range (with a 4-bit A/D) for the interference levels evaluated in the simulation portion of this investigation was not an issue. Dynamic range became a concern in the interference-rejection experiments with hardware in the loop, for which only 2-bits of A/D resolution were available. This is discussed in Chapter 4.

3.4 SIMULATION METHODOLOGY

This section describes the simulation methodology. The receiver tracking outputs could be compared directly with the known code-phase and carrier-phase input values from the signal simulation. In this way, it was possible to determine precisely the code-phase and carrier-phase biases due to antenna-induced distortion effects and array processing. For example, the tracking results in Figure 3.7 show the code-phase and carrier-phase biases from tracking with an adaptive array of non-isotropic antennas.

The software receiver estimates C/N_0 for received signals, which allows quantification of the noise and interference-rejection performance of the various array processing algorithms. However, when determining code-phase and carrier-phase biases, it is important to suppress the effects of noise in order to obtain a precise estimate. For example, because the code-phase standard deviations shown in Figure 3.7 are in the tens

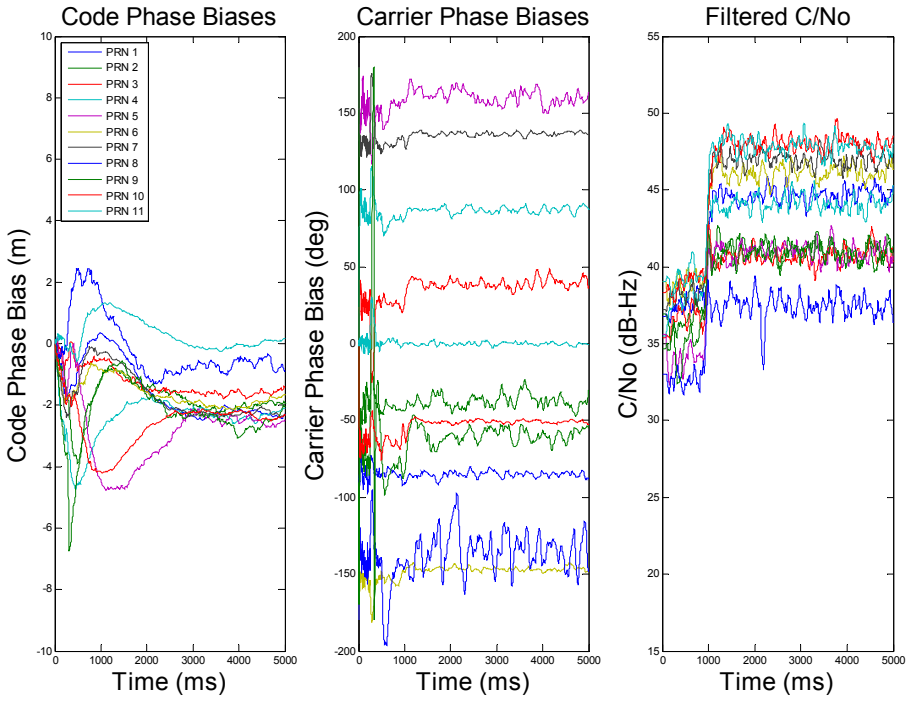

Figure 3.7. Software receiver tracking output and noise/bias estimation; Applebaum/MVDR-based STAP, C/N_0 = 40 dB-Hz plus six interference sources at J/S = 30dB.

of centimeters, substantial filtering would be needed to attenuate the noise effects. This would lead to excessively long simulation run-times.

Instead, a two-step process for bias estimation is implemented, shown in Figure 3.8. This process works for either a single-element FRPA or for deterministic or adaptive antenna arrays. Step #1 involves tracking the signals in the presence of WGN (noise correlated neither in time nor across elements) and interference. For adaptive arrays, the antenna weights are updated based on the selected adaptation scheme, and stored. Step #2 involves tracking the signals without noise or interference. For adaptive arrays, the stored weight vector is played back from step #1 at each processing epoch.

With this two-step method, the first step allows estimation of C/N_0 and calculation of the adaptive weight vector. Then, the second step allows estimation of code-phase and carrier-phase biases. In this way, bias values may be computed directly from a short-duration simulation. This is shown in Figure 3.9.

3.5 VERIFYING PHASE RESPONSE

The first step in analyzing receiver tracking output is verification that the code-phase and carrier-phase estimates coming from the tracking loops match those predicted from the signal simulation and the antenna response data. This verification process is important for two reasons: (a) it demonstrates that the previously-described two-step tracking methodology (noise then noise-free) can precisely estimate code-phase and carrier-phase biases to sub-centimeter in code-phase and to sub-degree in carrier-phase, and (b) it shows that the antenna characterization data are reproduced faithfully by simulation.

Verification is done in two ways: (a) for the array of isotropic antennas, verifying that there is zero error between the tracking output for each antenna and the code-phase and carrier-phase inputs based on satellite and array geometry, and (b) for the array of non-isotropic antennas, verifying that the tracking output from each antenna produces a carrier-phase error that, after geometry-based adjustment, is equal to the phase response from the antenna response input data (available from the response curves in Appendix B).

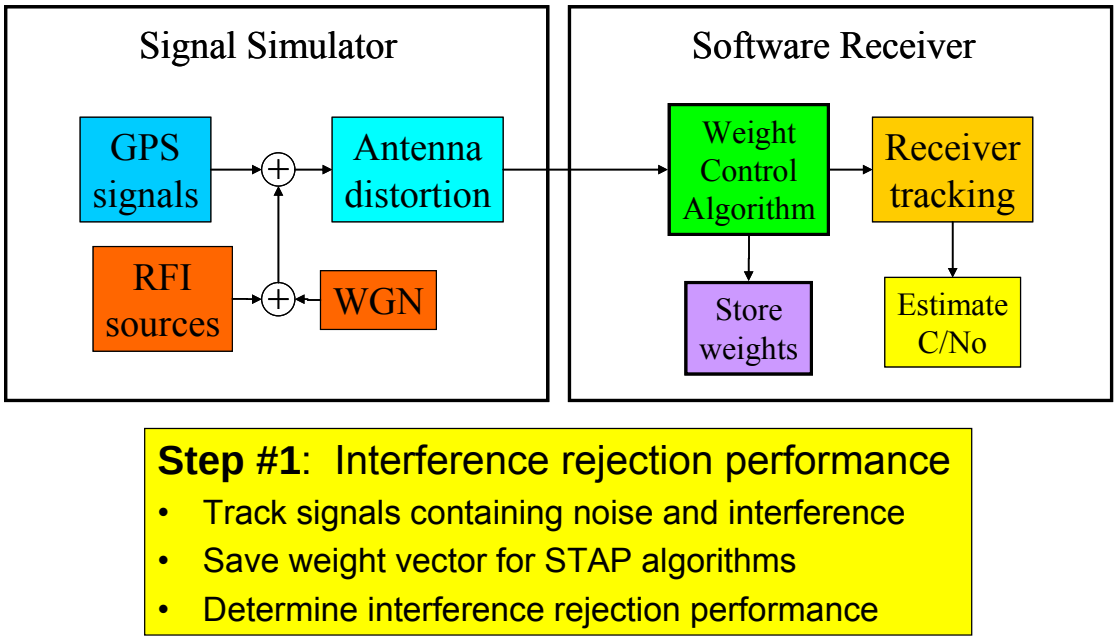

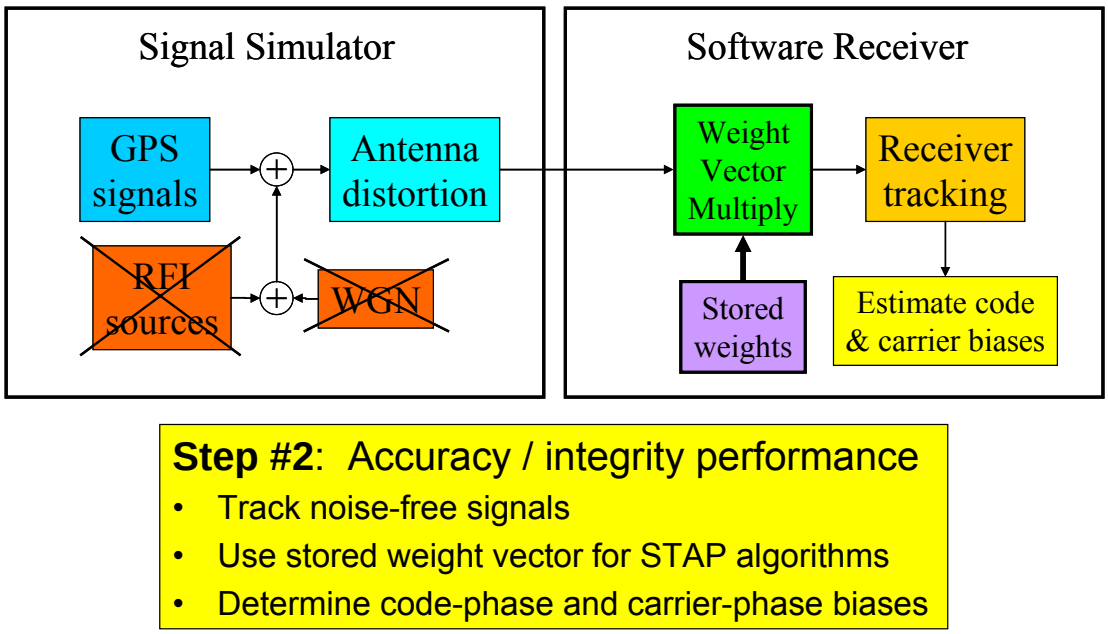

Figure 3.8. Methodology for estimating code/carrier biases and interference rejection performance for adaptive antenna arrays.

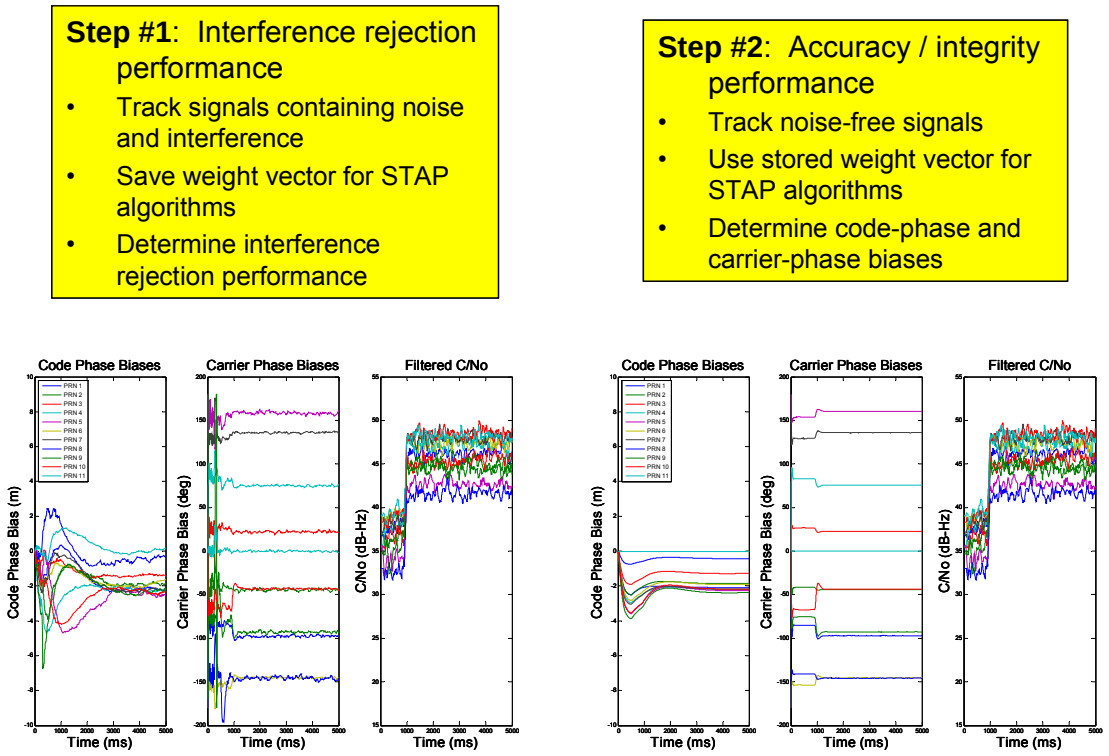

Figure 3.9. Two-step process for estimating interference rejection and code/carrier biases. This example shows 7-antenna Applebaum/MVDR-based space-time adaptive processing (with a single time-tap), C/N_0 of 40 dB-Hz, plus six interference sources at J/S of 30dB.

The receiver tracking output for each antenna in the isotropic array showed zero code-phase bias and zero carrier-phase bias. In this scenario, each of ten satellites was tracked on each of seven antennas (70 unique tracking scenarios). Then, the code-phase and carrier-phase tracking errors were found as the difference between the receiver's tracking output and the code-phase and carrier-phase inputs used to create the simulated signals.

For the slave antennas, there should be a phase advance or retard based on the array geometry and the incoming signal arrival direction. The code-phase and carrier-phase tracking errors are shown in Tables 3.3-a and 3.4-a, respectively. The geometrical phase for each slave antenna element is computed, relative to the center master element, in a manner similar to that described earlier for the calculation of Δt in the signal simulation.

Table 3.3-a. Code-phase difference (in cm) between receiver tracking output and signal simulation input, before geometric correction.
Isotropic Antennas

PRN	Antenna Number						
	1	2	3	4	5	6	7
1	0.0	8.4	3.3	-2.6	-7.0	-2.6	3.3
2	0.0	7.0	7.0	0.0	-7.0	-7.0	0.0
3	0.0	3.7	7.3	3.7	-4.0	-7.3	-4.0
4	-0.1	-0.1	5.4	5.4	-0.1	-5.3	-5.3
5	-0.1	-3.6	4.1	8.5	4.1	-3.6	-9.2
6	0.0	-4.0	0.0	3.3	3.3	0.0	-4.0
7	0.0	-2.6	-2.6	0.0	2.9	2.9	0.0
8	0.0	-4.0	-9.1	-4.0	4.1	9.2	4.1
9	0.0	0.0	-7.3	-7.3	0.0	7.0	7.0
10	0.0	0.7	-1.1	-1.8	-1.1	0.7	1.8

Table 3.3-b. Predicted code-phase (in cm), based on satellite and array geometry.
Isotropic Antennas

PRN	Antenna Number						
	1	2	3	4	5	6	7
1	0.0	7.3	3.6	-3.6	-7.3	-3.6	3.6
2	0.0	7.1	7.1	0.0	-7.1	-7.1	0.0
3	0.0	3.6	7.3	3.6	-3.6	-7.3	-3.6
4	0.0	0.0	5.3	5.3	0.0	-5.3	-5.3
5	0.0	-4.5	4.5	8.9	4.5	-4.5	-8.9
6	0.0	-4.1	0.0	4.1	4.1	0.0	-4.1
7	0.0	-2.8	-2.8	0.0	2.8	2.8	0.0
8	0.0	-4.5	-8.9	-4.5	4.5	8.9	4.5
9	0.0	0.0	-7.1	-7.1	0.0	7.1	7.1
10	0.0	0.8	-0.8	-1.6	-0.8	0.8	1.6

Table 3.3-c. Code-phase error between the geometrically-predicted values and the receiver tracking output.
Isotropic Antennas

PRN	Antenna Number						
	1	2	3	4	5	6	7
1	0.0	-1.2	0.3	-1.1	-0.3	-1.1	0.3
2	0.0	0.1	0.1	0.0	-0.2	-0.2	0.0
3	0.0	0.0	-0.1	0.0	0.4	0.0	0.4
4	0.1	0.1	-0.1	-0.1	0.1	0.0	0.0
5	0.1	-0.8	0.4	0.5	0.4	-0.8	0.2
6	0.0	-0.1	0.0	0.8	0.8	0.0	-0.1
7	0.0	-0.2	-0.2	0.0	-0.1	-0.1	0.0
8	0.0	-0.5	0.2	-0.5	0.4	-0.3	0.4
9	0.0	0.0	0.2	0.2	0.0	0.2	0.2
10	0.0	0.1	0.3	0.2	0.3	0.1	-0.2

Ensemble mean: 0.0 cm
Ensemble standard deviation: 0.4 cm

Table 3.4-a. Carrier-phase difference (in degrees) between receiver tracking output and signal simulation input, before geometric correction.
Isotropic Antennas

PRN	Antenna Number						
	1	2	3	4	5	6	7
1	0.0	137.9	68.9	-68.9	-137.9	-68.9	68.9
2	0.0	135.0	135.0	0.0	-135.0	-135.0	0.0
3	0.0	68.9	137.9	68.9	-68.9	-137.9	-68.9
4	0.0	0.0	100.2	100.2	0.0	-100.2	-100.2
5	0.0	-84.6	84.6	169.1	84.6	-84.6	-169.1
6	0.0	-77.9	0.0	77.9	77.9	0.0	-77.9
7	0.0	-53.3	-53.3	0.0	53.3	53.3	0.0
8	0.0	-84.6	-169.1	-84.6	84.6	169.1	84.6
9	0.0	0.0	-135.0	-135.0	0.0	135.0	135.0
10	0.0	15.6	-15.6	-31.3	-15.6	15.6	31.3

Table 3.4-b. Predicted carrier-phase (in degrees), based on satellite and array geometry.
Isotropic Antennas

PRN	Antenna Number						
	1	2	3	4	5	6	7
1	0.0	137.9	68.9	-68.9	-137.9	-68.9	68.9
2	0.0	135.0	135.0	0.0	-135.0	-135.0	0.0
3	0.0	68.9	137.9	68.9	-68.9	-137.9	-68.9
4	0.0	0.0	100.2	100.2	0.0	-100.2	-100.2
5	0.0	-84.6	84.6	169.1	84.6	-84.6	-169.1
6	0.0	-77.9	0.0	77.9	77.9	0.0	-77.9
7	0.0	-53.3	-53.3	0.0	53.3	53.3	0.0
8	0.0	-84.6	-169.1	-84.6	84.6	169.1	84.6
9	0.0	0.0	-135.0	-135.0	0.0	135.0	135.0
10	0.0	15.6	-15.6	-31.3	-15.6	15.6	31.3

Table 3.4-c. Carrier-phase error between the geometrically-predicted values and the receiver tracking output.
Isotropic Antennas

PRN	Antenna Number						
	1	2	3	4	5	6	7
1	0.0	0.0	0.0	0.0	0.0	0.0	0.0
2	0.0	0.0	0.0	0.0	0.0	0.0	0.0
3	0.0	0.0	0.0	0.0	0.0	0.0	0.0
4	0.0	0.0	0.0	0.0	0.0	0.0	0.0
5	0.0	0.0	0.0	0.0	0.0	0.0	0.0
6	0.0	0.0	0.0	0.0	0.0	0.0	0.0
7	0.0	0.0	0.0	0.0	0.0	0.0	0.0
8	0.0	0.0	0.0	0.0	0.0	0.0	0.0
9	0.0	0.0	0.0	0.0	0.0	0.0	0.0
10	0.0	0.0	0.0	0.0	0.0	0.0	0.0

Ensemble mean: 0.0°
Ensemble standard deviation: 0.0008°

These intermediate results are shown in Tables 3.3-b and 3.4-b. After this adjustment, the difference between the geometrically-predicted code-phase and carrier-phase and the estimates produced by the receiver's code and carrier tracking loops should be zero. This was indeed the case, as shown in Tables 3.3-c and 3.4-c.

The receiver tracking output for the array of non-isotropic antennas showed a match between the carrier-phase bias from simulation and that predicted from antenna characterization data. In this scenario, again each of ten satellites was tracked on each of seven antennas. Since these antennas are non-isotropic, there should be a carrier-phase error, even after geometrical correction, equal to the antenna's phase response at the GPS L1 carrier frequency. As before, the carrier-phase tracking error was found as the difference between the carrier-phase from the receiver tracking output and the carrier-phase used to create the simulated signals. This is shown in Table 3.5-a. The antenna carrier-phase response at the GPS L1 frequency is read from the antenna characterization curves. This information is contained in Table 3.5-b (data extracted from Appendix B). The difference between the antenna phase response and the estimates produced by the receiver's carrier-tracking loop, when corrected by the geometric phase of each antenna (refer back to Table 3.4-b) should be zero. This is the case, as shown in Table 3.5-c.

3.6 INTERFERENCE REJECTION VERSUS TRACKING BIASES

This section presents the characterization of code-phase and carrier-phase biases due to antenna anisotropy effects, adaptive array processing parameters, and wideband interference. This evaluates the effectiveness of deterministic bias compensation based on antenna and array calibration. Interference rejection is quantified by comparing C/N_0 for the adaptive arrays in the presence of jamming to the C/N_0 for the deterministic CRPA in the same interference scenarios. Results are found by isolating in turn each of the simulation variables and software receiver settings. Results are averaged over the ten satellites in the standard constellation, except for cases in which the receiver lost lock on some satellites due to excessive interference (this happened for satellites placed at small angular separation from jammers).

Table 3.5-a. Carrier-phase difference (in degrees) between receiver tracking output and signal simulation input, before geometric correction.
Non-Isotropic Antennas

PRN	Antenna Number						
	1	2	3	4	5	6	7
1	-85.0	42.4	-35.1	-172.0	-222.3	-168.7	-39.1
2	-41.7	86.8	89.1	-41.1	-179.0	-178.4	-45.0
3	26.5	83.6	155.6	99.1	-49.1	-116.0	-40.4
4	83.1	74.3	169.3	171.2	67.2	-26.8	-7.5
5	153.5	71.2	238.9	318.2	253.5	88.6	-0.2
6	-153.6	-216.1	-144.6	-64.7	-74.1	-135.7	-227.8
7	129.3	78.8	82.2	143.1	186.6	189.4	141.8
8	-141.3	-230.1	-313.6	-239.6	-78.5	26.5	-43.1
9	-75.7	-102.3	-232.0	-218.9	-104.3	43.0	41.3
10	-66.9	-26.5	-54.4	-72.9	-54.4	-22.9	-9.6

Table 3.5-b. Antenna phase response (in degrees) at the GPS-L1 frequency (1575.42 MHz).
Non-Isotropic Antennas

PRN	Antenna Number						
	1	2	3	4	5	6	7
1	-83.9	-95.1	-103.4	-103.0	-84.2	-99.7	-106.8
2	-39.7	-47.3	-44.8	-40.8	-43.2	-42.0	-43.9
3	28.3	15.3	19.4	31.3	20.3	21.6	29.2
4	83.1	74.3	68.9	71.5	67.7	73.3	93.2
5	154.2	156.0	154.8	150.0	170.8	174.7	168.3
6	-153.6	-137.5	-144.0	-141.9	-151.1	-134.8	-149.8
7	129.5	132.8	134.9	144.1	133.3	136.2	141.5
8	-139.4	-144.8	-144.2	-154.2	-162.2	-140.5	-126.0
9	-75.9	-101.4	-96.0	-83.3	-104.1	-92.2	-93.5
10	-67.4	-42.2	-38.1	-41.7	-38.3	-38.2	-40.5

Table 3.5-c. Carrier-phase error between antenna phase response and the receiver tracking output, after geometric adjustment (Table 3.2-b).
Non-Isotropic Antennas

PRN	Antenna Number						
	1	2	3	4	5	6	7
1	1.1	0.4	0.7	0.1	0.2	0.0	1.3
2	2.1	1.0	1.1	0.3	0.9	1.3	1.1
3	1.7	0.7	1.7	1.2	0.5	-0.3	0.6
4	0.0	0.0	-0.2	0.5	0.5	0.0	0.5
5	0.7	0.3	0.5	1.0	1.9	1.5	-0.6
6	0.0	0.7	0.6	0.7	0.9	1.0	0.0
7	0.2	0.7	-0.6	1.0	0.1	0.1	-0.3
8	1.8	0.7	0.3	0.8	0.9	2.1	1.6
9	-0.2	0.9	1.0	0.7	0.2	-0.2	0.2
10	-0.4	-0.1	0.7	0.0	0.4	0.3	0.4

Ensemble mean: 0.6°
Ensemble standard deviation: 0.6°

This section follows the organization shown in Table 3.6. The organization shown in this table might provide a useful resource in following the subsequent discussion of code-phase and carrier-phase biases versus interference rejection for isotropic and non-isotropic antenna arrays. As shown in the table, simulation cases are categorized according to antenna type (isotropic versus non-isotropic), noise and interference environment (WGN only versus both WGN and wideband interference), and array processing (spatial-only processing (either deterministic or adaptive) versus space-time adaptive processing). To aid understanding of the tables that follow, cells to which particular attention should be directed are shaded in blue. Also, for clarity of presentation, results are shown in the tables for wideband interference having a J/S power ratio of 50 dB on each of the six transmitters. The figures at the end of this section include results for J/S power ratios of 30 dB and 50 dB.

As developed in earlier sections of this investigation on adaptive array processing, the two adaptive algorithms utilized were a blind-adaptive array having a mean-square error cost function (LMS) and a constrained adaptive beamforming and nullsteering array

Table 3.6. Organization of simulation results - Tables 3.7-3.15;
code-phase and carrier-phase biases and RFI rejection.

<table>
<tr><th rowspan="2">Noise/RFI Environment</th><th rowspan="2">Spatial/Temporal Degrees of Freedom</th><th colspan="2">Antenna/Array Type</th></tr>
<tr><th>Isotropic</th><th>Non-Isotropic</th></tr>
<tr><td rowspan="3">C/No = 40 dB-Hz and No RFI</td><td rowspan="2">Spatial Only Processing</td><td rowspan="2">Table 3.7</td><td>Table 3.11 (no bias compensation)</td></tr>
<tr><td>Table 3.12 (w/ bias compensation)</td></tr>
<tr><td>STAP processing</td><td>Table 3.8</td><td>Table 3.13 (w/ bias compensation)</td></tr>
<tr><td rowspan="2">C/No = 40 dB-Hz plus Six Wideband RFI Sources, J/S = 50dB ea.</td><td>Spatial Only Processing</td><td>Table 3.9</td><td>Table 3.14 (w/ bias compensation)</td></tr>
<tr><td>STAP processing</td><td>Table 3.10</td><td>Table 3.15 (w/ bias compensation)</td></tr>
</table>

(MVDR). The adaptive algorithms were utilized in two ways: (a) with spatial processing only, and (b) with space-time adaptive processing using three or five time-taps (spatial-only adaptation is a special case of space-time processing with a single time-tap). The LMS algorithm performed equally well in both pre-correlation and post-correlation adaptation modes, while the MVDR algorithm suffered in the post-correlation mode due to excessive weight vector fluctuation. For this reason, the results shown in this section utilize pre-correlation adaptation only; refer to the upper block diagram in Figure 2.8.

3.6.1 Isotropic Antennas

Arrays of isotropic antennas, whether using deterministic or adaptive weight vector coefficients, introduce no code-phase or carrier-phase biases in the receiver's tracking output. This finding holds for spatial-only processing as well as for space-time adaptive arrays, and in the interference-free case or in the presence of wideband interference (Tables 3.7-10). The significance of this result is that when the signals input to the array processing operation contain no distortion (either through optimized antenna design or via frequency-domain antenna equalization), then the space-time adaptive algorithms investigated here (MVDR and LMS) introduce no code-phase or carrier-phase biases.

Antenna arrays improve C/N_0, and adaptive antenna arrays clearly outperform deterministic arrays in the presence of interference. For the interference-free case, as shown in Tables 3.7 and 3.8, the improvement in C/N_0 for the seven-element isotropic arrays with respect to the single-element FRPA is ~8.5 dB, going from 40 dB-Hz to approximately 48.5 dB-Hz. In the interference-free isotropic antenna case, there is no performance benefit for the adaptive arrays over the deterministic beamforming CRPA, since each weight calculation method produces the same steady-state antenna weighting coefficients.

The reason that the steady-state weight vectors for the adaptive algorithms are identical to those calculated deterministically is expanded upon next. The signals processed by the receiver are composed of the desired signals from the satellites as well as noise. For the

interference-free case, the noise is uncorrelated in both time and space among the antennas in the array. The structure of the covariance matrix associated with the desired signals is preserved either by the steering-vector constraint (MVDR) or by the constraint of matching the receiver-generated reference signal (LMS). Both of these constraints cause the optimal weight vector to match the Wiener solution (with the caveat that the received signals are distortion-free). To the extent that the noise is truly white, it

Table 3.7. Isotropic antennas, no RFI, C/No = 40 dB-Hz;
STAP arrays utilize spatial degrees of freedom only.

Averages over 10-satellite constellation	Deterministic		STAP w/ 1 time-tap	
	FRPA	CRPA	LMS	MVDR
Code-phase bias (m)	0.00	0.00	0.00	0.00
Carrier-phase bias (deg)	0.0	0.0	0.2	0.0
C/No (dB-Hz)	40.1	48.4	48.2	48.4

Table 3.8. Isotropic antennas, no RFI, C/No = 40 dB-Hz;
STAP arrays utilize spatial & temporal degrees of freedom.

Averages over 10-satellite constellation	Widrow/LMS			Applebaum/MVDR		
	# of time-taps			# of time-taps		
	1	3	5	1	3	5
Code-phase bias (m)	0.00	0.01	0.02	0.00	0.00	0.00
Carrier-phase bias (deg)	0.2	0.2	0.2	0.0	0.0	0.0
C/No (dB-Hz)	48.2	48.0	47.9	48.4	48.2	48.0

contributes nothing to the off-diagonal terms in the signal covariance matrix. In other words, there is no improvement to C/N_0 in changing the array sidelobes or nulls, since the Wiener weight vector solution already minimizes white-noise power. For this reason, any gain pattern changes are non-beneficial, and the adaptive arrays perform equally to the deterministic CRPA.

In the presence of wideband interference, the adaptive arrays of isotropic antennas show a clear C/N_0 advantage over the deterministic CRPA (the single-antenna FRPA does not track at all in the presence of six interference sources each at a J/S power ratio of 50 dB compared to the satellite signals). The advantages of adaptive spatial processing shown in Table 3.9 are significant. This table shows increases in C/N_0 of 7.6 dB for LMS adaptation and 5.9 dB for MVDR, when compared to the deterministic CRPA. The benefits of including temporal processing as well as spatial adaptation are greater still, as shown in Table 3.10. This table shows further increases of 3.0 dB for LMS and 1.8 dB for MVDR. Again, these improvements are realized without introducing any appreciable code-phase or carrier-phase navigation biases for arrays of isotropic antennas.

Table 3.9. Isotropic antennas, six 50dB J/S wideband RFI sources; STAP arrays utilize spatial degrees of freedom only.

Averages over 10-satellite constellation	Deterministic		STAP w/ 1 time-tap	
	FRPA	CRPA	LMS	MVDR
Code-phase bias (m)	N/A	0.00	0.00	0.00
Carrier-phase bias (deg)	N/A	0.0	3.0	0.0
C/No (dB-Hz)	N/A	27.7	35.3	33.5
Number of Tracked S/Vs	None	10	10	10

Table 3.10. Isotropic antennas, six 50dB J/S wideband RFI sources; STAP arrays utilize spatial & temporal degrees of freedom.

Averages over 10-satellite constellation	Widrow/LMS			Applebaum/MVDR		
	# of time-taps			# of time-taps		
	1	3	5	1	3	5
Code-phase bias (m)	0.00	0.01	0.01	0.00	0.00	0.00
Carrier-phase bias (deg)	3.0	1.0	0.5	0.0	1.7	5.5
C/No (dB-Hz)	35.3	36.9	38.3	33.5	35.3	35.1
Number of Tracked S/Vs	10	10	8	10	10	10

3.6.2 Non-isotropic Antennas

Non-isotropic antennas or arrays of non-isotropic antennas display significant code-phase and carrier-phase biases. For the antennas modeled in this investigation, code-phase biases are approximately two meters and carrier-phase biases are uniformly distributed from $-\pi$ to $+\pi$ (this is the range of the arctangent carrier-phase discriminator; carrier-phase is modulo 2π so greater biases simply toggle the polarity of the navigation data). For the single antenna, these results are shown in the left-most column of data in Table 3.11. The array results for the deterministic CRPA and for the LMS and MVDR adaptive arrays are shown in the next three columns. In addition to bias, there is attenuation of received signal power for the non-isotropic cases, with the tracked C/N_0 down by approximately 3.0 dB across the board as compared to the isotropic antenna and array cases (compare the bottom row of Table 3.11 to the bottom row of Table 3.7).

Table 3.12 shows that, in the absence of interference, deterministic bias compensation almost completely mitigates the code-phase biases for the MVDR spatial-only adaptive

Table 3.11. Non-Isotropic antennas, no RFI, C/No = 40 dB-Hz;
STAP arrays utilize spatial degrees of freedom only.

Averages over 10-satellite constellation	Deterministic		STAP w/ 1 time-tap	
	FRPA	CRPA	LMS	MVDR
Code-phase bias (m)	2.13	1.88	1.94	1.88
Carrier-phase bias (deg)	95.7	96.4	95.9	96.4
C/No (dB-Hz)	37.0	45.7	45.7	45.7

Table 3.12. Non-Isotropic antennas, no RFI, C/No = 40 dB-Hz;
bias compensation using FRPA-based antenna calibration
and CRPA-based array calibration.

Averages over 10-satellite constellation		Deterministic		STAP w/ 1 time-tap	
		FRPA	CRPA	LMS	MVDR
Bias corrections using single-element FRPA calibration	Code-phase residual (m)	- 0 -	0.28	0.23	0.28
	Carrier-phase residual (deg)	- 0 -	9.2	0.5	9.2
Bias corrections using 7-element CRPA calibration	Code-phase residual (m)	N/A	- 0 -	0.06	0.00
	Carrier-phase residual (deg)	N/A	- 0 -	9.3	0.0
C/No (dB-Hz)		37.0	45.7	45.7	45.7

array and the carrier-phase biases both for the MVDR and for the LMS adaptive arrays. The code-phase biases for LMS spatial-only adaptive processing are reduced to 6 cm in the interference-free case.

Regardless of the beamsteering algorithm (deterministic, MVDR, or LMS), mitigation of the biases due to non-isotropic antennas relies on calibration data. Deterministic bias compensation can use data derived from single-antenna FRPA calibration, from multi-element deterministic CRPA calibration, or from both. For adaptive arrays, the calibration data to use depends on which adaptive weight control scheme is considered.

Table 3.12 shows that the MVDR array benefits from code-phase and carrier-phase bias compensation derived from deterministic CRPA calibration (the C/N_0 values carry-over from Table 3.11). This is because the MVDR array uses a steering constraint equal to the weight vector for the deterministic CRPA. For this reason, the code-phase and carrier-phase biases in the absence of interference are equivalent between the deterministic CRPA and the MVDR adaptive array.

The LMS array uses a reference signal constraint, so in the presence of antenna anisotropy the weight vector does not match that of the deterministic CRPA. Antenna anisotropy causes the carrier-phase bias of the LMS adaptive array to not match the bias of the deterministic CRPA. Instead, single-element FRPA calibration is used to mitigate the LMS carrier-phase bias. This is effective for the following reason. The reference signal constraint of LMS adaptation steers signal energy preferentially to the inphase processing channel of the reference antenna element. The reference antenna element is the one for which single-antenna FRPA calibration is based. Therefore, this correction is almost completely effective in reducing the carrier-phase bias of the LMS array. In summary, for the LMS array, code-phase bias correction comes from the deterministic CRPA but carrier-phase bias correction comes from the single-antenna FRPA.

Table 3.13 shows the code-phase and carrier-phase bias residuals for the three and five time-tap LMS and MVDR adaptive arrays. There is no growth in carrier-phase bias

Table 3.13. Non-Isotropic antennas, no RFI, C/No = 40 dB-Hz;
STAP arrays utilize spatial & temporal degrees of freedom.

Averages over 10-satellite constellation		Widrow/LMS			Applebaum/MVDR		
		# of time-taps			# of time-taps		
		1	3	5	1	3	5
Bias corrections using single-element FRPA calibration	Code-phase residual (m)	0.23	0.24	0.26	0.28	0.29	0.32
	Carrier-phase residual (deg)	0.5	0.5	0.5	9.2	9.2	9.1
Bias corrections using 7-element CRPA calibration	Code-phase residual (m)	0.06	0.06	0.07	0.00	0.04	0.09
	Carrier-phase residual (deg)	9.3	9.3	9.3	0.0	0.1	0.2
C/No (dB-Hz)		45.7	45.9	45.8	45.7	45.9	45.7

residuals either for the LMS or for the MVDR array. In code-phase, the LMS array maintains virtually constant code-phase bias residuals of 6-7 cm, and the MVDR array experiences growth in code-phase biases from 0 cm for a single time-tap up to 9 cm for the five time-tap case. As can be seen in the bottom row of this table, there is no benefit in C/N_0, in the interference-free case, to increasing the number of time-taps.

Table 3.14 shows the results for non-isotropic antennas and six wideband interference sources each at a J/S power ratio of 50 dB. The bias residuals for LMS spatial-only adaptive processing increase to 34 cm in code-phase and 8.6° in carrier-phase. The bias residuals for MVDR spatial-only adaptive processing increase to 27 cm in code-phase and 2.1° in carrier-phase.

The improvement in C/N_0 for the adaptive arrays with respect to the deterministic CRPA has grown for the interference case when compared to the interference-free simulation. This can be seen by comparing the bottom row in Table 3.9 to the bottom row in Table

Table 3.14. Non-Isotropic antennas, six 50dB wideband RFI sources; bias compensation using FRPA-based antenna calibration and CRPA-based array calibration.

Averages over 10-satellite constellation		Deterministic		STAP w/ 1 time-tap	
		FRPA	CRPA	LMS	MVDR
Bias corrections using single-element FRPA calibration	Code-phase residual (m)	- 0 -	0.31	0.44	0.39
	Carrier-phase residual (deg)	- 0 -	10.5	8.6	8.0
Bias corrections using 7-element CRPA calibration	Code-phase residual (m)	N/A	- 0 -	0.34	0.27
	Carrier-phase residual (deg)	N/A	- 0 -	8.0	2.1
C/No (dB-Hz)		N/A	26.2	34.8	32.1
Number of Tracked S/Vs		None	8	9	9

3.14. Where before all ten satellites in the constellation were tracked successfully, now the deterministic CRPA tracks only eight satellites while the adaptive arrays maintain lock on nine satellites. This shows the advantage of adaptive array processing in maintaining lock on satellites with close angular separation to jammers.

Table 3.15 shows both the growth in bias residuals as well as the improvement in interference rejection for adaptive arrays of non-isotropic antennas in the presence of wideband interference. Adding temporal degrees of freedom by going from a single time-tap to three and five time-taps improves C/N_0 by approximately 2 dB for the LMS and MVDR adaptive arrays. Nine satellites are tracked successfully with one, three, or five time-tap adaptive arrays. Code-phase biases improve slightly for the LMS array, decreasing from 34 cm with one time-tap to 18 cm with five time-taps. However, there is

Table 3.15. Non-Isotropic antennas, six 50dB wideband RFI sources;
STAP arrays utilize spatial & temporal degrees of freedom.

Averages over 10-satellite constellation		Widrow/LMS			Applebaum/MVDR		
		# of time-taps			# of time-taps		
		1	3	5	1	3	5
Bias corrections using single-element FRPA calibration	Code-phase residual (m)	0.44	0.31	0.31	0.39	0.36	0.35
	Carrier-phase residual (deg)	8.6	9.0	14.4	8.0	8.8	12.8
Bias corrections using 7-element CRPA calibration	Code-phase residual (m)	0.34	0.25	0.18	0.27	0.21	0.19
	Carrier-phase residual (deg)	8.0	8.5	14.0	2.1	1.9	5.7
C/No (dB-Hz)		34.8	36.5	36.9	32.1	34.3	34.2
Number of Tracked S/Vs		9	9	9	9	9	9

growth in carrier-phase biases from 8.6° to 14.4°. For the MVDR array, code-phase biases improve slightly from 27 cm with one time-tap to 19 cm with five time-taps, and there is a growth in carrier-phase biases from 2.1° to 5.7°.

Table 3.16 contains a summary of the results described in Tables 3.7-15. This table shows that deterministic bias compensation based on single-element FRPA and multi-element deterministic CRPA calibration can largely reduce bias errors from the receiver tracking output. The bias residuals shown here are applicable to the patch antenna arrays for which gain and phase response data are available. Different antennas would perform differently, and yield different bias residual results. In the ideal case, if isotropic antennas are used, then the LMS and MVDR adaptive algorithms do not introduce code-phase or carrier-phase biases in either the interference-free case or in the presence of wideband interference (Tables 3.7-10).

Table 3.16. Code-phase and carrier-phase biases after deterministic compensation; the blue-shaded cells show the bias residuals after correction using values from single-antenna and/or array calibration.

Averages over 10-satellite constellation		Widrow/LMS (Blind-adaptive)	Applebaum/MVDR (Steering-vector)
Bias corrections using single-element FRPA calibration	Code-phase	23 cm	28 cm
	Carrier-phase	0.03 cm (0.5°)	0.5 cm (9.2°)
Bias corrections using 7-element CRPA calibration	Code-phase	5.6 cm	0.0 cm
	Carrier-phase	0.5 cm (9.3°)	0.0 cm (0°)

3.7 BIAS VERSUS INTERFERENCE SUMMARY

This section has analyzed the tradeoff between rejecting radio frequency interference and mitigating navigation biases resulting from non-isotropic antennas. This analysis leads to deterministic corrections. In the case of isotropic antennas, or antennas with limited signal distortion, these corrections are sufficient to reduce measurement biases below the levels required by Sea-based JPALS.

Figure 3.10 illustrates this summary. The top row of plots shows results for isotropic antennas. The bottom row of plots shows results for the non-isotropic antennas modeled in this simulation study. The left column of plots shows code-phase bias residuals versus interference rejection performance and the right column of plots shows carrier-phase bias residuals versus interference rejection performance. Interference rejection is measured as the increase in C/N_0 for the LMS and MVDR adaptive arrays as compared to the deterministic CRPA, in each of the specified interference scenarios.

As shown in Figure 3.10-a, for isotropic antennas the noise-free performance of the adaptive arrays is equal to that of the deterministic CRPA. Adaptive array processing

(a) Isotropic Antennas

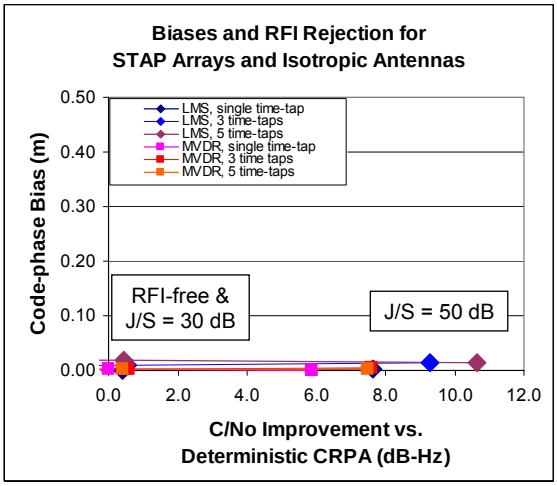

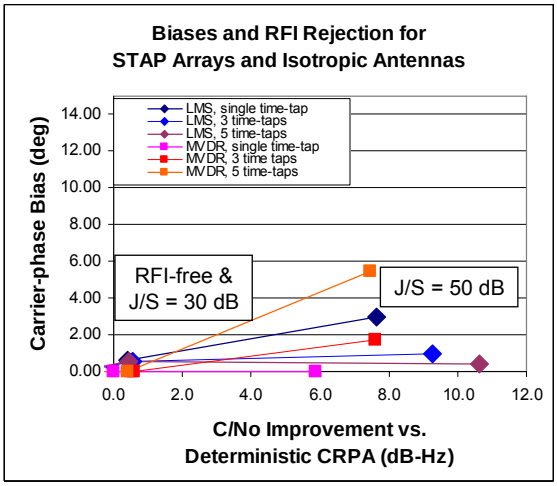

(b) Non-Isotropic Antennas

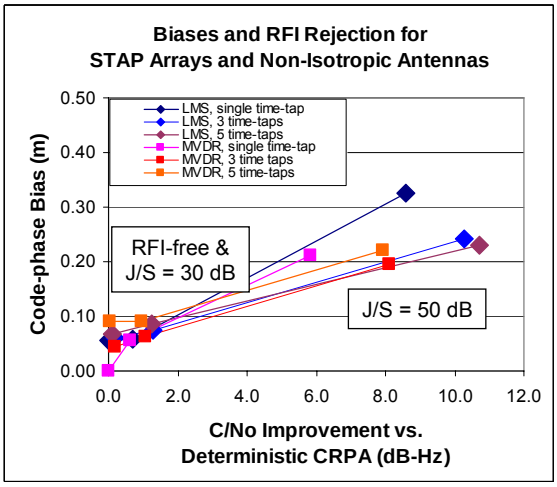

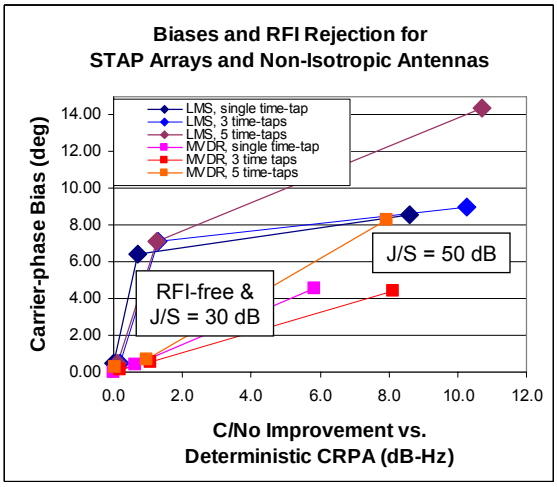

Figure 3.10. Average absolute errors and C/N0 improvement for space-time adaptive array algorithms and isotropic and non-isotropic antennas.

helps against interference, and introduces no code-phase or carrier-phase biases. The conclusion: for isotropic antennas, use adaptive array processing.

As shown in Figure 3.10-b, for non-isotropic antennas, the noise-free performance of the adaptive arrays is equal to that of the deterministic CRPA. Adaptive array processing is even more beneficial against interference than for the isotropic case, yet introduces code-phase and carrier-phase biases. These biases are partially mitigated by deterministic corrections. The conclusion: for non-isotropic antennas, selectively use adaptive array processing when interference power is high and accuracy demands are relaxed. Also, it is beneficial to implement improved antenna designs which display less distortion-induced signal tracking biases.

CHAPTER 4: EXPERIMENTAL VERIFICATION

This chapter demonstrates experimental verification by exercising the software receiver with operational hardware in the loop. This verification involves a two-tiered approach, addressing both interference rejection and bias mitigation.

Quantification of code-phase and carrier-phase biases and evaluation of bias mitigation performance is done with data from live open-air tests using a seven-element antenna array, custom analog hardware, and a dedicated data collection system. Evaluation of radio frequency interference rejection is done with data from a high-fidelity GPS RF hardware simulator, a wavefront generator which simulates a four-antenna front-end, and a four-receiver data collection system. Software receiver tracking of the signals recorded with this hardware was described previously in Section 2.4.

4.1 EXPERIMENTAL RESULTS – BIAS MITIGATION

This section describes the experimental results for bias characterization and mitigation with operational hardware in the loop. This hardware system collected live GPS C/A-code signals using a seven-element antenna array [87, 88]. A schematic of the system is shown in Figure 4.1. The data recording setup consisted of custom-designed front-ends performing downconversion and sampling, and one USB2 data bridge connected to a host computer. The front-end and the A/D converter for all antenna channels were connected to a common clock. The receiver-to-receiver phase biases were calibrated and removed during post-processing by the software receiver. The data processed in this investigation were from a ten-minute record collected in Sweden on November 7th, 2006. The array of commercial off-the-shelf patch antennas had a clear view of the sky and there were 13 GPS satellite signals present in the data, with an average tracked C/N_0 of 46 dB-Hz.

Table 4.1 shows bias characterization and mitigation results from testing with hardware in the loop. The first two rows of data show the code-phase and carrier-phase bias residuals for antenna array processing as compared to the single-element FRPA. The

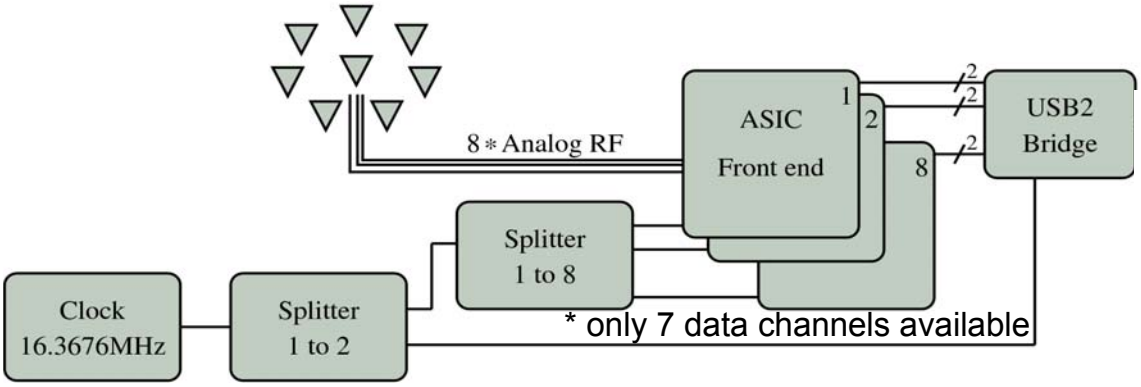

Figure 4.1. Hardware schematic – live GPS C/A-code signals and seven-antenna data collection system. Data courtesy Luleå University of Technology, Staffan Backén and Dr. Dennis Akos.

Table 4.1. Real data, seven-antenna receiving array, GPS C/A-code. Code-phase and carrier-phase biases after determinstic compensation. The blue-shaded cells show bias residuals using best calibration method.

Averages over 13-satellite constellation, Real signals, C/A-code		**Deterministic**		**STAP w/ 1 time-tap**	
		FRPA	**CRPA**	**LMS**	**MVDR**
Bias corrections using single-element FRPA calibration	**Code-phase**	- 0 -	4.42 m	4.37 m	4.43 m
	Carrier-phase	- 0 -	1.15 cm (21.8°)	1.22 cm (23.2°)	1.23 cm (24.2°)
Bias corrections using 7-element CRPA calibration	**Code-phase**	not applicable	- 0 -	25 cm	20 cm
	Carrier-phase	not applicable	- 0 -	0.4 cm (7.3°)	0.2 cm (4.2°)
C/No (dB-Hz)		45.9	53	53	53.1

residuals are found by subtracting the code-phase and carrier-phase estimates from tracking with the single-element FRPA from the estimates from tracking with the multi-antenna arrays. This method does not require actual calibration of the antennas, since the method presumes that the code-phase and carrier-phase biases of the single-element FRPA would be known from calibration and removed via deterministic compensation. Table 4.1 shows that for these antennas, absolute code-phase and carrier-phase biases using array processing are greater than the biases predicted from simulation. The two primary reasons for this difference are: (a) the use of real analog signal conditioning hardware, and (b) antennas of different design than were specified in simulation.

The next two rows of data in Table 4.1 show the code-phase and carrier-phase bias residuals for the MVDR and LMS adaptive antenna arrays as compared to the multi-element deterministic CPRA. Again, the method subtracts the code-phase and carrier-phase estimates from tracking with the deterministic CRPA from the estimates from tracking with the adaptive arrays. In this way, the results are equivalent to using the corrections from deterministic multi-element CRPA calibration for compensation of adaptive array biases.

Table 4.1 shows that the adaptive array post-compensation bias residuals from testing with hardware in the loop are greater than the results predicted from simulation. The carrier-phase bias residuals from hardware testing are 7.3 º for LMS and 4.2º for MVDR, compared to less than 1º in both cases for simulation testing (see Table 3.12). These biases are sufficiently small to meet the Sea-based JPALS carrier-phase bias requirement of 10º, shown previously in Table 1.2. The code-phase bias residuals from hardware testing are 25 centimeters for LMS and 20 centimeters for MVDR, compared to 6 centimeters for LMS and less than 1 centimeter for MVDR for simulation testing (with no interference; see Table 3.12). These biases are too large to meet the Sea-based JPALS code-phase bias requirement of 8 centimeters, shown previously in Table 1.2.

The last row of Table 4.1 shows the improvement in C/N_0 for the seven-element array as compared to the single-element FRPA. For this interference-free data, the average

increase is approximately 6 dB with respect to the single-antenna FRPA, which agrees well with simulation results and with theoretical array performance.

4.2 EXPERIMENTAL RESULTS – INTERFERENCE REJECTION

This section describes the experimental results for interference rejection performance with operational hardware in the loop. This hardware system collected simulated GPS C/A-code signals plus interference using a four-element antenna array [89, 90, 91]. A schematic of the system is shown in Figure 4.2. The hardware simulator can generate up to 48 individual signals, which includes signals from individual GPS or Galileo satellites, signal multipath, and interference. The simulator creates satellite and interference signals at baseband according to the geometry previously shown in Figure 3.3. The satellite and interference signals then are digitally weighted and combined by an external digital processing unit in order to map each signal to the antennas of a four-element array. In these experiments, the geometry was a 2-by-2 rectangular array with $\lambda/2$ baselines. After weighting and summing, the digital signals are fed back to the simulator for digital to analog conversion, mixing to a common intermediate frequency, and then upconversion to the RF carrier. The resultant signals are recorded by a NordNav-R30 Quad Front End. This data was used to quantify interference rejection performance of the adaptive algorithms.

Figure 4.3 illustrates the average C/N_0 tracking values over a ten satellite simulated constellation. Figure 4.3-(a) shows results for six jammers each at a J/S power ratio of 30 dB. Figure 4.3-(b) shows results for six jammers each at a J/S power ratio of 40 dB. The blue line shows the average C/N_0 versus time for the single-antenna FRPA; the average value is approximately 47 dB-Hz. The other lines plot the average C/N_0 versus time for the 4-element deterministic CRPA, LMS-based adaptive processing with pre-correlation and post-correlation adaptation, and MVDR-based adaptive processing with pre-correlation adaptation (MVDR with post-correlation adaptation did not produce acceptable results). Before the onset of interference, the average improvement in C/N_0 for the four-antenna array (regardless of weight calculation method) is approximately 4.5

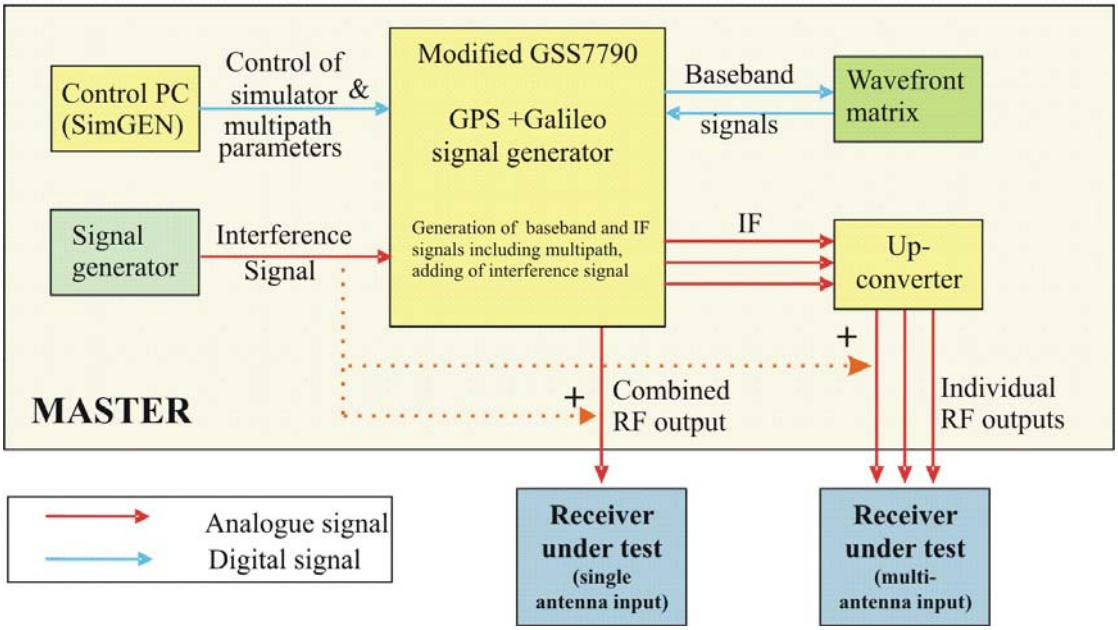

Figure 4.2. Hardware schematic – high-fidelity GPS C/A-code and interference simulator and four-receiver data collection system. Data courtesy DLR Institute of Communications and Navigation, Felix Antreich and Dr.-Ing. Achim Hornbostel.

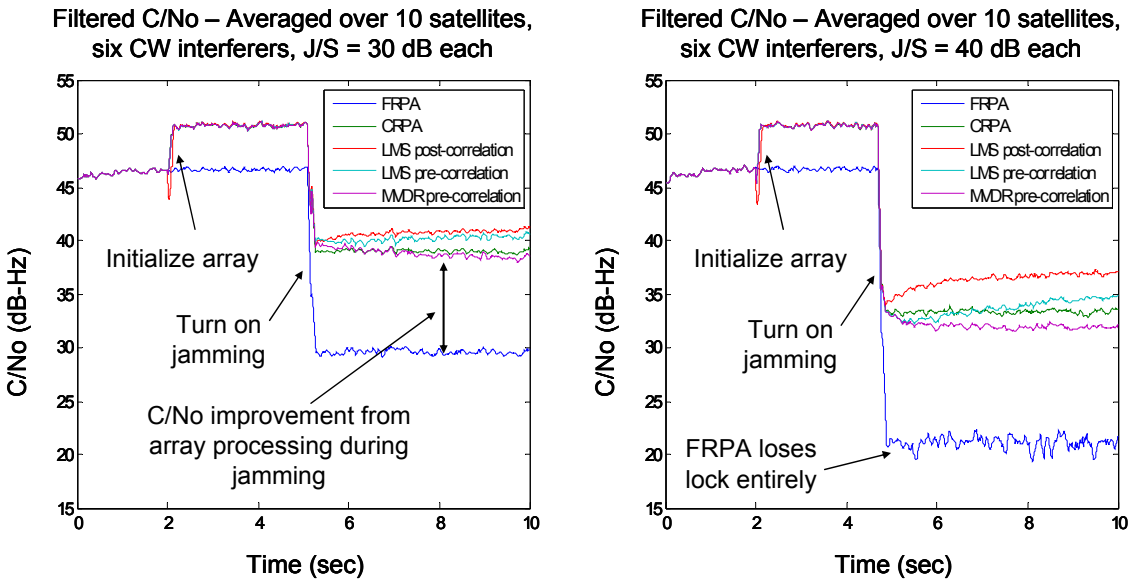

(a) (b)

Figure 4.3. Processing data from Spirent simulator, DLR wavefront generator, and four-channel NordNav receiver, using Stanford University multi-antenna space-time adaptive software receiver.

dB (this slightly underperforms the predicted value of 6 dB, and this minor degradation is due to analog hardware imperfections).

At 5000 milliseconds into the tracking window, narrowband jamming illuminates the antenna array. This is a sufficient time for the tracking loops to settle and for the adaptive algorithms to converge to steady-state values. As described in Section 3, the simulation portion of this investigation utilized six interference sources, to provide maximum stress to the adaptive algorithms in a seven-element receiver. Duplicate scenarios were created in the RF simulator, with interference from six jammers in the same locations as specified previously in Figure 3.3 (the limitation of using six jammers against a 4-element antenna array is discussed in Section 4.3.2).

Both wideband and narrowband interference were tested in the RF simulator. The hardware implementation allowed interference signals at J/S power ratios up to 55 dB for narrowband and 82 dB for wideband on each of the six jammers. However, signal tracking was not successful at the higher J/S power ratios. This limitation was discovered during data analysis, and attributable to the following two reasons: (a) the 2-bit A/D had insufficient dynamic range for the higher J/S power ratios, and (b) the four-element antenna array had insufficient spatial degrees of freedom to null six widely-separated interferers. The reduced performance due to limited A/D resolution underscores the importance of careful hardware design in systems that encounter high jamming levels.

As shown in Figure 4.3-(a), for the 30 dB case the FRPA tracks at an average C/N_0 of 30 dB-Hz, and the various array processing methods track at approximately 40 dB-Hz. The 10 dB drop in C/N_0 for array processing (compared to the interference-free case) is much less severe than the approximately 17 dB drop in C/N_0 for the single-antenna FRPA. As shown in Figure 4.3-(b), for the 40 dB J/S case the FRPA loses lock entirely. This represents a significant level of interference, and it is well beyond the capability of this GPS software receiver to maintain signal lock in single-antenna mode without special interference-rejection processing. The antenna arrays suffer reduction in C/N_0, but they all maintain signal lock with average C/N_0 in the range 32-37 dB-Hz.

Table 4.2 quantifies interference rejection performance for array processing when testing with hardware in the loop. In the interference-free case, the four-element arrays experience approximately 4.5 dB increase in C/N_0 as compared to the single-element FRPA. As expected, there is no benefit to adaptive processing in the interference-free case. (Note: as previously mentioned in Section 3.6, the post-correlation MVDR processing did not perform acceptably; these results are omitted here.)

As shown in Table 4.2, at a J/S power ratio of 30 dB on each of the six jammers, there is a 10 dB improvement for the four-element deterministic CRPA as compared to the single-element FRPA, and a further 2 dB increase with the LMS adaptive array. The MVDR adaptive array underperforms the deterministic CRPA by 0.5 dB (averaged over the ten satellites in the constellation). This degradation is due to channel-to-channel timing biases and receiver analog filter variation that introduce phase distortion on the received signals. At a J/S power ratio of 40 dB on each of the six jammers, the single-element FRPA loses lock entirely, and the deterministic CRPA tracks at an average C/N_0 of 33.4 dB-Hz. Now, the LMS adaptive array (in pre-correlation mode) yields approximately 3.5 dB improvement in C/N_0 compared to the deterministic CRPA. The MVDR adaptive array continues to underperform, now sacrificing approximately 1.5 dB compared to the deterministic CRPA.

Table 4.2. C/No from hardware-in-the-loop testing, six CW RFI sources;
STAP arrays utilize spatial degrees of freedom only.

C/No (Averages over 10-satellite constellation)	Deterministic		STAP w/ 4 antennas and 1 time-tap		
	FRPA	CRPA	LMS		MVDR
			post-correlation adaptation	pre-correlation adaptation	pre-correlation adaptation
no RFI	46.6 dB-Hz	50.8 dB-Hz	50.9 dB-Hz	50.8 dB-Hz	50.8 dB-Hz
6 CW RFI emitters, 30dB J/S ratio each	29.5 dB-Hz	39.0 dB-Hz	40.9 dB-Hz	40.4 dB-Hz	38.5 dB-Hz
6 CW RFI emitters, 40dB J/S ratio each	N/A (tracking failed)	33.4 dB-Hz	36.9 dB-Hz	34.4 dB-Hz	31.9 dB-Hz

4.3 LIMITATION OF EXPERIMENTAL RESULTS

The experimental set-up has demonstrated that the software receiver, in combination with operational hardware in the loop, rejects radio frequency interference while mitigating GPS navigation biases. However, there are limitations to these experimental results.

In particular, six specific unresolved issues identified here stand in the way of developing an operational prototype of this receiver. Three of the issues are hardware related. Two of the issues are software related. The sixth issue could arise either from software or from hardware. These six issues will be discussed one at a time.

4.3.1 Antenna Anisotropy

The unresolved issue of antenna anisotropy already has been described in Section 1.6 on page 16. For the L-band patch antenna design analyzed in simulation, the code-phase bias residuals in the presence of wideband interference exceed the limits established for Sea-based JPALS and therefore do not meet the auto-land requirements. However, with antennas that exhibit less signal distortion as a function of frequency and arrival direction, deterministic corrections are sufficient to reduce code-phase and carrier-phase biases below Sea-based JPALS limits (since isotropic antennas do meet Sea-based JPALS bias requirements, as established in Chapter 3). Therefore, with a suitable antenna design, space-time adaptive processing would be enabled for carrier-phase differential navigation, allowing aircraft auto-land while providing the benefits of interference rejection to the receiver.

4.3.2 Experimental Interference Rejection

NordNav receivers were used in the four-antenna data collection system of the hardware in the loop interference experiments. These receivers have a 2-bit A/D converter, as compared to the 4-bit A/D utilized in simulation. The 2-bit A/D provided insufficient dynamic range [5, 94], in this case precluding signal tracking at a J/S power ratio of 50

dB on each of six jammers. For this reason, it was not possible to verify interference rejection at J/S levels that were tested in simulation. Fortunately, this limitation did not affect the experimental results at moderate interference levels. This converter limitation was not identified until after completion of the data analysis from the experimental set-up. The obvious solution is to utilize a hardware receiver with greater A/D resolution.

The high-fidelity RF signal simulator used to create signals for testing with hardware in the loop was limited by a four-receiver data collection system. The simulation portion of this investigation utilized six interference sources, to provide maximum stress to the adaptive algorithms in a seven-antenna receiver. Since the hardware was limited to a four-antenna receiver, there were insufficient spatial degrees of freedom to adequately suppress jamming from six interference source. The obvious solution is to increase the number of data collection channels to recreate a seven-element array, or to create simulation and hardware scenarios that incorporate fewer jammers.

4.3.3 Receiver-to-Receiver Timing Biases

The multi-antenna hardware receivers were not properly synchronized, meaning that there was residual timing bias between the slave antenna channels and the master antenna. This observation applies both to the seven-antenna custom receiver system as well as to the four-antenna NordNav-based system, and was discussed in Section 2.4. The impact of this timing bias is to require additional phase rotation in the deterministically-computed antenna weights. The remedy is to use the LMS adaptive algorithm with blind initialization to calibrate the phase bias of each slave antenna channel. The preferred solution for an operational prototype system is improved hardware implementation that reduces this dependence on online phase calibration.

4.3.4 Convergence Speed

The adaptive algorithm parameter that controls convergence speed was set heuristically, as described in Section 2.3.2. The goal was to tie convergence speed of the adaptive

algorithms (LMS and MVDR) to the carrier-tracking loop noise bandwidth. The parameter that controls convergence speed is the misadjustment parameter γ that appears in Eq. (2.5) of Section 2.2.2. It would have been preferable to determine this parameter theoretically, and then to verify it experimentally. The desired value of γ is a function of the number of antennas, the sampling frequency, and the tracked C/N_0. The analytic determination of the convergence speed parameter is left for future work.

4.3.5 Post-correlation MVDR

The post-correlation MVDR adaptive algorithm did not perform as expected. This is discussed in Section 3.6. The LMS algorithm performed equally well both in pre-correlation and in post-correlation adaptation modes, while the MVDR algorithm suffered in the post-correlation mode due to excessive weight vector fluctuation. One possible cause is undetected errors in calculating the post-correlation steering vector constraint. For this reason, the results shown in this report utilize pre-correlation MVDR processing only. The resolution of this issue is left for future work.

4.3.6 LMS Blind Initialization

Some satellites displayed occasional weight vector instability with live GPS data during hardware in the loop experiments when using the LMS adaptive algorithm and blind initialization. This instability occurred for about half of the visible satellites, and manifested as occasional brief and rapid fluctuation (rotation) in the weight coefficients on all antennas. The instability appeared to be independent of satellite elevation angle and signal power. The instability never occurred either with the signal simulation discussed in Chapter 3 or with the high-fidelity hardware simulator covered in Chapter 4. This effect could be due to multipath or to hardware crosstalk. Crosstalk might be the most likely candidate, as isolation is particularly important for multi-antenna receiver hardware. The resolution of this important integrity issue is left for future work.

CHAPTER 5: CONCLUSIONS

5.1 SUMMARY

This thesis documents a multi-year effort to enable high-accuracy and high-integrity GPS navigation with interference rejection provided by a space-time adaptive antenna array. Chapter 1 reviewed Sea-based JPALS requirements and baseline architecture. Chapter 2 developed a GPS software receiver that implements a space-time adaptive multi-antenna array. Chapter 3 analyzed the tradeoff between rejecting radio frequency interference and mitigating navigation biases resulting from adaptive arrays of non-isotropic antennas. Chapter 4 provided experimental verification by exercising the software receiver with operational hardware in the loop.

This investigation demonstrates that a combination of carrier-phase differential navigation, space-time adaptive processing, deterministic measurement-domain bias compensation, and well-designed antennas will meet Sea-based JPALS requirements. The architecture of a GPS receiver that implements these features is illustrated in Figure 5.1. As interference power increases, GPS space-time adaptive algorithms become more desirable. Also, there is a balance between the ability to reject interference and the necessity of limiting errors. This investigation shows that the accuracy, integrity, and interference-rejection requirements of Sea-based JPALS can be met with a system architecture incorporating carrier-phase differential navigation and multi-element adaptive antenna arrays.

5.2 SUGGESTIONS FOR FUTURE WORK

The investigation and results described here can be considered as a "proof-of-concept" for GPS interference rejection using adaptive antenna arrays. The ultimate goal for future work is to create an operational prototype for a specific application (such as an aircraft landing on a carrier). Implementing that goal will require detailed system analysis and careful hardware design.

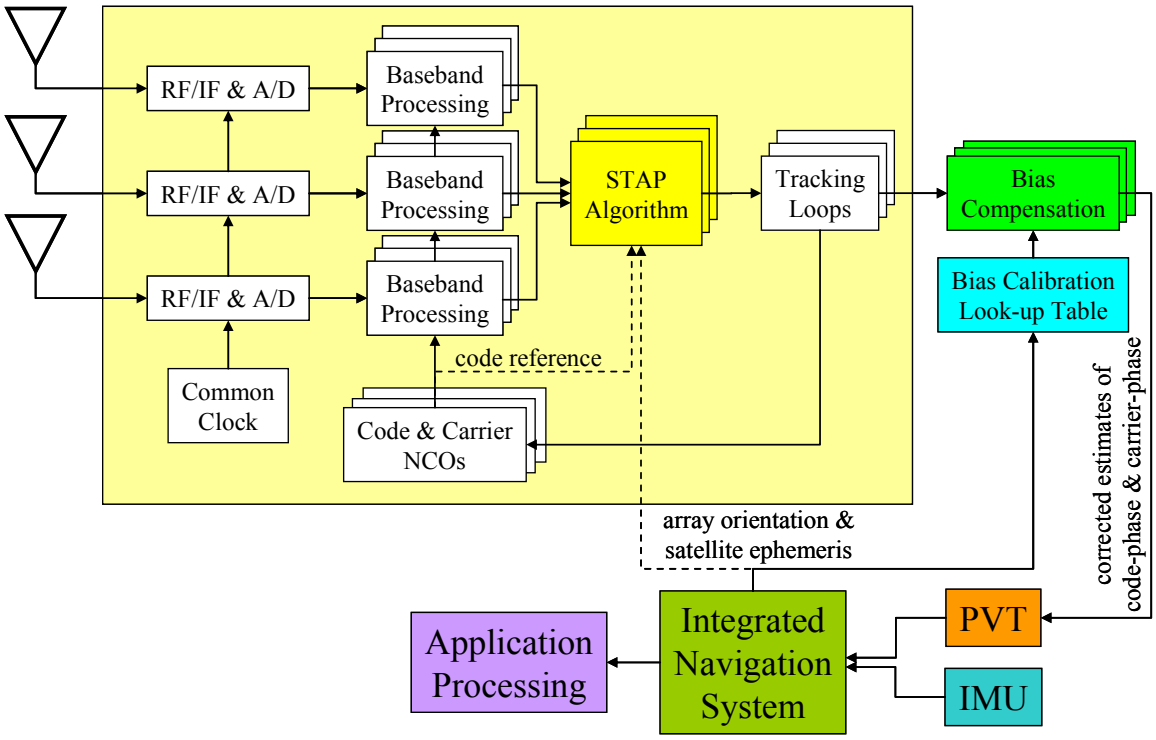

Figure 5.1. Final GPS receiver architecture with STAP array processing and code-phase and carrier-phase bias compensation.

Specific theoretical and practical extensions identified in this investigation to achieve an operational prototype are discussed here. Three areas for theoretical work are (a) testing additional adaptive algorithms in the software receiver, (b) comparing tested software receiver interference rejection performance to theoretical performance, and (c) pre-conditioning of the space-time covariance matrix to improve weight vector convergence speed and algorithm stability. The six key practical areas for future work were discussed in Section 4.3 on the limitations of experimental results. These six areas are (a) antenna anisotropy, (b) experimental interference rejection, (c) receiver-to-receiver timing biases, (d) convergence speed, (e) post-correlation MVDR, and (f) LMS blind initialization.

APPENDIX A: ACRONYMS

BOC	binary offset carrier
A/D	analog to digital
ADC	analog to digital converter
ASIC	application specific integrated circuit
C/N_0	carrier to noise ratio
COTS	commercial off-the-shelf
CRPA	controlled reception pattern antenna
CW	continuous-wave
D/A	digital to analog
DLL	delay-locked loop
FFT	fast Fourier transform
FLL	frequency-locked loop
FRPA	fixed reception pattern antenna
GNSS	global navigation satellite system
GPS	global positioning system
IMU	inertial measurement unit
INS	inertial navigation system
J/S	jammer to signal (power ratio)
JPALS	Joint Precision Approach and Landing System
LMS	least mean-square
MSE	mean-square error
MVDR	minimum variance distortionless response

NCO	numerically-controlled oscillator
PLL	phase-locked loop
PRN	pseudo-random noise
PVT	position, velocity, and time
RF	radio frequency
RFI	radio frequency interference
SFAP	space-frequency adaptive processing
SINR	signal to interference plus noise ratio
SMI	sample matrix inverse
SNR	signal to noise ratio
STAP	space-time adaptive processing
WGN	white Gaussian noise

APPENDIX B: ANTENNA DATA

This appendix contains antenna characterization data. The gain and phase information are for ten satellite look directions and for seven antennas, and the characterization data are as determined by simulation using the Ansoft FEM field solver. The ten satellite locations occupy the test constellation configuration proposed by Ung-Suok Kim, and the gain and phase data are for the patch antennas developed by him and then simulated by him in Ansoft.

The coordinate convention is shown in Figure B.1. The coordinate origin is at the physical center of the reference (or master) antenna, element #1, and the +x-axis passes through the center of antenna element #2. The remainder of the antennas are placed on the circumference of a circle in an anti-clockwise sense. With this hexagonal pattern of antenna elements, the baseline length separating any two adjacent antennas is equal to one-half of the wavelength of the GPS L1 carrier, or 9.5 centimeters.

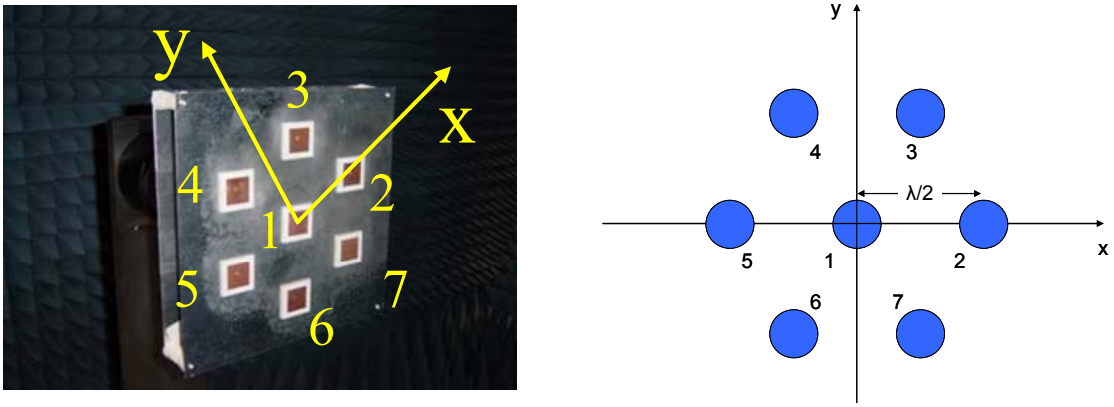

(a) (b)

Figure B.1. Antenna array configuration:
(a) antennas in anechoic chamber
(b) layout and coordinate definition

The look direction to the ten satellites in the constellation is shown in Figure B.2. Zero degrees azimuth lies along the +x-axis, and positive angles are measures in an anti-clockwise sense. Zero degrees elevation is at the horizon defined by the xy-plane, and positive angles are measured up towards the +z-axis of a right-hand coordinate system.

Figures B.3-B.12 show the gain and phase response of the seven antennas in the look directions defined by the ten satellites in the standard constellation. Gain response is in the upper plots (an isotropic antenna would have unity response for all frequencies), and phase response is in the lower plots. Phase response is specified with respect to the physical center of each antenna element (i.e., not to the physical center of the array).

PRN	Azimuth	Elevation
1	0	40
2	30	30
3	60	40
4	90	50
5	120	20
6	150	60
7	210	70
8	240	20
9	270	30
10	300	80

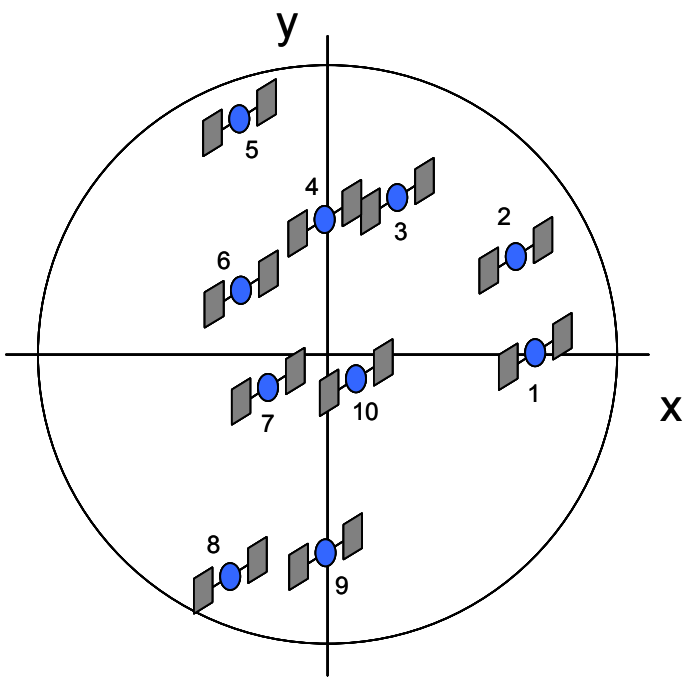

Figure B.2. Satellite locations and azimuth / elevation convention.

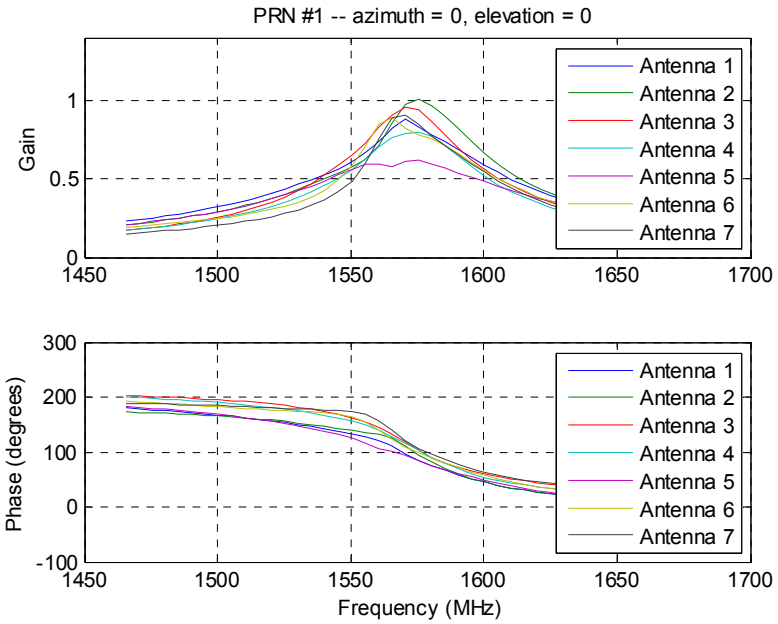

Figure B.3. Antenna response for PRN #1.

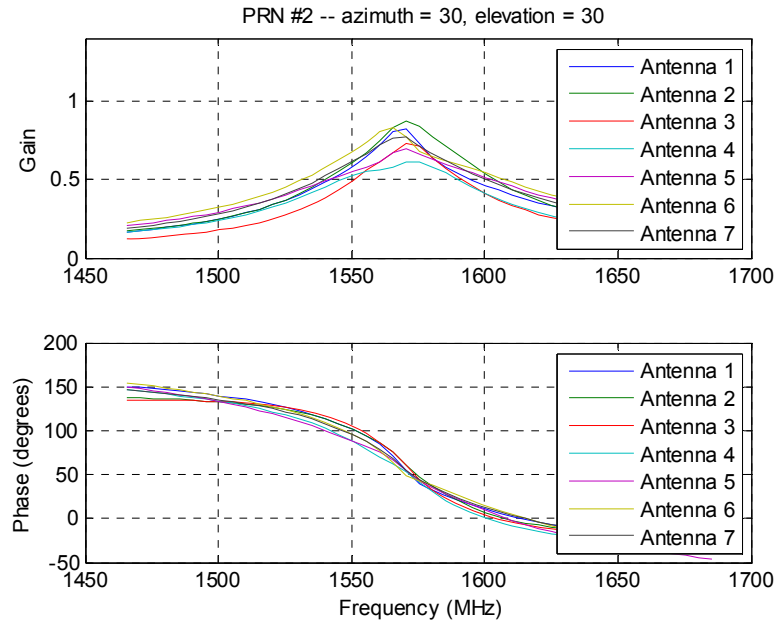

Figure B.4. Antenna response for PRN #2.

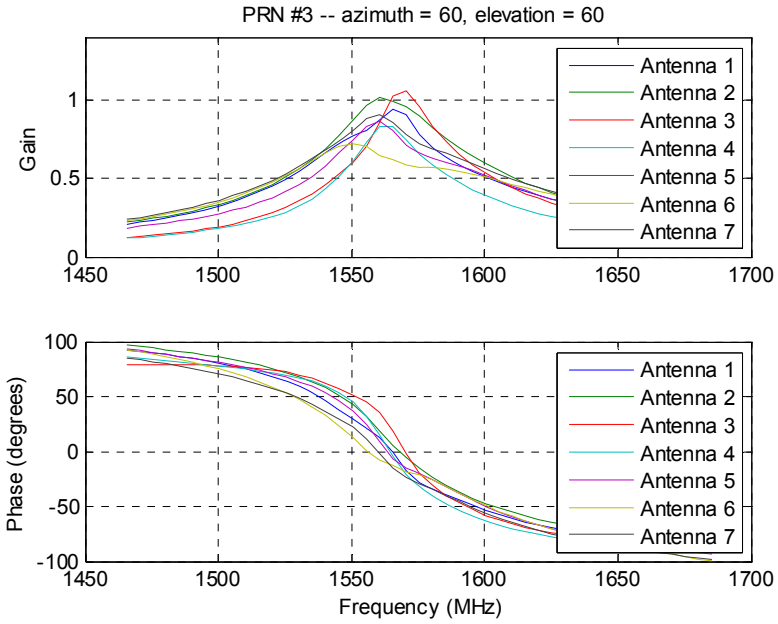

Figure B.5. Antenna response for PRN #3.

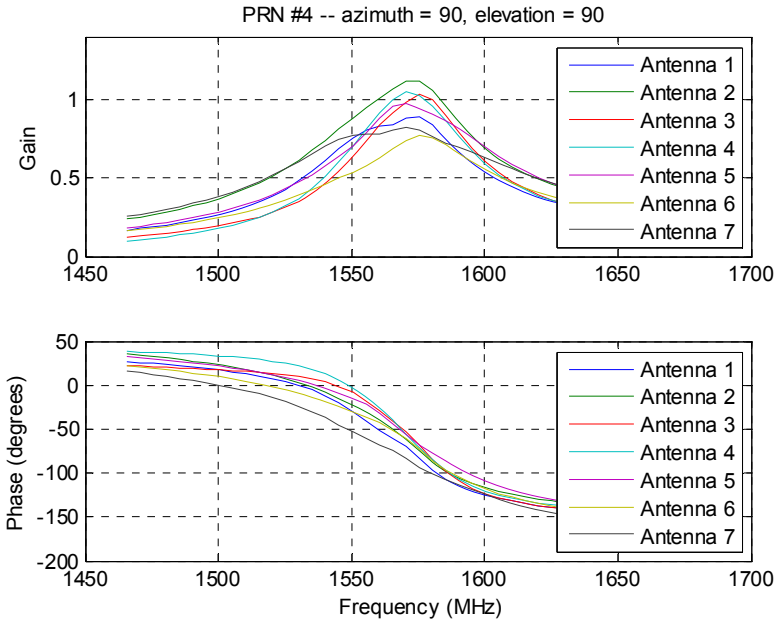

Figure B.6. Antenna response for PRN #4.

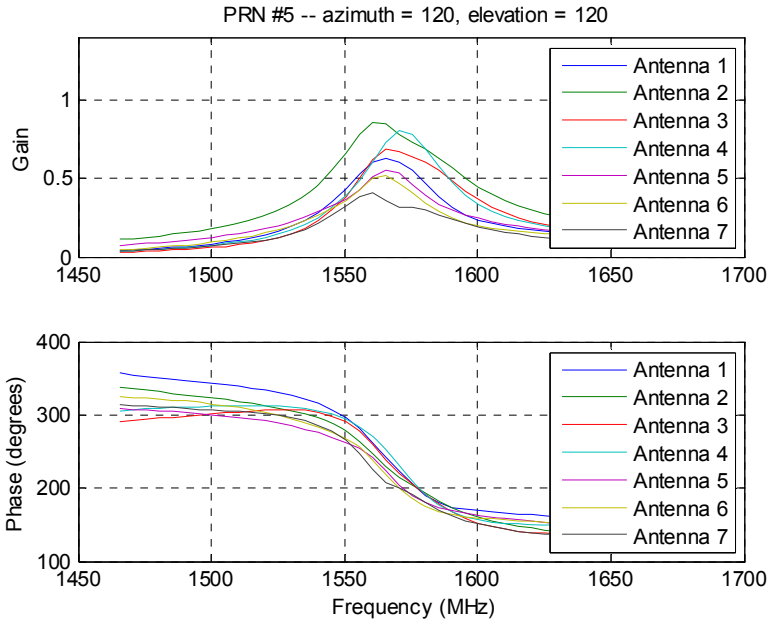

Figure B.7. Antenna response for PRN #5.

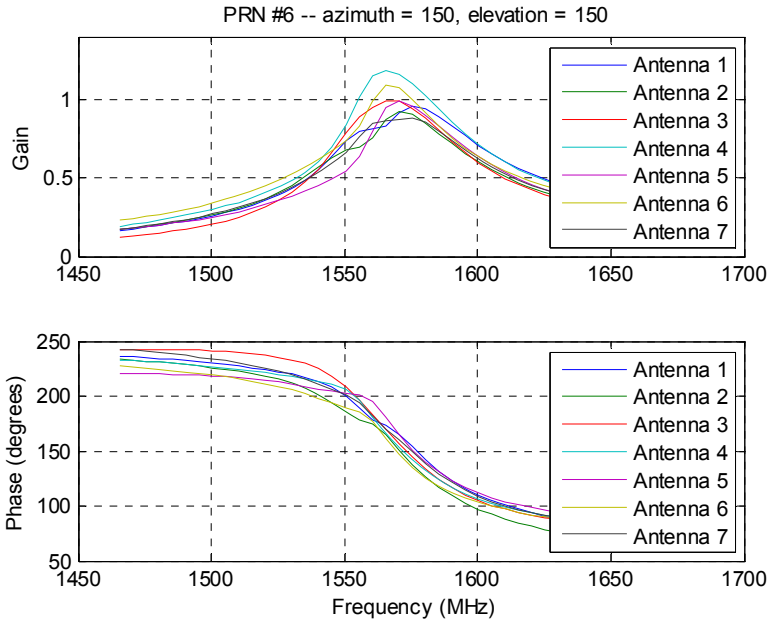

Figure B.8. Antenna response for PRN #6.

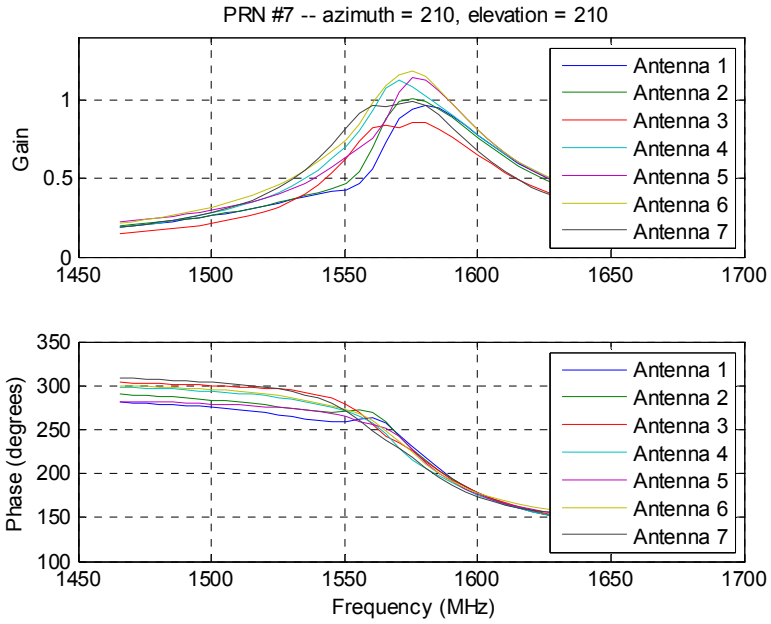

Figure B.9. Antenna response for PRN #7.

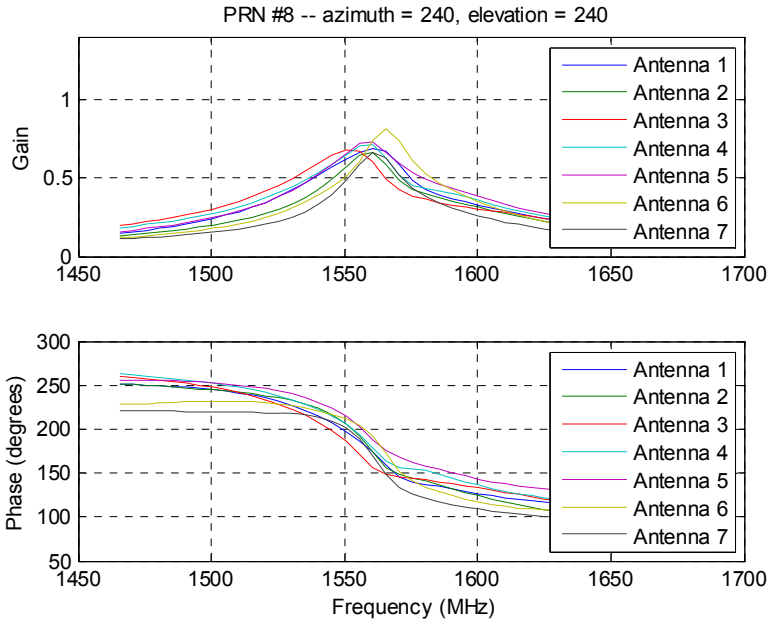

Figure B.10. Antenna response for PRN #8.

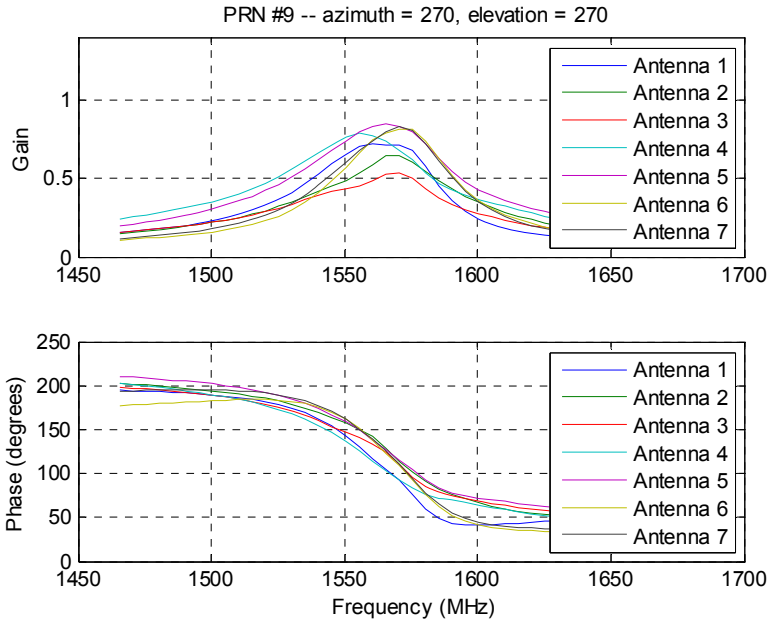

Figure B.11. Antenna response for PRN #9.

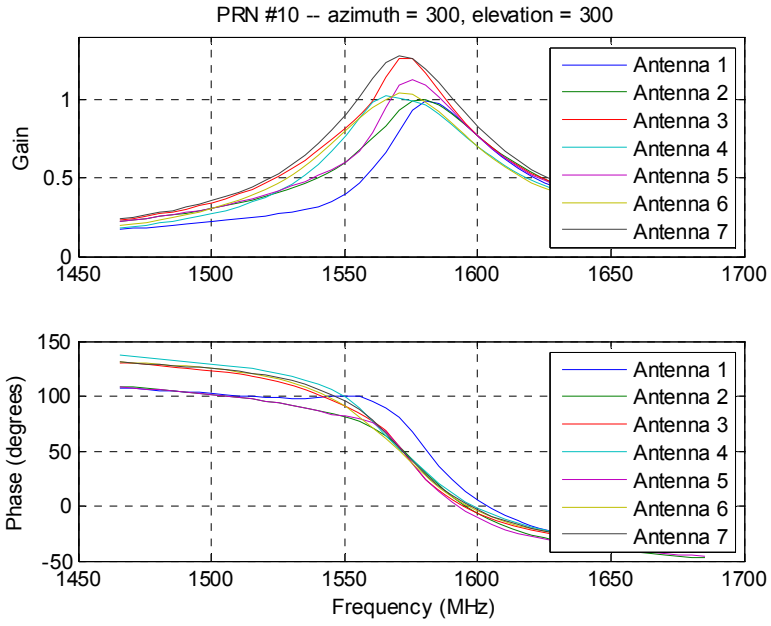

Figure B.12. Antenna response for PRN #10.

REFERENCES

1. B.W. Parkinson, T. Stansell, R. Beard, and K. Gromov, 1995, "A History of Satellite Navigation," *NAVIGATION*, vol. 42, no. 1, pgs. 109-164.
2. C. Kee, B.W. Parkinson, and P. Axelrad, 1991, "Wide Area Differential GPS," *NAVIGATION*, vol. 38, no. 2, pgs. 123-145.
3. B. Pervan, D. Lawrence, K. Gromov, G. Opshaug, J. Christie, P.-Y. Ko, A. Mitelman, S. Pullen, P. Enge, and B. Parkinson, 1997, "Flight Test Evaluation of a Prototype Local Area Augmentation System Architecture," *Proc. ION GPS 1997*, pgs. 1613-1621.
4. C.E. Cohen, H.S. Cobb, D.G. Lawrence, B.S. Pervan, J.D. Powell, B.W. Parkinson, G.J. Aubrey, W. Loewe, D. Ormiston, B.D. McNally, D.N. Kaufmann, V. Wullschleger, and R.J. Swider, Jr., 1995, "Autolanding a 737 Using GPS Integrity Beacons," *NAVIGATION*, vol. 42, no. 3, pgs. 467-486.
5. J.J. Spilker and F.D. Natali, 1996, "Interference Effects and Mitigation Techniques," in Global Positioning System: Theory and Applications I, B.W. Parkinson and J.J. Spilker (Eds.), AIAA, Reston, VA, pgs. 717-771.
6. R.T. Compton, Jr. 1988, Adaptive Antennas: Concepts and Performance, Prentice-Hall, Inc., Englewood Cliffs, N.J.
7. R.L. Fante and J.J. Vaccaro, 1998, "Cancellation of Jammers and Jammer Multipath in a GPS Receiver," *IEEE Aerospace and Electronic Systems Magazine*, vol. 13, no. 11, pgs. 25-28.
8. G.F. Hatke, 1998, "Adaptive Array Processing for Wideband Nulling in GPS Systems," *Proc. 32nd Asilomar Conference on Signals, Systems, and Computers*, vol. 2, pgs. 1332-1336.
9. K. Falcone, N.B. Jarmale, F. Allen, and J. Clark, 2000, "GPS Anti-Jam for CAT II Landing Applications," *Proc. ION GPS 2000*, pgs. 1301-1308.
10. W.L. Myrick, J.S. Goldstein, and M.D. Zoltowski, 2001, "Low Complexity Anti-jam Space-Time Processing for GPS," *Proc. IEEE ICASSP 2001*, pgs. 2233-2236.
11. S.G. Carlson, C.A. Popeck, M.H. Stockmaster, and C.E. McDowell, 2003, "Rockwell Collins' Flexible Digital Anti-Jam Architecture," *Proc. ION GPS/GNSS 2003*, pgs. 1843-1851.
12. R.L. Fante, M.P. Fitzgibbons, and K.F. McDonald, 2004, "Effect of Adaptive Array Processing on GPS Signal Crosscorrelation," *Proc. ION GNSS 2004*, pgs. 579-583.

13. G.A. McGraw, S.Y. Ryan Young, and K. Reichenauer, 2004, "Evaluation of GPS Anti-Jam System Effects on Code-phase and Carrier Phase Measurements for Precision Approach and Landing," *Proc. ION GNSS 2004*, pgs. 2742-2751.

14. D.S. De Lorenzo, J. Rife, P. Enge, and D.M. Akos, 2006, "Navigation Accuracy and Interference Rejection for an Adaptive GPS Antenna Array," *Proc. ION GNSS 2006*, pgs. 763-773.

15. G.A. McGraw, C. McDowell, and J.M. Kelly, 2006, "GPS Anti-Jam Antenna System Measurement Error Characterization and Compensation," *Proc. ION GNSS 2006*, pgs. 705-714.

16. JPALS SRD, 2003, "System Requirements Document (SRD) for the Joint Precision Approach and Landing System (JPALS) Common Program, Revision 2.4, Draft V13," Electronic Systems Center, Global Air Traffic Operations/Mobility Command and Control System Program Office, Hanscom AFB, MA.

17. Sea-based JPALS SRD, 2004, "Sea Based Joint Precision Approach and Landing System (JPALS) System Requirements Document, Version 2.0," Department of the Navy, Naval Air Systems Command, St. Inigoes, MD.

18. B.R. Peterson, S. Pullen, B. Pervan, G. McGraw, T. Skidmore, and S. Anderson, 2005, "Investigation of Common Architectures for Land- and Sea-Based JPALS," *Proc. ION GNSS 2005*, pgs. 26-37.

19. B.R. Peterson, G. Johnson, and J. Stevens, 2004, "Feasible Architectures for Joint Precision Approach and Landing System (JPALS) for Land and Sea," *Proc. ION GNSS 2004*, pgs. 544-554.

20. WAAS MOPS, 2001, "Minimum Operational Performance Standards for Global Positioning System / Wide Area Augmentation System Airborne Equipment," RTCA Special Committee 159 Working Group 2, RTCA Document Number DO-229C.

21. LAAS MASPS, 2004, "Minimum Aviation System Performance Standards for Local Area Augmentation System (LAAS)," RTCA Special Committee 159 Working Group 4A, RTCA Document Number DO-245A.

22. P. Misra and P. Enge, 2006, Global Positioning System: Signals, Measurement, and Performance, 2nd Edition, Ganga-Jamuna Press, Lincoln, MA.

23. B.D. Van Veen and K.M. Buckley, 1988, "Beamforming: A Versatile Approach to Spatial Filtering," *IEEE ASSP Magazine*, April, 1988, pgs. 4-24.

24. K.G. Gromov, 2002, "GIDL: Generalized Interference Detection and Localization System," PhD Dissertation, Stanford University.

25. A. Gecan and M. Zoltowski, 1995, "Power Minimization Techniques for GPS Null Steering Antenna," *Proc. ION GPS 1995*, pgs. 861-868.

26. R.L. Fante and J.J. Vaccaro, 2000, "Ensuring GPS Availability in an Interference Environment," *Proc. IEEE PLANS*, pgs. 37-40.

27. R.E. Cagley, S. Hwang, and J.J. Shynk, 2002, "A Multistage Interference Rejection System for GPS," *Proc. 36th Asilomar Conference on Signals, Systems, and Computers*, pgs. 1674-1679.

28. R.L. Fante and J.J. Vaccaro, 2000, "Wideband Cancellation of Interference in a GPS Receive Array," *IEEE Trans. on Aerospace and Electronic Systems*, vol. 2, no. 2, pgs. 549-564.

29. B. Pervan, F.-C. Chan, D. Gebre-Egziabher, S. Pullen, P. Enge, and G. Colby, 2003, "Performance Analysis of Carrier-Phase DGPS Navigation for Shipboard Landing of Aircraft," *NAVIGATION*, vol. 50, no. 3, pgs. 181-191.

30. U.-S. Kim, 2005, "Analysis of Carrier Phase and Group Delay Biases Introduced by CRPA Hardware," *Proc. ION GNSS 2005*, pgs. 635-642.

31. I.F. Progri, B.W. Nicholson, D.M. Upton, and W.E. Vander Velde, 1998, "Impacts of Frequency Dependent Mutual Coupling and Channel Errors on Digital Beam Forming Antenna Performance," *Proc. ION GPS 1998*, pgs. 275-283.

32. B.R. Rao, J.H. Williams, C.D. Boschen, J.T. Ross, E.N. Rosario, and R.J. Davis, 2000, "Characterizing the Effects of Mutual Coupling on the Performance of a Miniaturized GPS Adaptive Antenna Array," *Proc. ION GPS 2000*, pgs. 2491-2498.

33. E.C. Ngai and D.J. Blejer, 2001, "Mutual Coupling Analyses for Small GPS Adaptive Arrays," *Proc. IEEE Antennas and Propagation Society Intl. Symposium*, pgs. 38-41.

34. I.J. Gupta and S.W. Ellingson, 2003, "Adaptive Antenna Research at the ElectroScience Laboratory," *Proc. IEEE Antennas and Propagation Society Intl. Symposium*, pgs. 590-593.

35. U.-S. Kim, 2006, "Mitigation of Signal Biases Introduced by Controlled Reception Pattern Antennas in a High Integrity Carrier Phase Differential GPS System," PhD Dissertation defense, Stanford University.

36. B. Widrow and S.D. Stearns, 1985, Adaptive Signal Processing, Prentice-Hall, Inc, Englewood Cliffs, N.J.

37. B.W. Parkinson, J.J. Spilker, P. Axelrad, and P. Enge (Eds.), 1996, Global Positioning System: Theory and Applications, AIAA, Reston, VA.

38. J.B.-Y. Tsui, 2000, Fundamentals of Global Positioning System Receivers: A Software Approach, John Wiley & Sons, Inc., NY.

39. E.D. Kaplan and C. Hegarty (Eds.), 2006, Understanding GPS: Principles and Applications, 2nd Edition, Artech House, Inc., Norwood, MA.

40. K. Borre, D.M. Akos, N. Bertelsen, P. Rinder, and S. Holdt Jensen, 2006, A Software-Defined GPS and Galileo Receiver: A Single-Frequency Approach, Birkhäuser, Boston.

41. W.F. Gabriel, 1976, "Adaptive Arrays – An Introduction," *Proc. IEEE*, vol. 64, no. 2, pgs. 239-272.

42. L.C. Godara, 1997, "Applications of Antenna Arrays to Mobile Communications, Part I: Performance Improvement, Feasibility, and System Considerations," *Proc. IEEE*, vol. 85, no. 7, pgs. 1031-1060.

43. L.C. Godara, 1997, "Applications of Antenna Arrays to Mobile Communications, Part II: Beam-Forming and Direction-of-Arrival Considerations," *Proc. IEEE*, vol. 85, no. 8, pgs 1195-1245.

44. B.N. Agamata, 1991, "Time Domain Adaptive Filter Implementation of a Minimum Variance Distortionless Response (MVDR) Beamformer for a Sensor Array," *Proc. ION GPS 1991*, pgs. 443-451.

45. J.L. Milin, C. Terret, J.F. Diouris, and J. Saillard, 1993, "An Adaptative [*sic*] Array Processor Using the Analog L.M.S. Algorithm: An Efficient Solution for a N.A.V.S.T.A.R./G.P.S. Application," *Proc. Antennas and Propagation Society Intl. Symposium*, pgs. 678-681.

46. J.E. Miller and S.L. Miller, 1994, "An Adaptive Antenna Array for Multiple Received Signals in Direct-sequence Code-division Multiple-access Communication Systems," *Proc. IEEE MILCOM '94*, pgs. 733-737.

47. M.D. Zoltowski and A.S. Gecan, 1995, "Advanced Adaptive Null Steering Concepts for GPS," *Proc. IEEE MILCOM '95*, pgs. 1214-1218.

48. D.-J. Moelker and Y. Bar-Ness, 1996, "An Optimal Array Processor for GPS Interference Cancellation," *Proc. AIAA/IEEE Digital Avionics Systems Conference*, pgs. 285-290.

49. D.-J. Moelker, E. van der Pol, and Y. Bar-Ness, 1996, "Adaptive Antenna Arrays for Interference Cancellation in GPS and GLONASS Receivers," *Proc. IEEE PLANS*, pgs. 191-198.

50. J. Ramos, M. Zoltowski, and M. Burgos, 1996, "Robust Blind Adaptive Array: A Prototype for GPS," *Proc. IEEE Intl. Symposium on Phased Array Systems and Technology*, pgs. 406-410.

51. R. Arseneau, 1997, "Advantages of Adaptive Nulling in GPS Guided Munitions," *Proc. ION NTM*, pgs. 797-802.

52. B.W. Nicholson, D.M. Upton, S. Cotterill, J. Marchese, T. Upadhyay, and W.E. Vander Velde, 1998, "Computer Simulation of Digital Beam Forming Adaptive Antennae for GPS Interference Mitigation," *Proc. ION NTM*, pgs. 355-360.

53. J.M. Blas, R. Blázquez, and J.I. Alonso, 1999, "A Low Cost GPS Adaptive Antenna Array," *Proc. ION NTM*, pgs. 751-757.

54. K. Falcone, G. Dimos, C. Yang, F. Nima, S. Wolf, D. Yam, J. Weinfeldt, and P. Olson, 1999, "Small Affordable Anti-Jam GPS Antenna (SAAGA) Development," *Proc. ION GPS 1999*, pgs. 1149-1156.

55. J.I.R. Owen and M. Wells, 2001, "An Advanced Digital Antenna Control Unit for GPS," *Proc. ION NTM*, pgs. 402-407.

56. W.L. Myrick, M.D. Zoltowski, and J.S. Goldstein, 2000, "Exploiting Conjugate Symmetry in Power Minimization Based Pre-Processing for GPS: Reduced Complexity and Smoothness," *Proc. IEEE ICASSP 2000*, pgs. 2833-2836.

57. I.J. Gupta and T.D. Moore, 2001, "Space-Frequency Adaptive Processing (SFAP) for Interference Suppression in GPS Receivers," *Proc. ION NTM*, pgs. 377-385.

58. R.G. Lorenz and S.P. Boyd, 2002, "Robust Beamforming in GPS Arrays," *Proc. ION NTM*, pgs. 409-427.

59. F. Berefelt, B. Boberg, F. Eklof, J. Malmstrom, L. Paajarvi, P. Stromback, and S.L. Winkander, 2003, "INS/GPS Integration with Adaptive Beamforming," *Proc. ION GPS/GNSS 2003*, pgs. 1096-1106.

60. D.S. De Lorenzo, J. Gautier, P. Enge, and D. Akos, 2004, "GPS Receiver Architecture Effects on Controlled Reception Pattern Antennas for JPALS," *Proc. ION GNSS 2004*, pgs. 2010-2020.

61. G.F. Hatke and T.T. Phuong, 2004, "Design and Test of a GPS Adaptive Antenna Array Processor: The Multipath Adaptive Multibeam Array (MAMBA) Processor," MIT Lincoln Laboratory Project Report GPS-16.

62. K.F. McDonald, R. Raghavan, and R. Fante, 2004, "Lessons Learned Through the Implementation of Space-Time Adaptive Processing Algorithms for GPS Reception in Jammed Environments," *Proc. IEEE PLANS*, pgs. 418-428.

63. G.A. McGraw, C. McDowell, R.S.Y. Young, and D.W. Glessner, 2005, "Assessment of GPS Anti-Jam System Pseudorange and Carrier Phase Measurement Error Effects," *Proc. ION GNSS 2005*, pgs. 603-617.

64. D.S. De Lorenzo, J. Gautier, J. Rife, P. Enge, and D. Akos, 2005, "Adaptive Array Processing for GPS Interference Rejection," *Proc. ION GNSS 2005*, pgs. 618-627.

65. G. Carrie, F. Vincent, T. Deloues, D. Pietin, A. Renard, and F. Letestu, 2006, "Stabilizing the Phase Response of Blind Array Processors for GNSS Interference Cancellation," *Proc. IEEE/ION PLANS*, pgs. 319-323.

66. C. Prades and F.A. Rubio, 2004, "Robust Space-Time Beamforming in GNSS by Means of Second-Order Cone Programming," *Proc. IEEE ICASSP 2004*, vol. II, pgs. 181-184.

67. G. Carrie, F. Vincent, T. Deloues, D. Pietin, and A. Renard, 2005, "A New Blind Adaptive Antenna Array for GNSS Interference Cancellation," *Proc. 39th Asilomar Conference on Signals, Systems, and Computers*, pgs. 1326-1330.

68. G. Seco-Granados, J.A. Rubio, and C. Prades, 2005, "ML Estimator and Hybrid Beamformer for Multipath and Interference Mitigation in GNSS Receivers," *IEEE Trans. on Signal Processing*, vol. 53, no. 3, pgs. 1194-1208.

69. S.-S. Hwang and J.J. Shynk, 2006, "Blind GPS Receiver with a Modified Despreader for Interference Suppression," *IEEE Trans. on Aerospace and Electronic Systems*, vol. 42, no. 2, pgs. 503-513.

70. D.S. De Lorenzo, F. Antreich, H. Denks, A. Hornbostel, C. Weber, and P. Enge, 2007, "Testing of Adaptive Beamsteering for Interference Rejection in GNSS Receivers," *Proc. ENC 2007*, in press.

71. T.-S. Chiou, 2007, "On the Probability Density Function and Stability Properties for a Cross-Product Frequency-Locked Loop," *Proc. ION GNSS 2007*, in press.

72. G.X. Gao, J. Spilker, T. Walter, P. Enge, and A.R. Pratt, 2006, "Code Generation Scheme and Property Analysis of Broadcast Galileo L1 and E6 Signals," *Proc. ION GNSS 2006*, pgs. 1526-1534.

73. G.X. Gao, D.S. De Lorenzo, A. Chen, S.C. Lo, D.M. Akos, T. Walter, and P. Enge, 2007, "Galileo Broadcast E5 Codes and their Application to Acquisition and Tracking," *Proc. ION NTM*, in press.

74. G.X. Gao, D.S. De Lorenzo, T. Walter, and P. Enge, 2007, "Acquisition and Tracking of GIOVE-A Broadcast L1/E5/E6 Signals and Analysis of DME/TACAN Interference on Receiver Design," *Proc. ENC 2007*, in press.

75. M. Quigley, Y. Gu, S. Bolouki, P. Abbeel, D.S. De Lorenzo, A. Ng, and D.M. Akos, 2007, "Portable GPS Baseband Logging," *ION GNSS 2007*, in press.

76. E.C. Jordan and K.G. Balmain, 1968, Electromagnetic Waves and Radiating Systems, Prentice-Hall, Inc., Englewood Cliffs, N.J.

77. W.L. Stutzman and G.A. Thiele, 1998, Antenna Theory and Design, 2nd Edition, John Wiley & Sons, Hoboken, N.J.

78. R.A. Monzingo and T.W. Miller, 1980, Introduction to Adaptive Arrays, John Wiley & Sons, Ltd., NY.

79. B. Allen and M. Ghavami, 2005, Adaptive Array Systems: Fundamentals and Applications, John Wiley & Sons, Ltd., West Sussex, England.

80. O.L. Frost, 1972, "An Algorithm for Linearly Constrained Adaptive Array Processing," *Proc. IEEE*, vol. 60, no. 8, pgs. 926-935.

81. S.P. Applebaum, 1976, "Adaptive Arrays," *IEEE Trans. on Antennas and Propagation*, vol. 24, no. 5, pgs. 585-598.

82. B. Widrow, P.E. Mantey, L.J. Griffiths, and B.B. Goode, 1967, "Adaptive Antenna Systems," *Proc. IEEE*, vol. 55, no. 12, pgs. 2143-2159.

83. R.T. Compton, Jr., 1988, "The Relationship Between Tapped Delay-Line and FFT Processing in Adaptive Arrays," *IEEE Trans. on Antennas and Propagation*, vol. 36, no. 1, pgs. 15-26.

84. R.T. Compton, Jr. 1989, "Comments on 'The Relationship Between Tapped Delay-Line and FFT Processing in Adaptive Arrays' (Author's Reply)," *IEEE Trans. on Antennas and Propagation*, vol. 37, no. 4, pg. 523.

85. C.W. Reed, R. Van Wechel, I. Johnston, B. Baeder, and E. Hogan, 2004, "FaSTAP: A Scalable Anti-Jam Architecture for GPS," *Proc. IEEE PLANS*, pgs. 496-502.

86. A.J. Van Dierendonck, 1996, "GPS Receivers," in Global Positioning System: Theory and Applications I, B.W. Parkinson and J.J. Spilker (Eds.), AIAA, Reston, VA, pgs. 329-407.

87. S. Backén and D.M. Akos, 2006, "GNSS Antenna Arrays – Hardware Requirements for Algorithm Implementation," *Proc. ENC 2006*.

88. S. Backén and D.M. Akos, 2006, "Antenna Array Calibration using Live GNSS Signals, *Proc. NAVITEC 2006 – 3rd ESA Workshop on Satellite Navigation User Equipment Technologies*.

89. A. Hornbostel, A. Schroth, H. Denks, and M. Holbrow, 2004, "A New Signal Simulation Tool for Testing of Receivers with Controlled Reception Pattern Antennas," *Proc. ION GNSS 2004*, pgs. 2595-2603.

90. A. Hornbostel, 2006, "MASTER: Multi-output Advanced Signal Test Environment for Receivers," DLR Institute of Communications and Navigation.

91. A. Konovaltzev, 2007, "Galileo Antenna Demonstrator," GALANT Workshop, DLR-Oberpfaffenhofen, March 9th 2007.

92. U.-S. Kim, D.S. De Lorenzo, J. Gautier, P. Enge, D. Akos, and J.A. Orr, 2004, "Precise Phase Calibration of a Controlled Reception Pattern GPS Antenna for JPALS," *Proc. IEEE PLANS*, pgs. 478 – 485.

93. U.-S. Kim, D.S. De Lorenzo, J. Gautier, P. Enge, and J.A. Orr, 2004, "Phase Effects Analysis of Patch Antenna CRPAs for JPALS," *Proc. ION GNSS 2004*, pgs. 1531-1538.

94 . P.W. Ward, J.W. Betz, and C.J. Hegarty, 2006, "Interference, Multipath, and Scintillation," in Understanding GPS: Principles and Applications, 2nd Edition, E.D. Kaplan and C. Hegarty (Eds.), Artech House, Inc., Norwood, MA.